# Thermal Cycling of Composite Honeycomb Sandwich Structure for Space Application

Sandesh Rathnavarma Hegde

A Thesis

In the Department

of

Mechanical Industrial and Aerospace Engineering

Presented in Partial Fulfillment of the Requirements

for the Degree of

Master of Applied Science (Mechanical Engineering)

at Concordia University

Montreal, Quebec, Canada

November 2018

# CONCORDIA UNIVERSITY
## School of Graduate Studies

This is to certify that the thesis prepared

By:             Sandesh Rathnavarma Hegde

Entitled:       Thermal Cycling of Composite Honeycomb Sandwich Structure for
                Space Application

and submitted in partial fulfillment of the requirements for the degree of

## Master of Applied Science (Mechanical Engineering)

complies with the regulations of the University and meets the accepted standards with respect to originality and quality.

Signed by the final Examining Committee:

_____ Chair
            *Dr. Masoumeh Kazemi-Zanjani*

_____ Internal Examiner
            *Dr. Farjad Shadmehri*

_____ External Examiner
            *Dr. Ahmed M Soliman*

_____ Examiner and Supervisor
            *Dr. Mehdi Hojjati*

Approved by    _____
                    Chair of Department or Graduate Program Director

November 2018    _____
                    Dean, Gina Cody School of Engineering and Computer Science

**ABSTRACT**

Thermal Cycling of Composite Honeycomb Sandwich Structure for Space Application

Sandesh Rathnavarma Hegde

A spacecraft during its operation, can experience temperature variations as high as ± 185 °C. Materials used in its structure such as carbon fiber reinforced polymer (CFRP) solid laminates and sandwich structures with honeycomb core are sensitive to the hostile space environment. One of the most common types of defect is microcracking. This thesis aims to study the effect of thermally induced microcracks on the mechanical property of the composite honeycomb sandwich structure. Composite honeycomb sandwich structure with Kevlar core and facesheet made of carbon fiber/ cyanate ester resin was studied. Sandwich material made of the different core and facesheet thickness were examined to study the thickness effect. To expose the samples to cryogenic temperature, the samples were submerged in Liquid Nitrogen ($LN_2$). To get it to elevated temperature, samples were placed in a convection oven. Two different experimental setups for cryogenic conditioning was used, one with accelerated cooling and the other with a slower rate of cooling. This was done to study the effect of the cooling rate on the formation of microcracks. Longitudinal microcracks were primarily observed between the facesheet and core interphase. Microscopic observation was done on two perpendicular polished cross-sections of the samples (ribbon and transverse ribbon directions). Microcracks were quantified using parameters such as crack density and crack length. Flatwise tensile mechanical test was performed on the samples to study the effect of microcracks. Good correlation was made between the crack area and the mechanical strength with the increase in thermal cycles. It is observed that the crack formation get saturated after a number of cycles, avoiding the need to conduct more thermal cycles. Microcrack formation both at the free edge and middle of laminate was observed. The crack density at the middle was comparatively less than the ones found on the free edges. Results for non-contact cooling and direct nitrogen contact cooling were compared. Microscopic inspection and flatwise test show significant difference between contact and non-contact cooled samples. The effect of thermal cycling on the different core and facesheet thicknesses for the same material system was compared. Samples with thicker core seemed to be more sensitive to microcracking. 3D finite element analysis (FEA) was conducted on the sandwich structure geometry to predict the experimental observations. The FEA results are in good agreement with the experimental findings.

# Table of Contents

# List of figures

# List of Tables

# Acknowledgements

# Dedication

**To my beloved father,**

for the sacrifices he made to provide me all the comforts

**To my dear mother,**

for the unconditional love and patience

**To my brother,**

for the support and guidance

**To my late grandmother,**

for her blessings

**and to my mentors, teachers, friends and family members.**

# Chapter 1: Introduction

## 1.1 Introduction

Over the years, use of composite materials for space and aerospace applications have grown significantly. The ability to tailor structures to achieve the required directional mechanical properties have made composite materials an ideal candidate for space applications. Among the wide range of options available, carbon fiber reinforced polymer (CFRP) in the form of solid laminates and sandwich structures are most frequently used [1-4]. There is a significant demand in the aerospace industry to reduce the structural mass. Reduction in structural mass provides more margin to accommodate payload mass for spacecraft and launch vehicles. Therefore, choosing materials with higher stiffness to density ratio which also satisfy other operational requirements such as the ability to operate in extreme temperature in space is of primary importance. Composites structures offer features such as higher bending stiffness, superior dimensional stability, low thermal conductivity and acoustic insulation compared to metal counterparts.

## 1.2 Application in space structures

Composite materials were initially developed for space missions where more emphasis was given on fabricating light weight structures without compromising required mechanical properties. Even though the cost of materials and processing are high, composite materials were preferred for space structures that are subjected to challenging working conditions. A mission critical structural failure would jeopardize the mission. Also, there is no scope for repair after the spacecraft is operational. Figure 1 shows various space applications where composite materials are used. Figure 1.1 (a) presents a spacecraft primary structure made of composite honeycomb sandwich material. The spacecraft structure is subdivided into primary, secondary and tertiary structures [5-6]. The objective of a spacecraft primary structure is to withstand launch loads and maintain structural integrity during launch as well as operational phase. Figure 1.1 (b) presents antenna assembly which is an example for a secondary structure. Figure 1.1 (c) presents a large cryogenic fuel tank for launch vehicle application. The requirement is to develop a tank to contain the internal pressure and resist formation of microcracks that results in leakages. Composite materials are prone to microcracking due to its heterogenous composition.

(a)



(b)



(c)

*Figure 1.1: (a) Spacecraft primary structure [7], (b) Antenna components[8], (c) Composite cryogenic fuel tank made of carbon/epoxy[9].*

## 1.3    Composite sandwich structure

Composite sandwich structure comprises of two facesheets separated by a core. Core in the form of honeycomb or foam-based core are widely used. Figure 1.2 shows various types of sandwich materials. Some of the most common types of facesheets used are glass fiber reinforced polymers (GFRP), carbon fiber reinforced polymers (CFRP) and sheet metal based facesheets. The facesheets are bonded to the core using suitable structural adhesive. The processing can be done either by co-curing or by secondary curing method. Co-curing involves curing both laminates and structural adhesive simultaneously. Secondary bonding (curing) involves curing of laminates separately and then bonding the cured laminates with adhesive. The adhesives are available in the form of thin film.
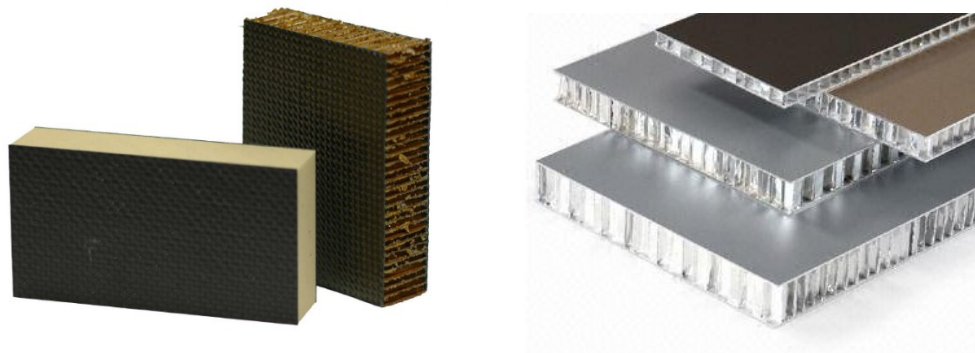


*Figure 1.2: Types of sandwich structures [10-11].*

Honeycomb cores made of aluminium and Kevlar [12] are most frequently used for space applications. By varying the geometry of the core cell, different density of the core can be manufactured. Honeycomb cores are manufactured by expansion process or by corrugation process [13]. Expansion process involves stacking of sheets consisting of printed adhesive node lines, by means of a substrate to form honeycomb before expansion (HOBE®) blocks. Furthermore, these blocks are sliced to suitable thickness followed by expansion of blocks. The expanded blocks are then trimmed to desire length along ribbon and transverse ribbon direction. Figure 1.3 illustrates manufacturing of core using expansion process.
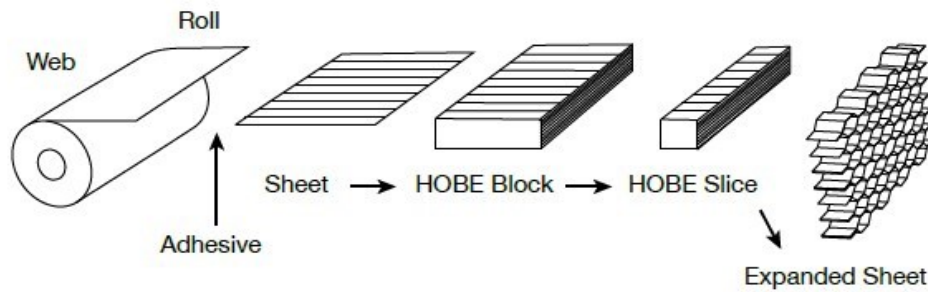
*Figure 1.3: Expansion process [13].*

Corrugation process involves passing of sheets of desired material through corrugated rolls, as shown in Figure 1.4. Adhesive is applied on corrugated nodes. The sheets with impregnated adhesive are then stacked to form blocks. The blocks are then cut to desired shape and dimensions. Corrugation process is generally performed to manufacture cores in high density range.
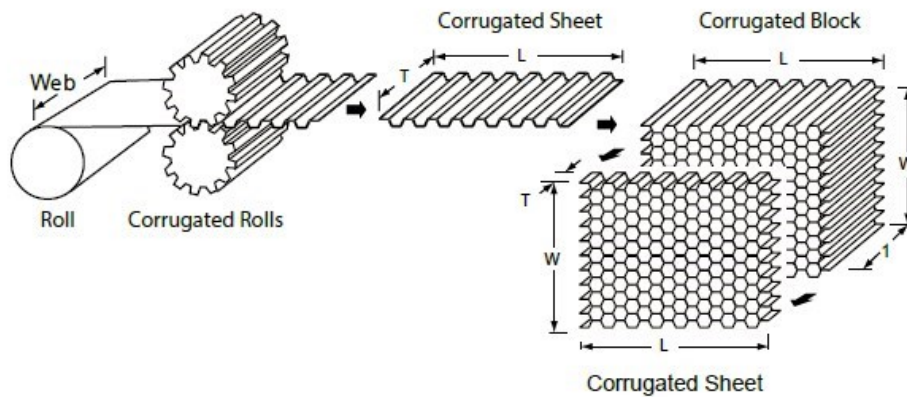


*Figure 1.4: Corrugation process [13].*

## 1.4    Literature review

### 1.4.1    Effect of space environment on composite materials

Space environment poses challenging working conditions for spacecraft. Spacecraft is exposed to hostile environment comprising of atomic oxygen, ultraviolet radiation, man-made debris, micrometeoroids and harsh thermal environment [14-17]. During a spacecraft's operation, it can experience temperature variations as high as ± 185 °C. A spacecraft experiences cryogenic temperature condition during the eclipse region of the orbit and elevated temperature due to the exposure to sun rays. This fluctuating thermal environment results in formation of microcracks.

The microcracks are in the form of fiber/matrix de-bonding and delamination between layers for composite structures.

### 1.4.2 Microcracking

Mahdavi S studied [18] the effect of thermally induced microcrack on the mechanical properties of solid laminates. The solid laminates made of unidirectional and woven carbon/epoxy prepregs were fabricated using the Out Of Autoclave (OOA) curing technique. The aim was to investigate the flight worthiness of the OOA cured laminates subjected to thermal cycling. Samples were exposed to thermal environment ranging between -194 °C to 150 °C. The panels comprised of voids. Microscopic observation showed the presence of microcracks after 10 thermal cycles. Cross-section of the samples were observed. Longitudinal cracks surfaced on unidirectional laminates connecting voids. Transverse cracks were observed around the voids in 90° tow of woven fabric laminates as shown in Figure 1.5. Short beam shear test showed reduction in interlaminar shear strength after subsequent thermal cycles.
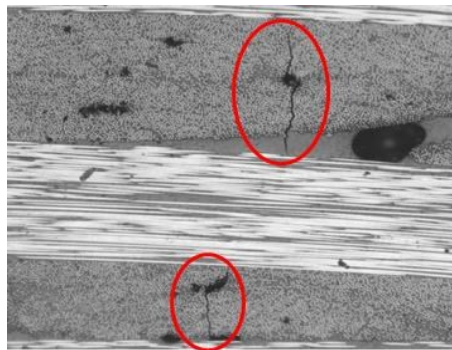


*Figure 1.5: Microcracks around voids [18].*

Bechel V. T et al. [19] studied the effect of thermal cycling for three types of carbon/polymer solid laminates (IM7/977-2, IM7/977-3, and IM7/5250-4). The thermal cycling temperature range was set between cryogenic temperature to +170 °C and room temperature (RT) to cryogenic temperature. Microcracks were quantified at the ply level as a function of thermal cycles. Up to 1000 thermal cycles were conducted and cracks were quantified by means of crack density (cracks/unit length). Effect of fiber angle on the formation of microcrack was also determined. It was reported that samples with cryogenic temperature to +170 °C thermal cycle had 64 times greater microcrack density than RT to cryogenic temperature cycling [20-24]. Microscopic observation was made at both free edges and midsection of the sample. Presence of microcracks

were significant even at the midsection of the samples. This observation indicates microcracking is not only at the free edges where material comes in contact with cryogen or heat, but also at the midsection of the sample.

Grogan et al. conducted damage investigation of carbon/PEEK laminates subjected to cryogenic thermal cycling. Three types of carbon/PEEK were tested. Laminates with cross ply and quasi-isotropic configuration was studied. To assess the effect of thickness on the microcrack formation, ply counts of 8, 16 and 32 were manufactured. Ply numbers were varied; however, thickness of each ply was kept constant. The temperature of thermal cycle ranged between +46 °C to -194 °C. Crack growth was monitored using optical microscopy and X-ray CT. Microcracking density was extensive for thicker (32 ply) laminates in comparison with 16 ply laminates and 8 ply laminates for same number of thermal cycles. Microcracks, in the form of transverse cracks and delamination were observed. The comparatively high sensitivity of microcracks for thicker laminates was mainly attributed to large thermal gradients.



(a)

(b)

(c)

(d)
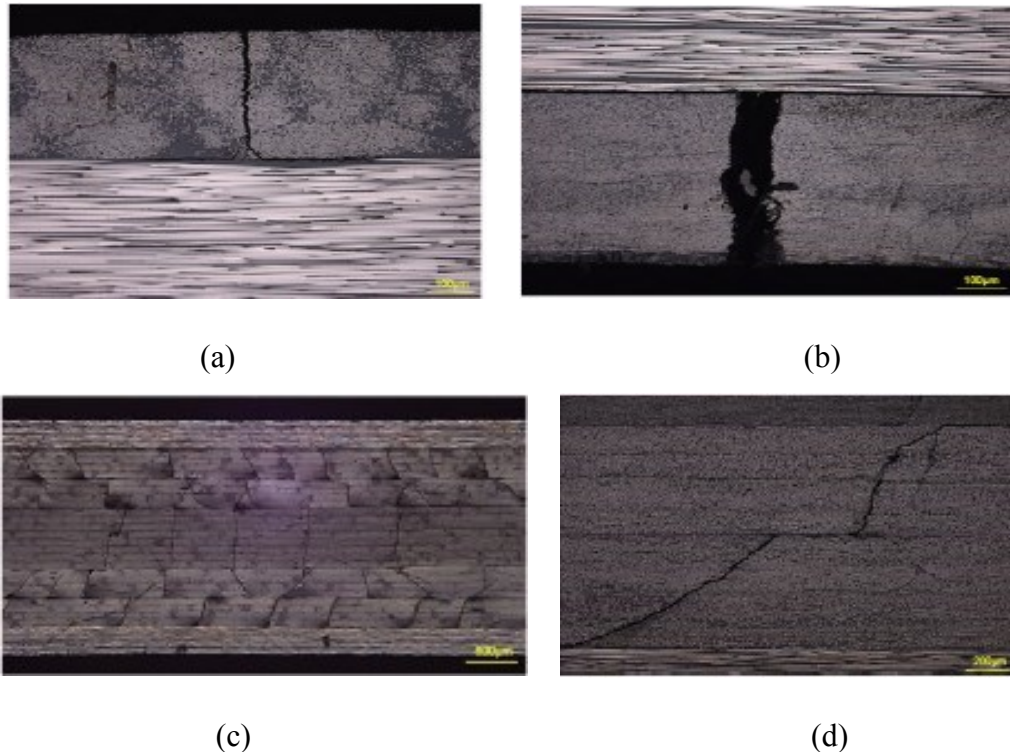
*Figure 1.6: (a) Transverse microcrack and associated delamination, (b) significant delaminated crack opening displacement in the laminate, (c) microcrack networks in quasi-isotropic laminate and (d) cracks in adjacent ply groups joined by a delamination [19].*

Mathilde et al [25], studied the effect of thermal cycling on composite honeycomb sandwich structure and three different varieties of carbon/cyanate ester resin solid laminates. Up to 360 thermal cycles were conducted on the samples and damage evolution in the form of microcracks were monitored by microscopic observation. Cracks were quantified by crack density, both at the polished free edges and at the mid-section. Three types of damages were observed on the edges such as, transverse microcracks, debonding between the fibers and the matrix; and delamination. On the mid-section only transverse microcracks were observed in the 90° tow. Longitudinal microcracks were observed between facesheet and core for sandwich material. In-plane shear test and tensile test of solid laminates showed significant reduction in the mechanical properties.

## 1.5    Objectives

This thesis is focussed on studying the effect of thermal cycling on the performance of composite honeycomb sandwich structure. Most of the studies done in the past addresses thermal cycling of solid laminates. To the best of the author's knowledge, the information on thermally induced microcracks and its effect on the de-bonding strength between facesheet and core is still a void. The main objectives of the present research are as follows:

- Develop a test plan for thermal cycling of composite honeycomb sandwich structure.
- Develop the test setup to achieve fast and slow rate of cooling and observe its influence on microcrack formation.
- Study the evolution of microcracks with increase in thermal cycles. Classify types of microcracks and understand the reasons behind the formation and growth of microcracks.
- Quantify microcracks by means of parameters such as crack density and crack length.
- Make a correlation between microcracks and mechanical strength.
- Develop a finite element model that can capture the experimental observation.
- Determine the effect of thermal cycling on the samples with different facesheet and core thickness.

## 1.6    Thesis outline

This thesis comprises of five chapters and formatted as per manuscript-based thesis format. Three chapters (Chapter 2 to 4) consists of three journal articles. Chapter two is published and chapter three and four are submitted for publication. Each chapter addresses different objectives. However,

cohesion is maintained between the chapters and some parts are duplicated. Outline of each chapters are given below.

**Chapter 1** provides the brief introduction to different types of composite materials used for space applications with relevant examples. Detailed description about various types of composite honeycomb sandwich structures and manufacturing process are given. Literature review of the problems associated with the thermal cycling of polymeric composites followed by the objectives of the present work is described.

**Chapter 2** Reproduced from: S. R. Hegde, M. Hojjati.," Thermally Induced Microcracks and Mechanical Property of Composite Honeycomb Sandwich Structure: Experiment and Finite Element Analysis" *Journal of Sandwich Structures and Materials*, 2018, DOI: 10.1177/1099636218802432.This chapter presents the material under investigation, test plan and test setup to study the effect of thermal cycling on composite honeycomb sandwich structures. Experimental and simulation results (finite element analysis) were presented based on the thermal cycles which contain dipping the samples in liquid nitrogen (direct contact). High cooling rate is achieved.

**Chapter 3** Reproduced from: S. R. Hegde, M. Hojjati.," Performance of Composite Sandwich Structures under Thermal Cycling" submitted to the *Journal of Composite Materials*, 2018. This chapter presents the experimental test setup to achieve lower rate of cooling (non-contact cooling). Microscopic observation and quantification of microcracks was performed. Comparison of microcracks for contact cooling and non-contact cooled samples and its effect on the mechanical property was investigated. Finite element analysis of sandwich cross-section geometry was performed.

**Chapter 4** Reproduced from: S. R. Hegde, M. Hojjati.," Effect of Core and Facesheet Thickness on the Mechanical property of Composite Sandwich Structures Subjected to Thermal Fatigue" submitted to the *International Journal of Fatigue*, 2018. This paper investigates the effect of thermal cycling on different core and facesheet thickness of samples made of the same material. Comparison of microcrack formation and evolution for different configuration was performed. Comparison of flatwise tensile mechanical strength with the microcrack area for all the configuration of samples chosen for study was made.

**Chapter 5** summarises the conclusions drawn from the experimental findings, contributions from the author, followed by recommendations for future work.

# Chapter 2: Thermally Induced Microcracks and Mechanical Property of Composite Honeycomb Sandwich Structure: Experiment and Finite Element Analysis

## ABSTRACT

Microcracking in composite honeycomb sandwich structure and its effect on mechanical properties are studied in this paper. A methodology is presented to study the extent of mechanical strength degradation of composite sandwich structure, subjected to thermal fatigue. The material under study is used for spacecraft structural applications. The test coupons were exposed to thermal cycling at elevated temperature as high as +150 °C inside the oven and cryogenic temperature of -190 °C by dipping in liquid nitrogen, which is comparable to the thermal environment experienced by spacecraft structures. After each thermal cycle, coupons were inspected for microcracks under an optical microscope at the cross-section. The microcracks were then quantified using parameters like crack length and crack density with increase in the number of cycles. Flatwise tensile test was conducted on the coupons after every ten thermal cycles, up to sixty cycles, to make a correlation between crack density and mechanical strength. It was observed that by increasing the number of thermal cycles the crack density increases and the flatwise tensile strength decreases up to a specific number of cycles. Finite element analysis was performed to predict the possible location of microcracks formation and compared with experimental observation. Good correlation was observed.

## 2.1 Introduction

Composites materials made of Fiber Reinforced Polymers (FRP) offer superior mechanical properties, such as, the ability to offer orthotropic strength and stiffness, great stiffness to density ratio, resistance to corrosion, acoustic insulation and thermal stability at extreme temperature environment that makes it an attractive option, when compared to the metal counterpart.

---

Composites sandwich structures, among other available composite materials, imparts superior flexural stiffness which makes it an ideal choice for structures that are subjected to flexural loads, more often for aerospace applications [26].

Sandwich construction primarily consists of a core, sandwiched between much stiffer facesheets using suitable adhesive. The core is available in various forms, more prominently, honeycomb and foam made from a wide range of materials. That includes sheet metal, fiber reinforced plastics, unreinforced polymers and paper-based. Most common type of facesheet chosen for aerospace application is aluminium and Carbon Fiber Reinforced Polymers (CFRP). Mathematically the distance of the outer most layers from the midplane of the material results in higher flexural stiffness of the structure [27]. This is achieved in sandwich structures where the distance of the facing from the midplane of the core results in the outer layer (facesheet) contributing more to the bending stiffness. However, this feature also introduces more potential material failure modes. A study on the several types of failure modes of the sandwich beam, made of Graphite Fiber Reinforced Polymer (GFRP) and Nomex honeycomb core, with different skin thickness to span length, subjected to three-point bending was conducted by Petras et al. [28]. Some of the most commonly observed failure modes include face yielding, face wrinkling, intracell dimpling, core shear or local indentation and core-facing delamination.

Sandwich structures have multiple components and interphases. Their applications involve an interaction of the material with cryogenic fuel in launch vehicle fuel tanks or the space environment which exposes the spacecraft structures to extreme thermal fluctuations [29], and therefore, their behaviour under severe environmental conditions needs to be investigated. One such investigation was conducted by Gates et al. on the facesheet delamination of composite sandwich materials at cryogenic temperatures [30]. A novel test method to determine the core-facing debonding strength at cryogenic temperature and the effect of specimen orientation were considered. Matrix and fiber induced cryogenic of different varieties of carbon fiber and epoxy was characterised by Timmerman et al. [31], a method of microcrack quantification was also conducted. Thermal expansion of honeycomb sandwich panels was studied by Chen et al. [32]. The study involved the comparison of experimentally measured thermally induced deformation with the classical laminate theory for layered structures. Grimsley et al. [33], studied the advantages of layered hybrid composite liquid hydrogen fuel tank, over the conventional sandwich

structure with CFRP facesheet and kevlar-based core fuel tanks. The study involved reducing the permeation of the cryogenic fuel from entering the core region due to microcracking in the polymer matrix. Lee et al. [34] studied the mechanical behaviour and failure process during compressive and shear deformation of the honeycomb composite at elevated temperatures. They observed that the compressive and shear strengths reduce when tested at the higher temperature. Tompkins [35] studied the change in crack density with an increase in the thermal cycles, followed by conducting the tensile test to determine the tensile strength and tensile modulus of CFRP based solid laminates. It was found that the tensile properties reduced with the increase in thermal cycles. Weinhold et al. [36], investigated the change in flatwise tensile properties of honeycomb sandwich structure at elevated temperatures and found slight degradation in material properties. Most researchers have conducted a thermal fatigue test [37] and correlated the degradation of mechanical strength with thermal cycling [38-43] for solid laminates. The studies involving careful microscopic observation of the microcrack growth and its effect on mechanical properties, particularly for composite honeycomb structures, is still a void. This work is primarily focussed on quantifying the microcrack growth and determining the mechanical strength degradation of composite honeycomb sandwich structure after subjecting the material to thermal fatigue at both cryogenic and elevated temperatures. Finite element analysis was also performed to predict the possible location of microcracks formation and compared with experimental observation.

## 2.2   Material

The sandwich composite material under study is made of a 6.4 mm (0.25 inch) thick Kevlar honeycomb core (cell size 3mm, core wall thickness 46 micrometer and density 48 kg/m$^3$), with two 0.25 mm thick facesheets (stacking sequence - [( ±45),(0/90),core]$_S$), made of Cyanate Ester based resin reinforced with a high modulus 5 harness satin woven carbon fiber. The facesheets were cured separately at a laminate level and then bonded to the core using a modified epoxy film adhesive cured at 120 ºC.

## 2.3   Sample Preparation

The samples were cut from a large panel as shown in Figure 2.1a using a diamond saw cutting machine to the size of 25.4 mm by 25.4 mm (1 in by 1 in). The sample size was decided considering the size requirement for flatwise tensile test and limitation on the thermal cycling setup size. Figure

2.1b shows the sample after preparation and Figure 2.1c shows the size of the sample in comparison with a scale.



(a)                        (b)                        (c)
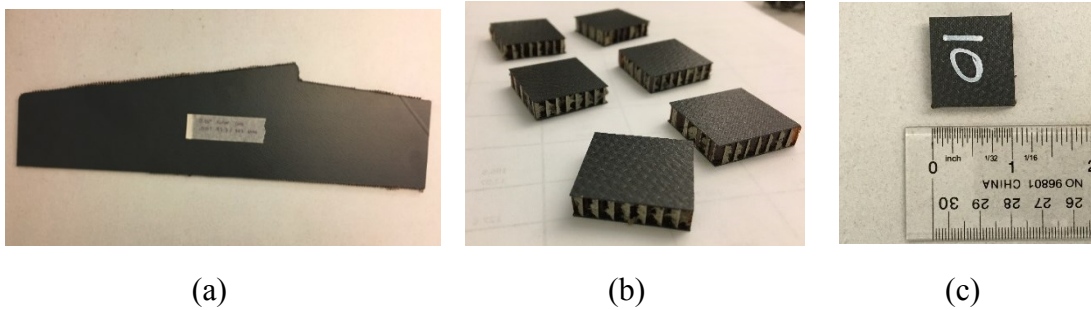
*Figure 2.1: Images of material under study (a) sandwich panel, (b) sample cut from the panel, (c) size comparison of the sample with the scale.*

Two edges of the sample were polished using Mecatech 234™ polishing machine [44]. Polishing the cross section of the samples for microscopic observation was a very crucial step. Unlike solid laminates, the sandwich structure with thin facesheet loses material quickly if polishing is done using sandpaper with grit size in the range of 200 to 300 microns which corresponds to rougher surface finish. As a result, first polishing was done at 600-micron grit size sandpaper which was followed by 9-micron and 3-micron grit size surface finish.

## 2.4    Surface under observation

Due to the orthotropic behaviour of the material under mechanical or thermal loading, the samples are observed on two crossed sides. Ribbon direction side (side 1 as shown in figure 2.2) where the cut was made along the direction of the ribbon and transverse ribbon direction (side 2 as shown in Figure 2.2) where the cut was made in the direction perpendicular to the ribbon direction.
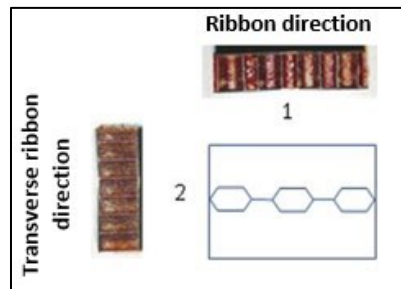


*Figure 2.2: The geometry of the sample with views of ribbon and transverse ribbon direction cross- section.*

## 2.5 Experimentation

### 2.5.1 Test plan

The test plan was developed to subject the samples to the thermal fatigue which is experienced by the structures used in spacecraft. A spacecraft during its operation is exposed to elevated temperature environment roughly around 185 °C because of incident sun rays, and cryogenic environment which is close to -185 °C during the eclipse region of the orbit. One complete cycle comprises of one cold and one hot conditioning. The cold case is achieved by dipping the sample in Liquid Nitrogen (LN2) to reach cryogenic temperature, and the hot case is achieved by placing the samples in a convection oven to get to the higher temperature.

### 2.5.2 Dry-out Test

The sandwich coupons tend to absorb water from the environment and the water used during cutting and polishing stage. Both processes utilize water for lubrication to prevent carbon particle from circulating in the air, which could be harmful. A dry out test was carried out by holding the sample to a temperature of 70 °C and measuring the mass of the sample at an interval of 30 minutes, the results from the test are shown in figure 2.3.
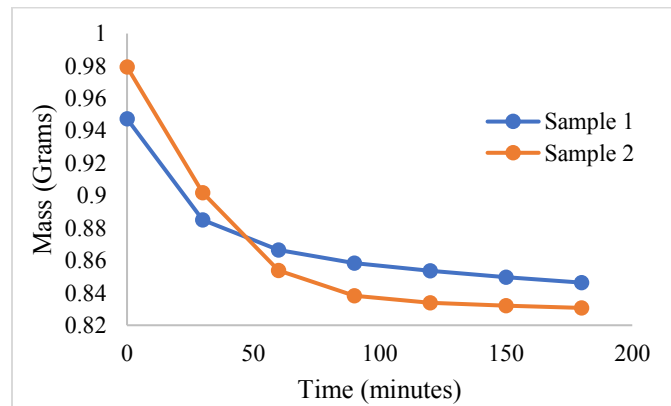


*Figure 2.3: Change in mass with time.*

It is interesting to notice that there is a significant drop in the mass of the sample after 30 minutes of holding at 70 °C, which indicates absorption of water during polishing and cutting process. The dry out test was continued for 3 hours to measure the variation in mass, the change was not significant after 30 minutes of drying. The sample cross-section was observed using the ProgRes® Speed XT core microscope camera [45]. Some minor microcracks were observed after drying in the adhesive region as shown in Figure 2.4.
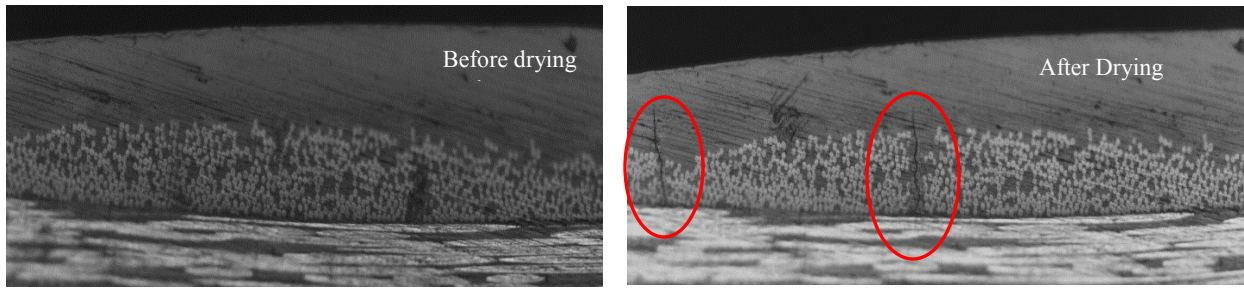
*Figure 2.4: Microcrack formation after sample drying by holding at 70 °C.*

### 2.5.3 Thermal cycling

Two samples were used for thermal cycling. To monitor the temperature change with respect to time and to make sure the samples reached desire temperature during the thermal cycle, a reference sample (spare sample) was used with a thermocouple mounted at the centre of the core by means of a 0.5 mm hole drilled from one of the free edges. The hole was then covered with clay to prevent liquid nitrogen from entering the center of the sample.

The change in temperature of the sample subjected to both cryogenic and hot conditioning is shown in Figure 2.5a. The samples were submerged in liquid nitrogen (LN₂) using a metallic meshed container as shown in Figure 2.5b, to allow direct contact of $LN_2$ with the samples. It took close to 20 seconds to reach -194 °C from room temperature. The samples were then brought to room temperature and placed in the convection oven as shown in Figure 2.5c, to expose the samples to an elevated temperature of 150 °C. Based on the thermocouple readings, it took about 15 minutes to reach the desired temperature.



(a)                              (b)                              (c)
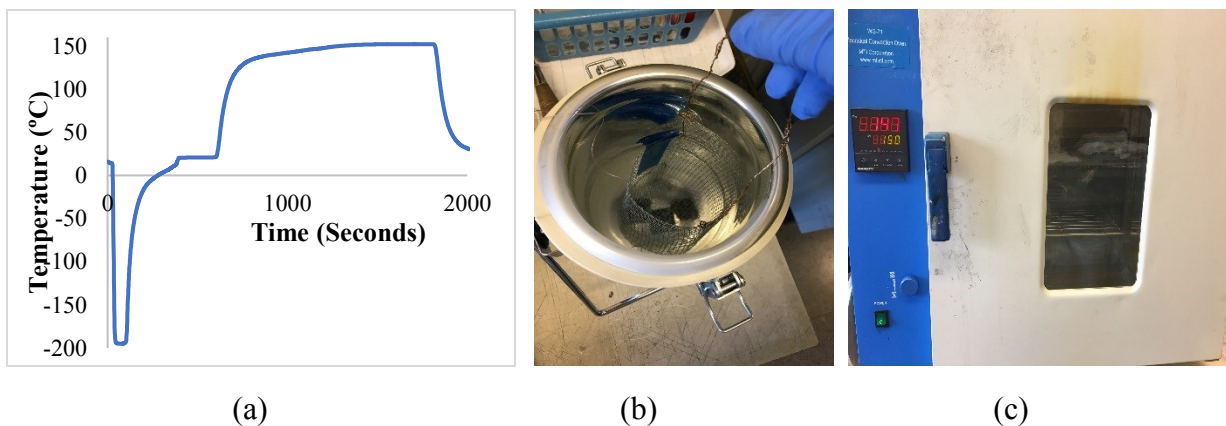
*Figure 2.5: (a) Temperature history captured by the thermocouple, (b) Samples dipped in LN₂, (c) samples placed in the oven.*

## 2.6  Microscopic Inspection

The microscopic inspection was done after every half cycle until 10 thermal cycles, to inspect how the samples would react to the different thermal environment, cryogenic and elevated temperature. As discussed in the test plan section, the samples were inspected for microcracks on two sides, ribbon direction side and transverse ribbon direction side. Figure 2.6 (a) indicates various constituents of a sandwich structure. No voids were observed in the facesheet as the laminate was thin. However, some voids were found in the adhesive region.

## 2.7  Microcrack formation

Microcracks were observed under the microscope at room temperature. Cracks started to form right from the first thermal cycle, at the adhesive region, between the facesheet and core. Microcrack growth/formation was clearly observed after every half a cycle until the $10^{th}$ cycle. Old cracks would grow in length and new cracks would form after subsequent cycles. Cracks form longitudinally along the facesheet and core interface. However, after the $10^{th}$ cycle cracks growth and formation was relatively slow, so the inspection interval was increased to 3 and then subsequently to 10 cycles. Figure 2.6 (a) to 2.6 (f) indicates crack growth up to 60 thermal cycles.

(a)



(b)



(c)

(d)



(e)



(f)
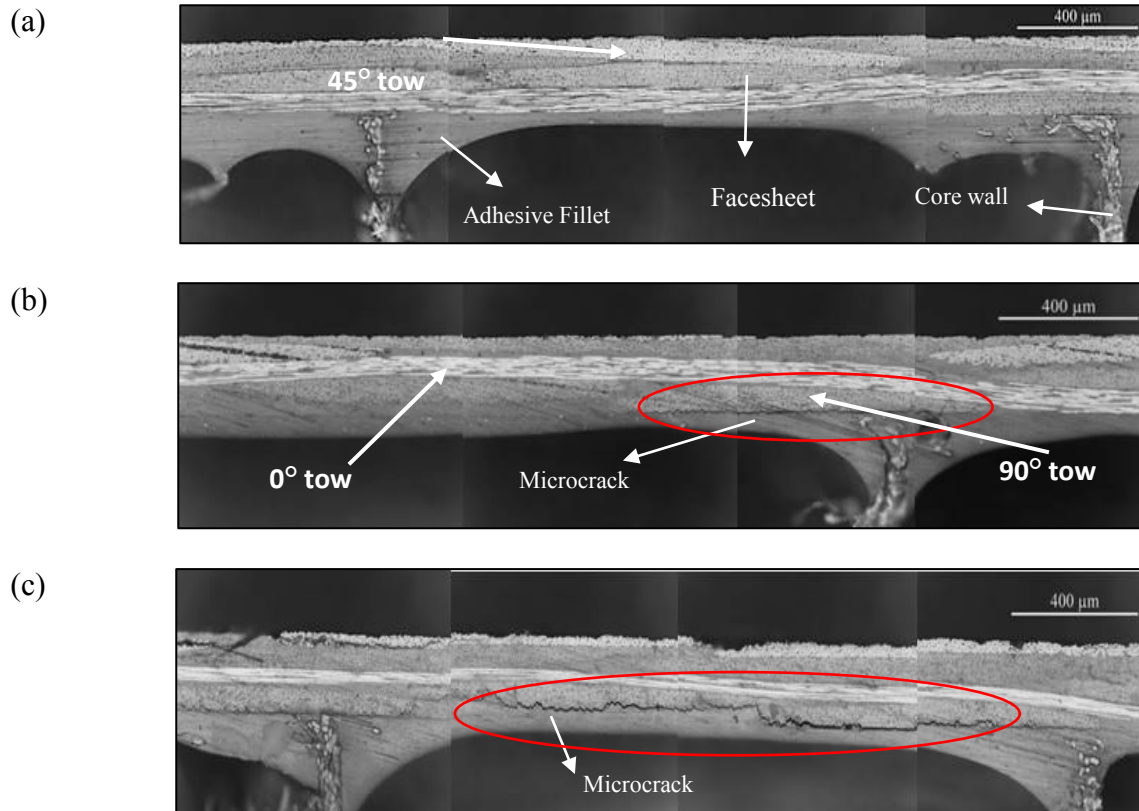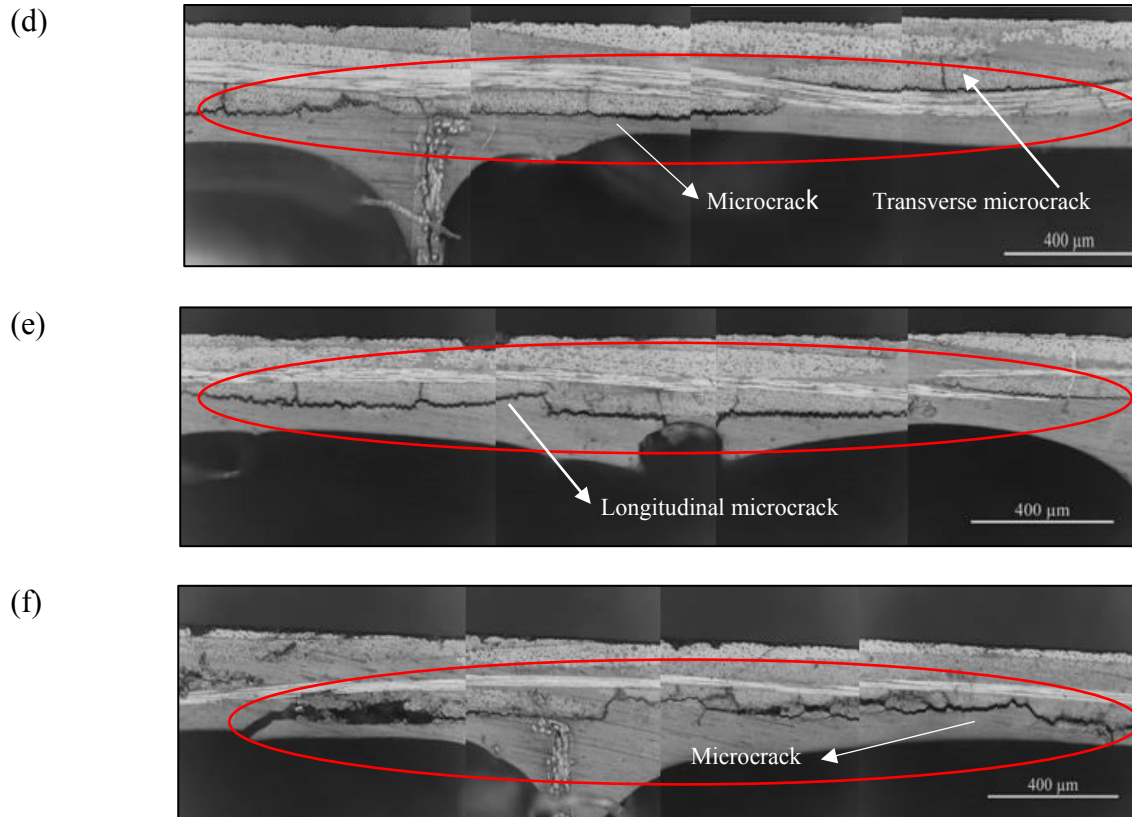


*Figure 2.6: Stitched microscopic images taken after sample preparation, a) No thermal cycle, b) after 10 thermal cycles, c) after 20 thermal cycles, d) after 30 thermal cycles, e) After 40 cycles, f) After 60 cycles*

## 2.8 Types of Microcracks

Two types of microcracks were observed in the cross section of the sample, longitudinal and transverse. Longitudinal microcracks appeared between facesheet and core interface where the trend is the same in both the samples under observation. Figure 2.6a and 2.6b shows the co-ordinate system of the tow orientation. The contact region between 90° tow and adhesive is more prone to longitudinal microcracking, compared to 0° tow and the adhesive contact region. As can be seen, cracks initiate at the adhesive and 90° tow interface, reach the 0° tow and adhesive interphase, then jump to the adjacent 90° tow. After 10th thermal cycle, small cracks join to form larger cracks, as shown in Figure 2.7.
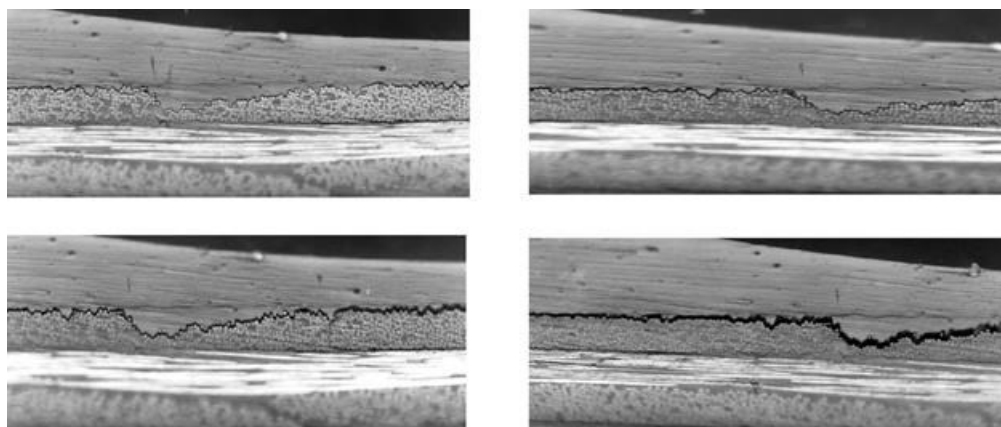
*Figure 2.7: Small cracks combining to form larger cracks.*

Transverse microcrack surfaced after 30 thermal cycles, primarily in 90° tow as shown in Figure 2.8. After 30 thermal cycles, longitudinal cracks start appearing between the plies inside facesheets. However, the microcracking is more on the core side of the sandwich and not on the mold or bag side.
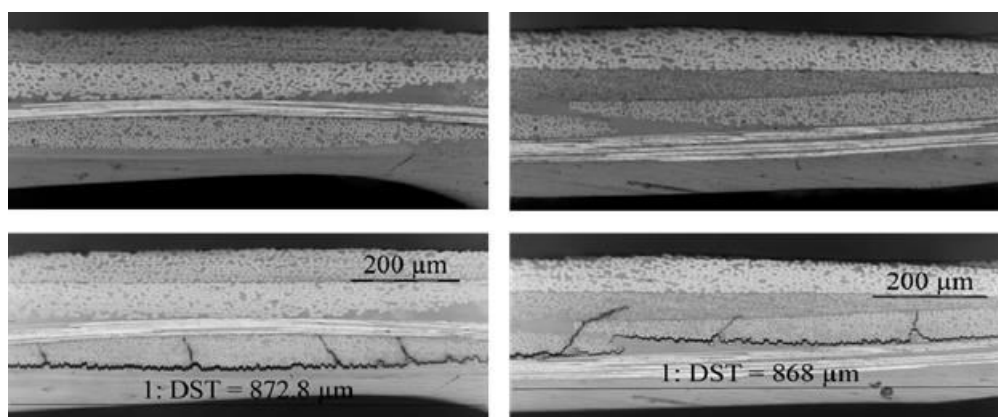


*Figure 2.8: Growth of transverse cracks.*

## 2.9    Mechanics of microcrack formation

Based on the experimental observation of microcracks under an optical microscope at room temperature, two factors that primarily affect microcrack formation/ propagation are moisture and difference in Coefficient of Thermal Expansion (CTE) of the respective constituents used in the composite sandwich structure. Microcracks first surfaced after drying at 70° C for three hours, as observed in Figure 2.4a and 2.4b. This is mainly due to the expansion of trapped moisture during the drying process [46]. The cracks would form in cryogenic cycle and grow in high temperature part of the cycle. The growth was progressive after 2 cycles in both high and low-temperature

exposure. Longitudinal cracks in the form of delamination form mainly due to the difference in the CTE of laminate and adhesive. Transverse microcrack appeared at higher thermal cycles mainly due to the difference in CTE of fiber and resin [47-48].

## 2.10  Quantification of micro-cracks

### 2.10.1  Crack density

Crack density gives an idea about the number of cracks with the observed area under consideration as shown in Figure 2.9. Samples were inspected for microcracks on two sides, as described in the test plan. The area under observation was confined to the facesheet and core-facesheet interface region, as the cracks would occur in that area. Crack density is calculated using Equation 2.1. The area under observation corresponds to the area of the facesheet cross-section multiplied by a factor of two as each side comprises of two facesheets.

$$\text{Crack density} = \text{Number of cracks/ Area} \qquad [2.1]$$
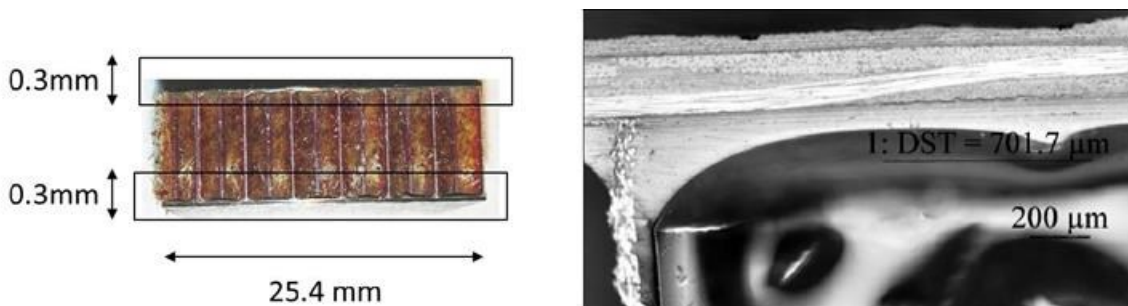


*Figure 2.9: Area under observation.*

The change in crack density with the increase in cycles is shown in Figure 2.10. For the first 10 cycles observations were done after every half a cycle, then the observation interval was increased. It is interesting to notice that the crack density starts increasing in the ribbon direction side, right from the first thermal cycle, compared to the transverse ribbon direction side of the sample where cracks start appearing only after 4th thermal cycle. The initial observed increase in microcrack in the ribbon direction side of the sandwich sample is mainly due to more positive CTE of the core in the ribbon direction side compared to the transverse ribbon direction side [32]. A steep increase in the number of crack formation is observed up to 6th thermal cycle followed by saturation. The number of microcracks remains constant between 6 and 12 thermal cycles, but as it will be shown later, the crack length increases. Increase in number of microcracks is again observed between 12

to 20 thermal cycles, this is due to the formation of new longitudinal microcrack's between the ply's and the adjacent tows, as shown in figure 2.6d and 2.6e at higher cycles. After 30 thermal cycles, it can be observed from the above plot that the difference between the crack density, in both ribbon and transverse direction side reduces, indicating the equal number of cracks on both ribbon and transverse ribbon direction by the end of the 40th cycle.
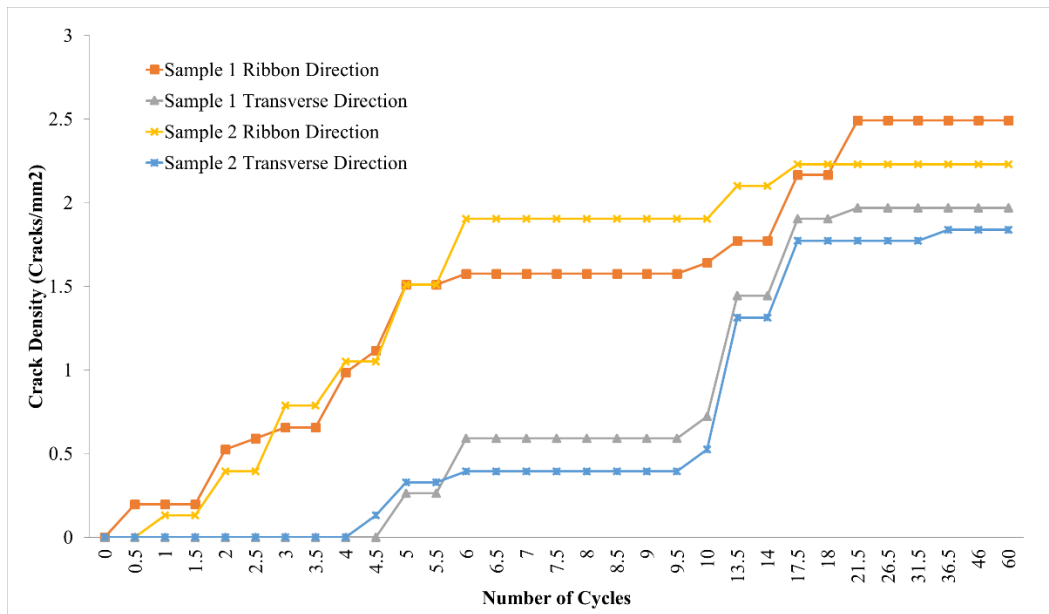


*Figure 2.10: Change in crack density with the increase in thermal cycles.*

### 2.10.2 Crack Length

Crack length refers to the summation of all the microcrack length observed on the sample cross section. Figure 2.11 indicates the change in crack length with the increase in the number of thermal cycles, up to 60 cycles. Even though the crack density tends to saturate between the 6 to 12 cycles, and between 20 to 30 cycles, crack length significantly grows until 40 cycles. After 40 cycles, the strain energy induced by the thermal environment might not be sufficient to influence the formation and propagation of more microcracks. As a result, the crack growth saturates after 40 thermal cycles.

20
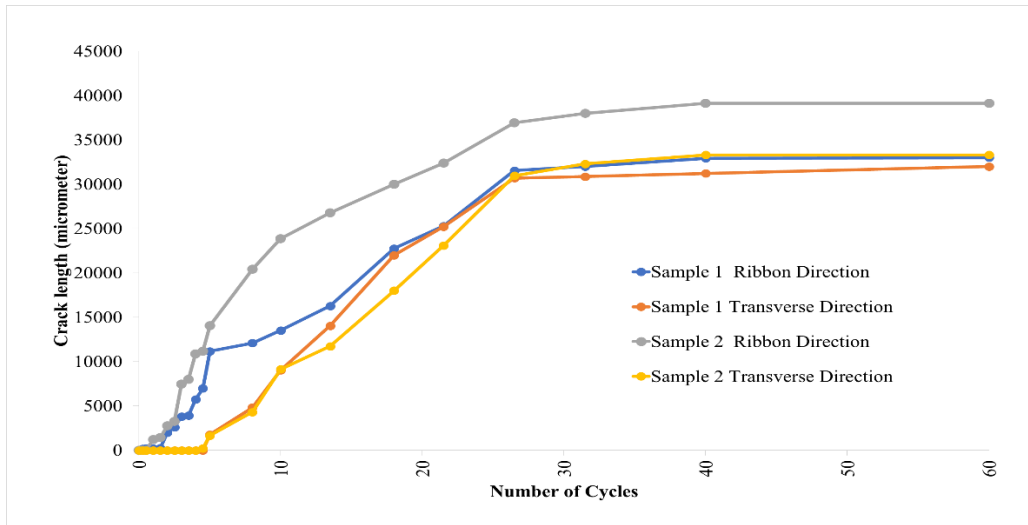
*Figure 2.11: Change in crack length with the increase in thermal cycles.*

### 2.10.3 Normal distribution of individual crack lengths

Individual crack lengths were measured at the cross section during microscopic observation, using PROGRES speed XT core software. Figure 2.12 shows the normal distribution of crack lengths of four test samples at the end of 10 and 50 thermal cycles. After 10 cycles, it is interesting to notice that the majority of the crack length of individual cracks are between 250-500 micrometres. The cracks taken into consideration are longitudinal microcracks. The similar observation was done after 50 thermal cycles. It can be noted that the majority of individual crack length range at the end of the 50th cycle is between 500 to 1000 micrometers.
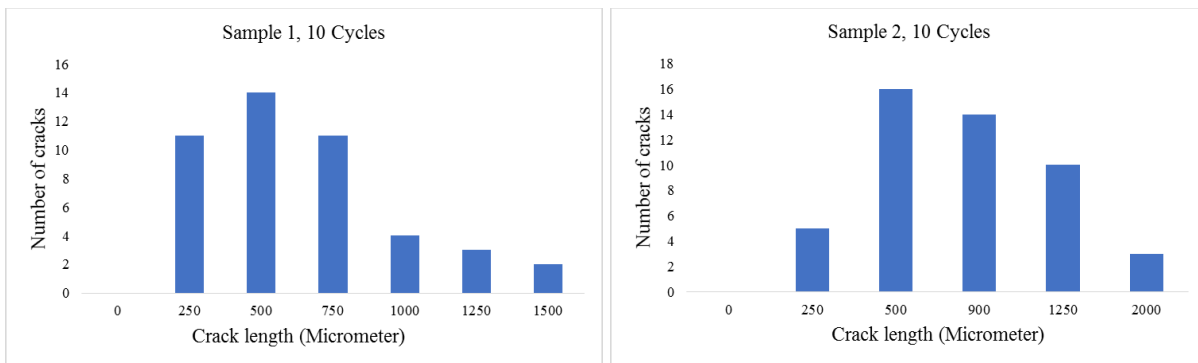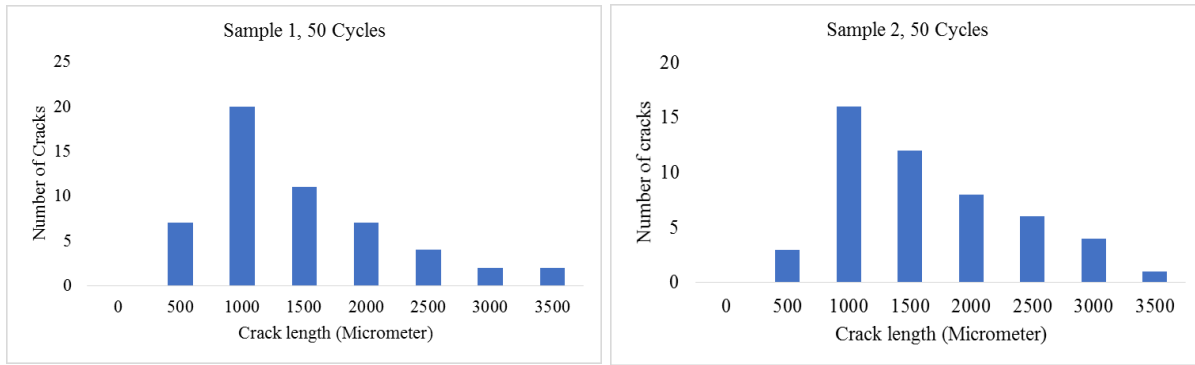
*Figure 2.12: Normal distribution of crack lengths after 10 and 50 thermal cycles.*

## 2.11   Mechanical Test

The mechanical test was performed to determine the effect of microcracks on the mechanical strength of the sandwich structure. Based on microscopic observation, most microcracks appeared in the adhesive zone between the core and facesheet interface which directly affects the interfacial bonding strength between them. Flatwise tensile test was selected. The test involves the application of tensile load perpendicular to the facesheet planes by bonding the facesheet to the loading blocks. The test was conducted as per ASTM standard C297 [48], which is a test method to determine the flatwise tensile strength between the core to facing bond. To make a correlation between microcrack density, number of thermal cycles and the sandwich tensile strength, flatwise tensile test was conducted on the test coupons after subjecting the specimens to 0, 10, 20, 30, 40 and 60 thermal cycles.

### 2.11.1  Sample preparation and test setup

Samples were prepared as per the recommendations from ASTM C297 standard. As the core cell size was 3 mm, the corresponding specimen size was 25.4 mm by 25.4 mm. These criteria influenced us, to decide the sample size of 25.4 mm by 25.4 mm even for thermal cycling. Samples were carefully cut to the dimensions mentioned above, using a diamond saw cutting machine, such that the edges were straight from top to bottom and the dimensional tolerance is within ± 0.5 mm. Testing samples with small damages and higher dimensional deviation may lead to a significant difference in the strength values. Surface preparation for both sample and loading block is essential part of the test. An excellent adhesion is very essential to have an acceptable mode of failure.

For the flatwise test the only acceptable failure modes are the one that fails within the sample and not on the adhesion between the sample and loading blocks. The samples and loading blocks were initially cleaned using ethanol to remove surface greases and dust particles. The sample's facesheet surface was lightly sanded with 320-micron grit size sandpaper for better adhesion with the loading blocks. To bond the samples to the loading blocks a two-component, high-performance aerospace grade adhesive from LOCTITE, named Hysol 9392 Qt aero [49], was used. Figure 2.13 (a) shows the alignment jig used to make sure both the loading blocks are aligned well, to avoid eccentricity. The adhesive was cured in the oven with the attached alignment jig, as per the manufacturer recommended curing cycle. After complete curing is achieved the sample along with the loading fixture are then clamped to the tensile machine, to conduct flatwise tensile test. The tests were performed on displacement control mode with the rate of 0.5 mm/min and the force values are recorded at a sampling rate of 3 readings per second.



(a)                                                                              (b)

*Figure 2.13: a) Sample alignment jig, b) sample under flatwise tensile loading.*

### 2.11.2 Flatwise tensile test results and failure modes

The load at failure corresponds to the ultimate flatwise tensile strength was recorded for different samples as shown in Table 2.1. The flatwise tensile strength is calculated using the equation below.

$$F_z^{ftu} = P_{max} / A \qquad\qquad [2.2]$$

where $F_z^{ftu}$ is ultimate flatwise tensile strength in MPa, $P_{max}$ is ultimate force prior to failure in Newton and A is the cross-sectional area in mm$^2$. The results are shown in table 2.1.

*Table 2.1: Bond strength and failure modes of the samples after testing.*

| Sample No | Cycles | Ultimate failure load (N) | Ultimate flatwise tensile strength (MPa) | Failure Mode |
| --- | --- | --- | --- | --- |
| 1 | 0 | 3130 | 5.005 | Adhesive failure of core-facing adhesive |
| 2 | 10 | 2895 | 4.638 | Adhesive failure of core-facing adhesive |
| 3 | 20 | 2679 | 4.28 | Adhesive failure of core-facing adhesive |
| 4 | 30 | 2164 | 3.46 | 97% Adhesive failure of core-facing adhesive, 3 % facing tensile failure. |
| 5 | 40 | 2236 | 3.56 | Adhesive failure of core-facing adhesive |
| 6 | 60 | 2138 | 3.42 | Adhesive failure of core-facing adhesive |

Samples after failure were removed from the fixture and examined for identification of failure modes (Figure 2.14). The failure was mainly due to the adhesive failure which happens at the interface between the fillet ends and the facesheets and left hexagonal impression on the facesheets, as shown in Figure 2.14. It shows that the bonding between the adhesive and facesheets was not strong which can be related to the fact that those sandwich panels are made using co-bonding techniques. It is interesting to see the layer of adhesive retained in samples that are subjected to thermal cycling, as shown in Figure 2.14b. This retention of adhesive is due to the microcracks formed between the facesheet and adhesive. The sample tested after 20 cycles underwent interfacial failure in the adhesive region on both sides of the core. Some of the samples tested after the 30th cycle had some per cent of facing tensile failure, this is mainly due to the microcracks formed between the plies at higher cycles, as shown in Figure 2.14d. Samples tested after 30 thermal cycles would show partial debonding between facesheet and the adhesive layer, on either side of the core. After 30 thermal cycles, the change in the magnitude of mechanical strength at failure is very marginal. This result correlates with the variation of microcrack length and density with respect to thermal cycles which also indicates saturation after 30 thermal cycles. The width of the adhesive fillet retained, in the samples tested after 60 thermal cycles as shown in Figure 2.14f is more, compared to the samples tested without any thermal cycling as shown in figure 2.14a, indicating the presence of microcrack.
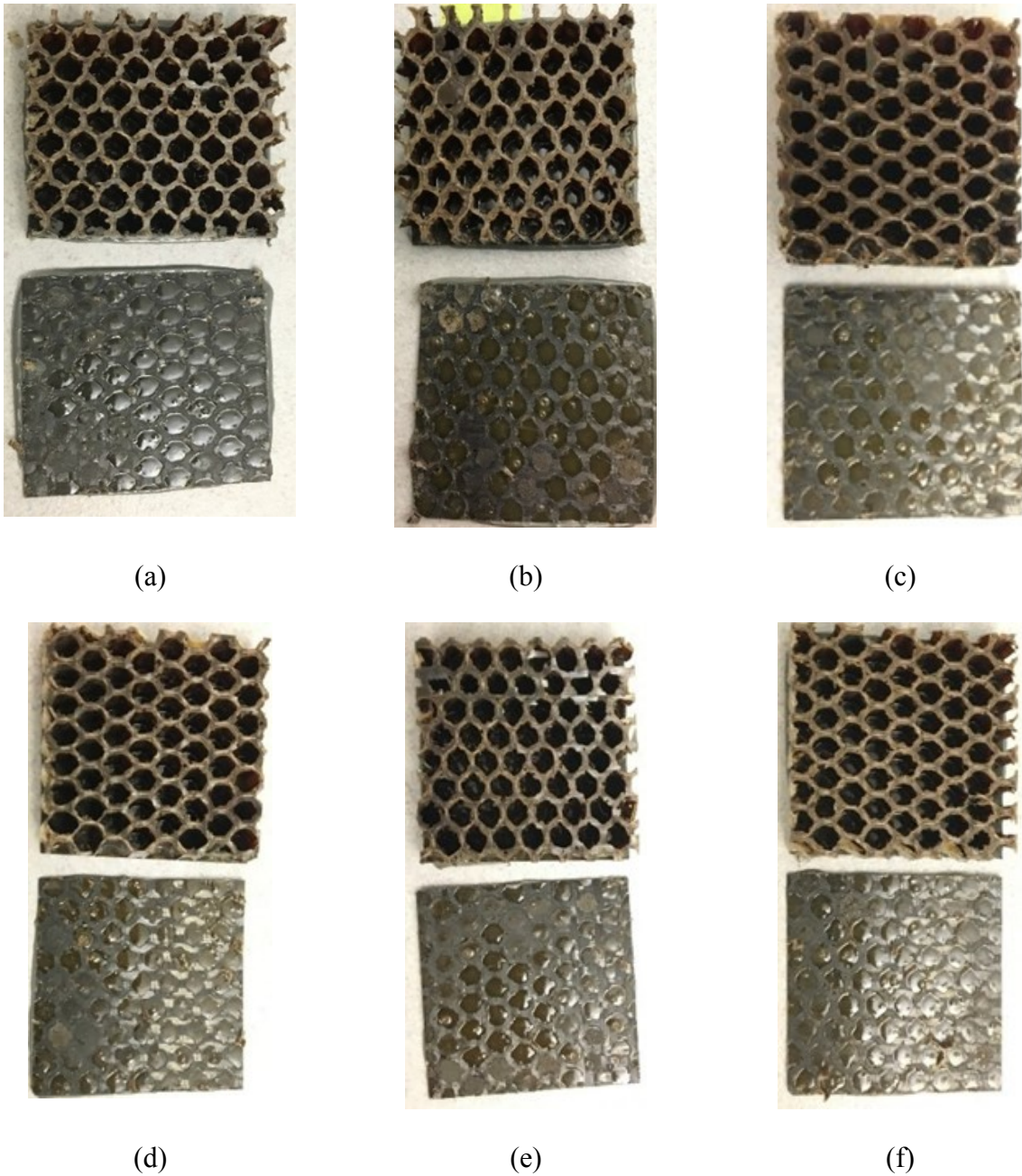
*Figure 2.14: Images indicating residue of adhesive on the core side of the sample, a) no thermal cycle, b) after 10 thermal cycle, c) after 20 thermal cycles, d) after 30 thermal cycles, e) after 40 thermal cycles, f) after 60 thermal cycles.*

## 2.12 Correlation between crack area and mechanical strength

The crack area was defined and calculated by multiplying the total crack length on two perpendicular edges of the adhesive-facesheet interphase, on one side of the core. The cracks between the adhesive-facesheet were considered and the cracks within the facesheet were omitted, as the failure mainly occurred in that region. Figure 2.15 shows the variation of the crack area and

flatwise strength for different samples thermally cycled from zero to 60. It is interesting to note from the plot that both crack length and strength value saturates around 30-40 cycles. It seems there is a linear relationship between the crack area and strength with the number of thermal cycles up to saturation point.
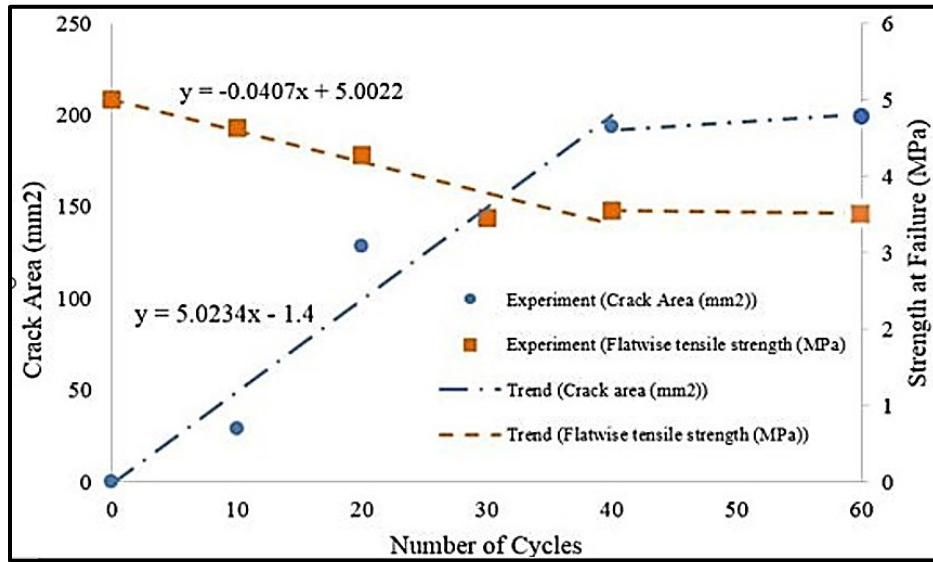


*Figure 2.15: Change in the crack area and mechanical strength at failure with the increase in thermal cycle.*

## 2.13    Finite Element Analysis

In the previous sections, formation and propagation of microcracks were studied and its effect on the mechanical property was investigated. The approach was quantitative in nature. The major factor that affected the formation of stress was interlayer stress, due to the composition of the sandwich structure under study. To qualitatively simulate the stress induced within the facesheet, adhesive and core interface, a three-dimensional finite element analysis was conducted on the sandwich construction subjected to the thermal loading. The simulation was conducted to observe the stress [51-52] and strain component development of the constituents under temperature changes using the finite element method. Details of the study and results are presented in this section.

### 2.13.1  Geometric model

Finite element analysis of the composite sandwich structure was done in ANSYS™ workbench [50]. A three-dimensional 25.4 mm by 25.4 mm area sandwich structure with 6.25 mm thick core was modelled in CATIA V5™ software that replicates the sample used in the experiment. The

elements of sandwich construction such as embedding matrix, carbon tow, adhesive film and core (made by combining aramid paper ribbon), was separately modelled and assembled as shown in figure 2.16. The elements were modelled by referring to various microscopic images. Each facesheet was made of resin envelope and fiber tow. As the geometry of weave is complex with overlapping yarns, a simplified 3-dimensional model of 5 Harness Satin (5HS) yarns, running parallel (warp) and perpendicular (weft) to each other were modelled. The thickness of each facesheet was 0.125 mm. Width and thickness of the tow were set to 1.2 mm and 0.1 mm respectively. The distance between adjacent tows was set to 0.06 mm.
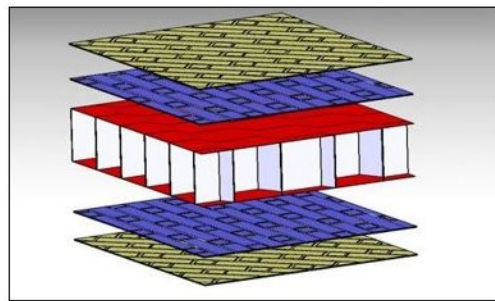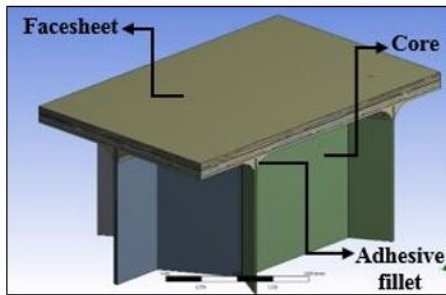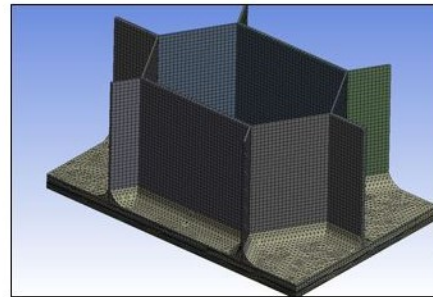


*Figure 2.16: (a) Exploded view of the assembly, (b) Representative volume element, (c) Meshed geometry.*

### 2.13.2 Model Elements Mechanical Properties

The properties of different sandwich constituents are summarized in table 2.

*Table 2.2: Material properties of the respective constituents used in the sandwich structure.*

| Sl. No | Material name | Density (g/cm³) | Coefficient of Thermal Expansion (C⁻¹) | Elastic Modulus (GPa) | Poisson's Ratio | Specific Heat (Cal g⁻¹ K⁻¹) | Tg °C | Tensile strength (MPa) |
|---|---|---|---|---|---|---|---|---|
| **1.** | Resin | 1.19 | $43*10^{-6}$ | 3 | 0.3 | 1.2 | 254 | 80 |
| **2.** | Carbon tow impregnated with resin | 2.1 | $\alpha_x = -1.8*10^{-8}$ $\alpha_y = 2.4*10^{-5}$ $\alpha_z = 2.4*10^{-5}$ | $E_x=155$ $E_y=12$ $E_z=12$ | 0.248 0.0193 0.0193 | 0.9 | - | 3830 |
| **3.** | Kevlar paper | 1.4 | $-2*10^{-6}$ | 3.1 | 0.36 | 1.4 | - | - |
| **4.** | Adhesive film | 1.2 | $75*10^{-6}$ | 5 | 0.2 | 0.2 | 148 | 7.1 |



*Figure 2.17: Co-ordinate system of resin impregnated tows oriented at 0, 90 and +/- 45 degrees with respect to global coordinates.*

As the mechanical properties of the resin impregnated tows are transversely isotropic, the local coordinates of the tows were changed with respect to the orientation of the tows as shown in Figure 2.17. The direction of the red arrow in the coordinate system represents the fiber direction. The

local coordinates of the resin, adhesive and core wall were not changed as they are isotropic materials. The assigned material properties are independent of temperature, as the idea behind conducting FEA is to make a qualitative correlation with experimental findings. To make a quantitative study of the stress and strain level induced at cryogenic temperature, one must use the mechanical properties corresponding to the temperature.

### 2.13.3 Boundary conditions and constraints

The CAD (Computer-aided design) model was imported to ANSYS$^{TM}$ workbench. Material properties mentioned in table 2.2 were assigned to the respective elements of the sandwich construction. Bonded contact was selected as the means of contact between the surfaces of sandwich structure constituents. The model was meshed by the auto mesh command option. Due to the intricacy of the model, mesh size was selected such that the skewness of the element is low as shown in Figure 2.16c. Initially the mesh size was set to 0.3 mm, however, the mesh quality was satisfactory. To achieve convergence, mesh size was reduced by 0.05 mm in every mesh iteration. The mesh size was finalized to 0.1 mm as the stress results tend to converge. As shown in figure 2.18b, the mesh elements of matrix and tows show good connectivity which is necessary to achieve the stable transfer of thermal loads. For the embedding matrix, 3D Solid-186 tetrahedron shaped elements were chosen. For tows and core wall, 3D Solid-186 hexahedron shaped elements were chosen. The resulting meshed geometry comprised of 2,14,895 elements and 5,15,557 nodes. Representative volume element (RVE) was considered for analysis to reduce the number of nodes which would in turn reduce computational time.

The RVE considered was approximately 4 mm by 10mm in the area and 3.25 mm thick. Only half the thickness was considered, as the structure is symmetric about the midplane of the core. The rationale behind choosing this size was to make sure all the geometric features of the sandwich construction was considered. The size selected represents a smallest repetitive unit of the sandwich panel.

Steady state condition was chosen as the thermal environment. The cryogenic thermal induced stress is maximum. As the stress induced is proportional to the thermal strain, which is a function of the difference in process temperature and the stress-free temperature. When the samples are dipped in liquid nitrogen, the induced stresses between the constituents are maximum, compared to the elevated temperature exposure. As a result, the cryogenic environment was chosen to study

29

the stress induced between the layers. The simulation was run and equivalent von misses stress and strain results were extracted.

## 2.14    Results

A region from the samples which contain microcrack developed during the experiment (Figure 2.18 (a)) was selected to compare with FEA results. The model cross section related to this sample configuration is shown in Figure 2.18 (b). The stress and strain developed during the cooling stage are shown in Figure 2.19. It is interesting to note that the stress and strain distribution in the adhesive region, particularly in between the facesheet and adhesive interface is higher compared to the stress distribution in the other part of the sample. This result correlates with the experimental microscopic observations as shown in Figure 2.18, where the microcracks are between facesheet and the adhesive layer.



(a)



(b)
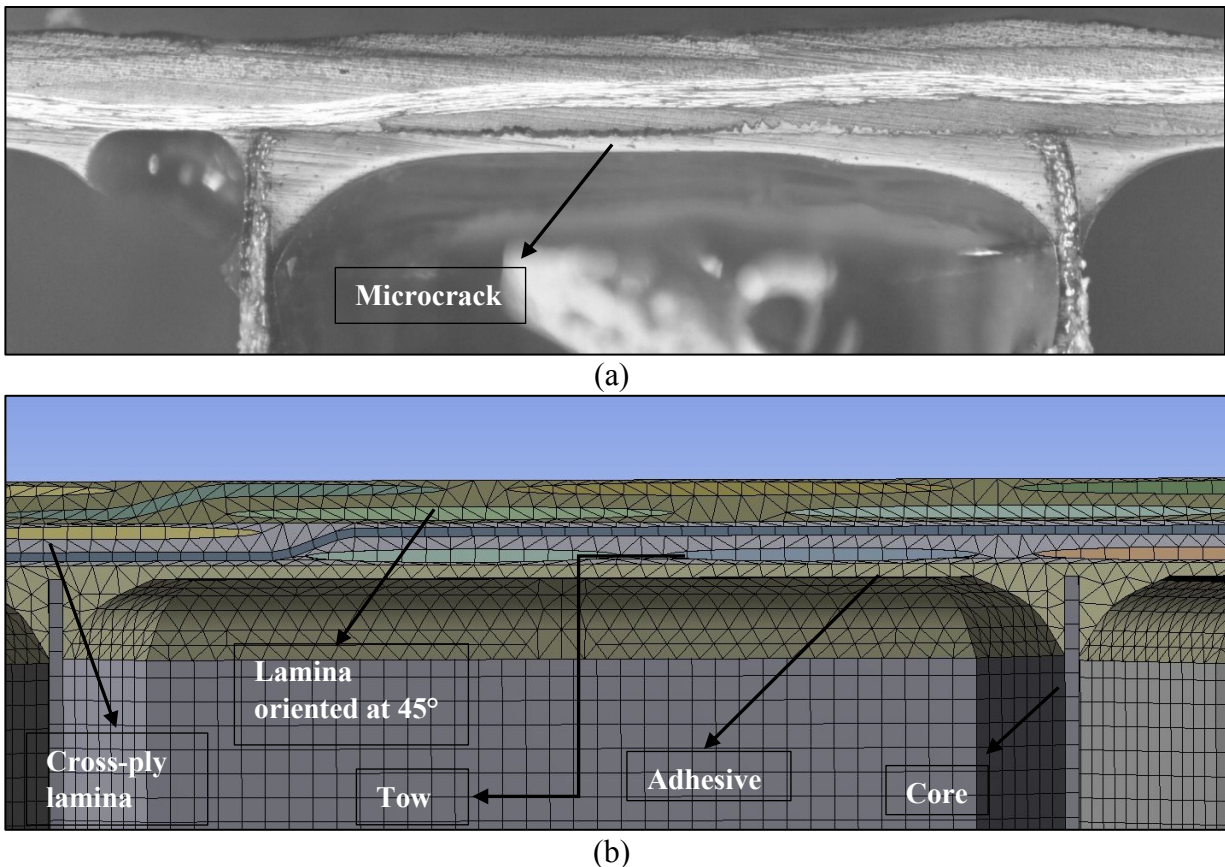
*Figure 2.18: (a) Microscopic image of the sample with microcrack, (b) Meshed closeup view of the facesheet, adhesive layer and core.*
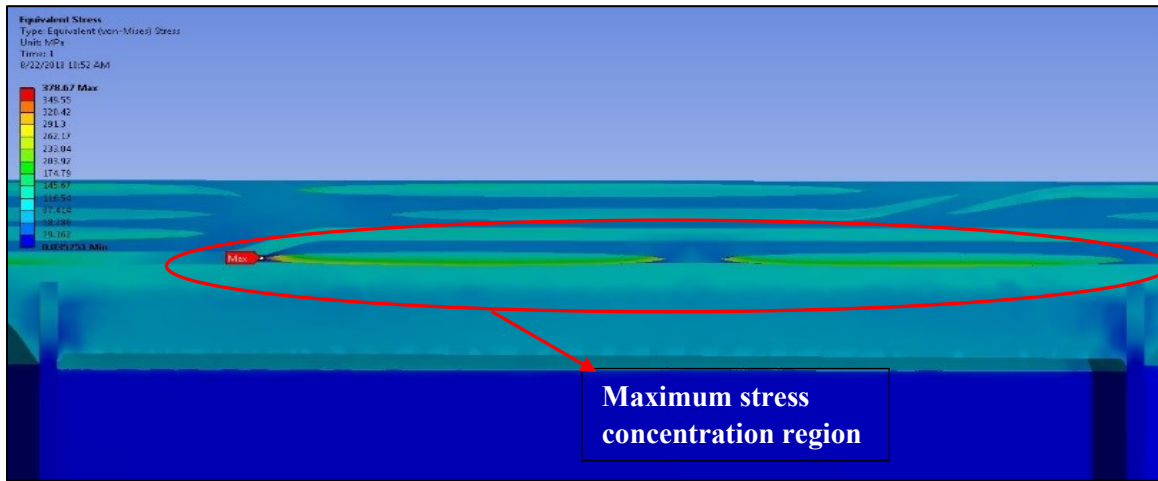
(a)
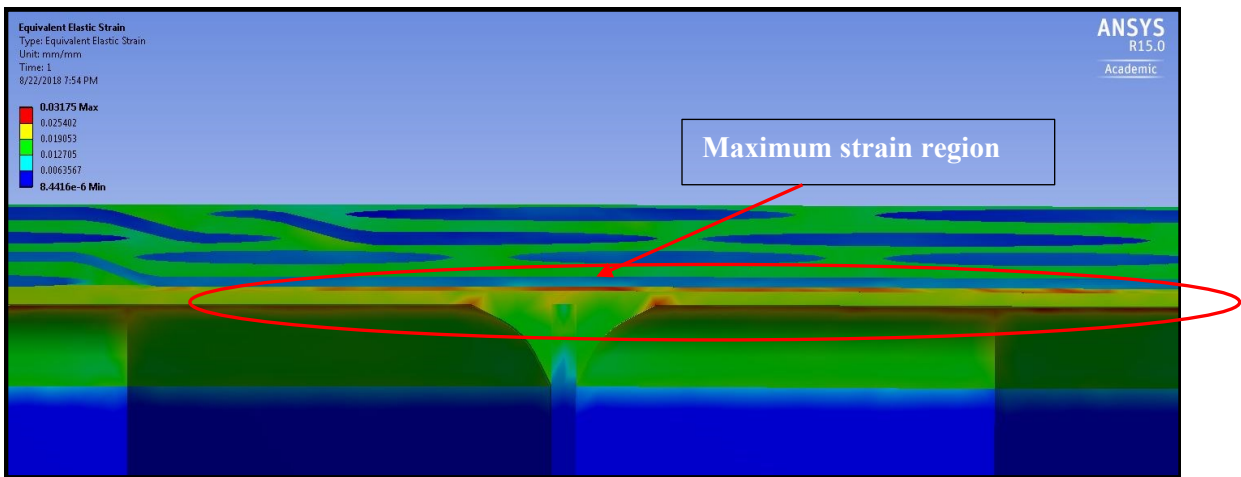


(b)
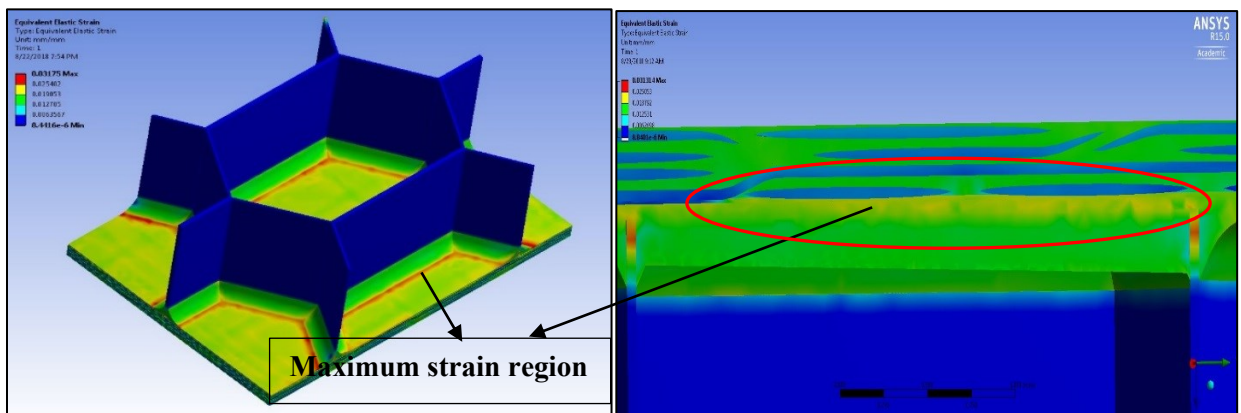


(c)

*Figure 2.19: Structure exposed to the cryogenic thermal environment (a) stress variation, (b) and (c) strain variation.*

The analysis accurately predicts the regions where initial microcracks formed. As per the result scale, the red colored regions are the ones with high magnitude. After close observation of the results from the cross-section, it can be clearly noticed that the magnitude of stress and strain reduces as it approaches the outer surface of the skin, away from the core. Figure 2.19 (b) shows fibers in blue contours which corresponds to very low strain, this is in good agreement with the theory. The resin impregnated fibers have a negative coefficient of thermal expansion (near zero). The tows tend to resist any movement under the influence of environmental temperature, whereas the resin and adhesive tend to expand and contract freely.

## 2.15    Conclusions

A methodology to study the effect of thermal cycling and microcracks formation and propagation on composite honeycomb sandwich structure was developed. The test plan was made to conduct the thermal cycle which involves subjecting the test samples to space like thermal environment. Then cycles were repeated to observe crack formation and growth at the cross section under the microscope followed by mechanical testing. The formation of cracks was significant at the early stage of thermal cycling, then tends to saturate due to the stress relieving after the $40^{th}$ cycle. It was observed that the majority of microcracks are formed at the interface of the adhesive and the composite facesheets which should be related to the co-bonding process during the sandwich manufacturing. Results from flatwise tensile test indicate a considerable reduction in bond strength with the increase in thermal cycles up to 40 cycles. After that, no significant reduction in flatwise strength was observed that shows the damage has already been done.  Therefore, it is not required to run hundreds of thermal cycles to investigate its effect on the sandwich mechanical properties. Based on the simulation results of the sample exposed to the cryogenic environment, a qualitative analysis indicated the higher magnitude of stress at the adhesive region than the other parts of the sample which aligns with our microscopic observation results. Therefore, the finite element simulation can be used to identify the possible location of stress concentration and microcrack formation and therefore to optimize the ply orientation and stacking sequence to reduce the thermal stresses.

# Chapter 3: Performance of Composite Sandwich Structures under Thermal Cycling

## Abstract

This paper presents a laboratory-based test procedure to study the effect of thermally induced microcracks on the performance of laminated sandwich structure by subjecting the material to cryogenic temperature as low as -170 ºC and high temperature as high as 150 ºC. A simple non-contact set-up using liquid nitrogen was developed to subject the material to low temperature. The set-up can provide a cooling rate of 24 ºC/min up to -170 ºC. Samples were subjected to the elevated temperature of 150 ºC inside an oven. A correlation was made between the number of cycles and flatwise mechanical strength after quantifying the microcracks. It was observed that the crack formation gets saturated at about 40 cycles, avoiding the need to conduct more thermal cycles. Microcrack formation both at the free edge and middle of the laminate was observed. The crack density at the middle was comparatively less than the ones found on the free edges. Results for non-contact cooling and direct nitrogen contact cooling were compared. Microscopic inspection and flatwise test shows a significant difference between contact and non-contact cooled samples. Flatwise tensile strength for non-contact cooled samples reduces by 15%, compared to the contact cooled samples which recorded a 30% reduction in bond strength. A 3D finite element analysis (FEA) was conducted on the geometry that resembles the cross-section of the samples tested, to predict the observations from the experiment. Good correlation between experiment and analysis was observed.

## 3.1    Introduction

Composite sandwich structures have replaced traditional metallic space structures in the past three decades, in a bid to reduce weight, resulting in reduced launch cost. A satellite during its operational cycle is exposed to harsh environment involving, high vacuum, ultraviolet radiation, atomic oxygen, and extreme temperature conditions, as a result of spacecraft's orbit around the earth. The fluctuating thermal environment poses some serious challenges on the composite sandwich material used in spacecraft, in particular, the resistance to microcracking.

---

Composite sandwich construction comprises of a core, which is available in various forms such as honeycomb and foam, sandwiched between facesheets that are available in the form of a metal sheet or carbon fiber/ glass fiber reinforced polymer (CFRP/ GFRP). It is primarily used for structural applications subjected to flexural loads. The composite material in the form of solid laminates and sandwich structures are used in spacecraft. Sandwich structures are used as antenna reflectors and support structures for various subsystems in spacecraft. One of the most common types of defect that arise due to thermal cycling during the spacecraft's operational cycle is microcracking. This is a very critical issue in composite sandwich structure as they possess higher geometric and material anisotropy compared to solid laminates. Due to the coefficient of thermal expansion mismatch, microcracking occurs at the laminate level, in case of the solid laminates and between laminate and core for the sandwich structures [53]. The longitudinal and transverse microcrack which is a result of thermal cycling causes deterioration in mechanical properties including strength. Grimsley et al., [33] described one such example of failure due to microcracking. A liquid hydrogen tank made of sandwich CFRP material failed the validation test, when the outer skin and core separated from inner skin, due to the microcracking of the polymer matrix in the sandwich inner skin.

A.J Hodge [54] studied the evaluation of microcracking in two carbon fiber epoxy-based matrix composite cryogenic tanks. The microcracking characteristics of two different cryogenic tanks were evaluated by conducting the tensile test at room and cryogenic temperature and followed by microscopic observation at the cross section after failure. T. L. Brown [55] studied the effect of layer thickness, orientation, matrix and fiber type, on the formation of microcrack. Gupta et al. [43] studied the effect of thermal cycling on solid laminates. The crack formation was monitored by means of its occurrences at voids and void-free areas using a microscope. It was noticed that the microcracks grow both around voids and void-free areas. With the increase in the number of cycles, microcrack growth is faster around void compared to the void-free areas. Timmerman et al. [31] conducted thermal cycling on symmetric carbon fiber/epoxy laminates. The study indicates that the laminates comprising of fibers with higher tensile modulus and linear coefficient of thermal expansion had higher crack density. Results from microscopic observation at the cross section also indicate that microcracking was significant only in first ten cycles and then tend to saturate. Richard [56] and Stucky [57] studied the effects of long-duration space exposure on the mechanical properties of a set of carbon fiber reinforced resin matrix composites. The long

duration exposure facility (LDEF) incorporated a spacecraft carrying 86 experiment and about 10,000 samples were studied. The spacecraft was launched by the space shuttle and ejected into the low earth orbit. The LDEF lasted for six years and then recovered. The recovered samples were subjected to a set of experiments such as visual observation, weight loss determination, cross-sectional examination of panel integrity and mechanical testing. Superficial erosion of the resin rich surface by atomic oxygen and microcracks through the thickness of the laminates were some of the primary observations made. David et al., [58] conducted experiments to evaluate the bonding and sealing performance of sandwich structures meant for cryogenic tanks. The author performed the flatwise tensile test on the sandwich structure made of different combinations of core and facesheet materials. The adhesives to bond the core and the facesheets were PR 1664, EA 9394, Crest 3170, FM-300 and HT 435. The tests were conducted at room temperature after subjecting the samples to the elevated and cryogenic temperatures. Cracking and popping sounds were heard when the samples were dipped in liquid nitrogen for cryogenic conditioning. Of all the adhesives used, HT 435 performed better. It was interesting to note that a certain set of samples where FM 300 adhesive was used performed better after cycling at the elevated temperature. It was suspected that the post-curing could be the primary reason for the higher bond strength.

During the literature study, it was found that most experiments involved submerging of test samples in liquid nitrogen for cryogenic conditioning. As a result, samples experience thermal shock. Materials used for cryogenic fuel tanks experience this condition. However, this method may not be ideal to study the effect of low-temperature environment on space structures that are not subjected to thermal shocking. For example, composite honeycomb panels used in the primary and secondary structure of the spacecraft. This article is focussed on studying the mechanical property of composite honeycomb sandwich structure subjected to the lower rate of cooling. The other objective is to define a methodology to make a correlation between the presence of crack and its influence on the mechanical properties. Finite element analysis FEA is conducted to predict experimental observations.

## 3.2    Materials and Manufacturing

The sandwich composite material under study is made of a 6.4 mm (0.25 inch) thick Kevlar honeycomb core (cell size 3mm, core wall thickness 46 micrometer and density 48 kg/m$^3$), with two 0.25 mm thick facesheets, made of Cyanate Ester based resin reinforced with a high modulus

5 harness satin woven carbon fiber. Each facesheet comprised of two laminas. The outer most lamina was oriented at the 45º angle with respect to ribbon direction of the core, and the inner lamina was oriented at 0º angle. The facesheets were cured separately at a laminate level and then bonded to the core using a modified epoxy film adhesive cured at 120 ºC.

## 3.3    Coupon preparation

Coupons were cut from a large panel using diamond saw cutting machine to the size of 25.4mm by 25.4mm area. Care was taken to make sure edges were straight from top surface to bottom surface of the panel. Two edges of the sample were polished using a polishing machine. Ribbon direction side (side 1 as shown in Figure 3.1) is where the cut was made along the direction of the ribbon and transverse ribbon direction (side 2 as shown in Figure 3.1) is where the cut was made in the direction perpendicular to the ribbon direction.
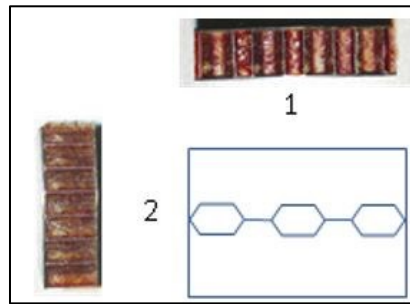


*Figure 3.1: Geometry of the sample with views of ribbon and transverse ribbon direction cross-section.*

Using lower grit size sandpaper that corresponds to courser surface finish resulted in wearing of material, as the facesheet was thin. As a result, polishing was done with sand paper of 600-micron grit size sand paper which was followed by 9-micron and 3-micron grit size surface finish.

## 3.4    Test Plan

The test plan was made (Figure 3.2) to study the effect of thermal cycling on the formation of microcracks. Two samples were prepared. Both ribbon direction and transverse ribbon direction edges were observed under the optical microscope at 20X resolution. Thermal cycling was initiated by cold conditioning the samples using a non-contact cooling process explained in the next section of the report. After cold conditioning, the samples were observed for microcracks followed by hot conditioning using a convection oven. Again, microscopic observation was conducted. One thermal cycle comprises one cold and one hot conditioning. This process of observing samples at

every half cycle was conducted until 10 thermal cycles. Furthermore, microscopic observation was conducted after every three cycles until 20 thermal cycles and then the observation interval was increased to five and ten cycles, as the crack growth was not significant.
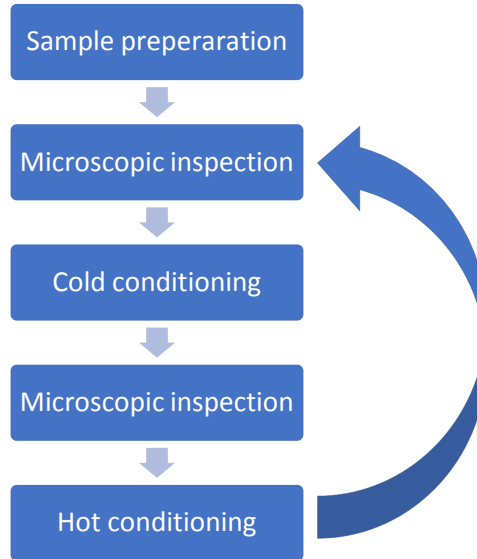


*Figure 3.2: Test plan of thermal cycling.*

## 3.5    Test setup

A test setup was developed in-house to cold condition the samples at a slower rate of cooling. Most of the work done in the past [38] involved direct dipping of samples in liquid nitrogen ($LN_2$) as a representation of materials exposed to space like cryogenic environment. However direct dipping of samples in $LN_2$ produces a thermal shock load which may not be representative of spacecraft structures environment conditions in eclipse region of the orbit. Efforts were made to create a setup which exposes the sample to the slower rate of cooling as shown in Figure 3.3.

As shown in Figure 3.3 (a), the setup comprises of a stainless-steel container placed in the $LN_2$ bath that encloses the samples. As a result, samples are not directly in contact with $LN_2$ as there is a blanket of air surrounding it. The mode of heat transfer is convection which facilitates the slower rate of cooling. One reference sandwich sample was placed in addition to samples that were tested. The reference sample comprised of a thermocouple attached to it at the center of the core, by drilling a hole from one of the sides. The thermocouple was connected to a computer operated data acquisition system that records the change in the temperature with time.
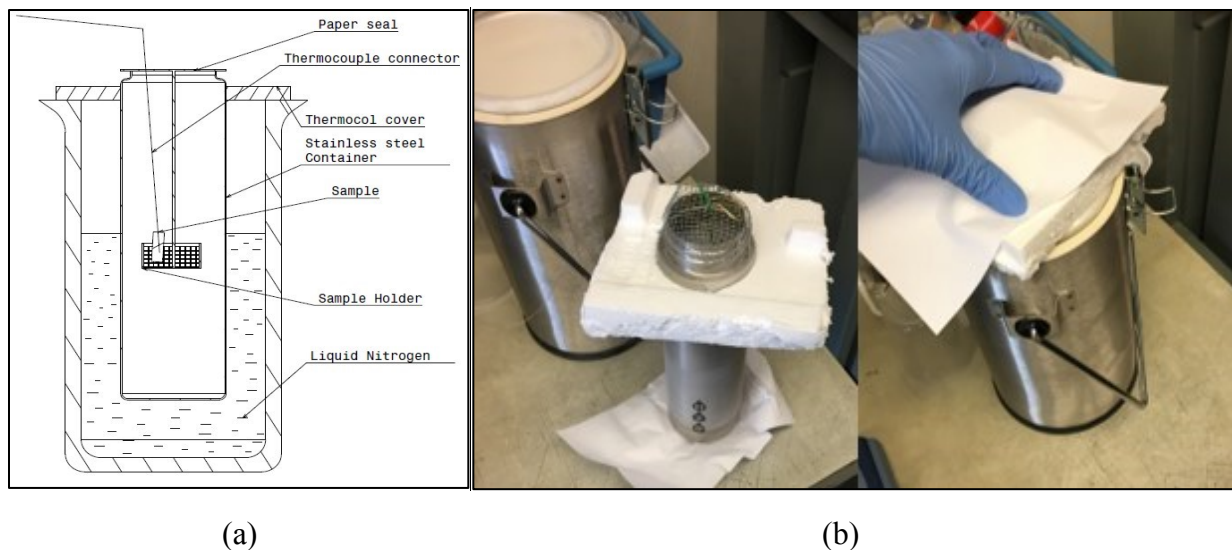
*Figure 3.3: Non-contact cooling (a) Schematic of test setup (b) Actual setup.*

To start the cold conditioning process, the stainless-steel container which housed the samples were inserted in the bath of $LN_2$ and held firmly in position with the help of a thermocol barrier. Hot conditioning was done by placing the test coupons with reference coupons inside a convection oven and temperature with respect to time was recorded in the same manner. Temperature history of a complete thermal cycle is shown in Figure 3.4. It is interesting to notice that a temperature of -170 ºC is reached in eight minutes, in comparison to 20 seconds, in case of cold conditioning by means of direct dipping in $LN_2$.
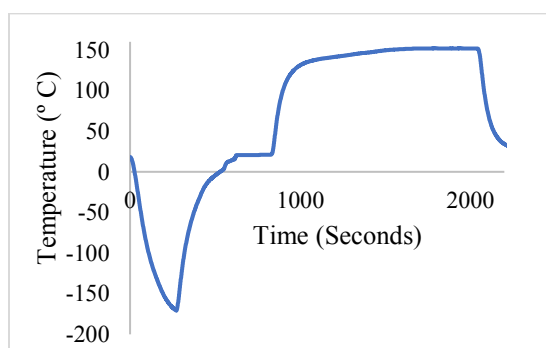


*Figure 3.4: Change in temperature with time.*

## 3.6    Microscopic Observation

As mentioned in the previous section, microscopic observation was conducted on the cross-section on two sides, ribbon and transverse ribbon direction side using the optical microscope. Microscopic images were taken after sample preparation and after subsequent thermal cycles to see the behaviour of crack growth/propagation and compare it with previous cycles. For the first

38

couple of cycles, the inspection was done at every half cycle as the growth in crack formation was significant.

### 3.6.1 Effect of the thermal cycle on microcrack formation

Microcracks were observed right from the first cold conditioning. Figure 3.5 indicates various stages of microcrack growth with an increase in the thermal cycle [59-61]. Most microcracks were longitudinal, in the form of delamination cracks primarily between facesheet and adhesive interface. They were formed below the 90º tow and then propagate until they reach to the 0º crimp section and then jump to the corresponding 90º tow adjacent to it. Some transverse microcracks were observed after 30 thermal cycles in 90º tow.

(a)



(b)



(c)



(d)

(e)



(f)
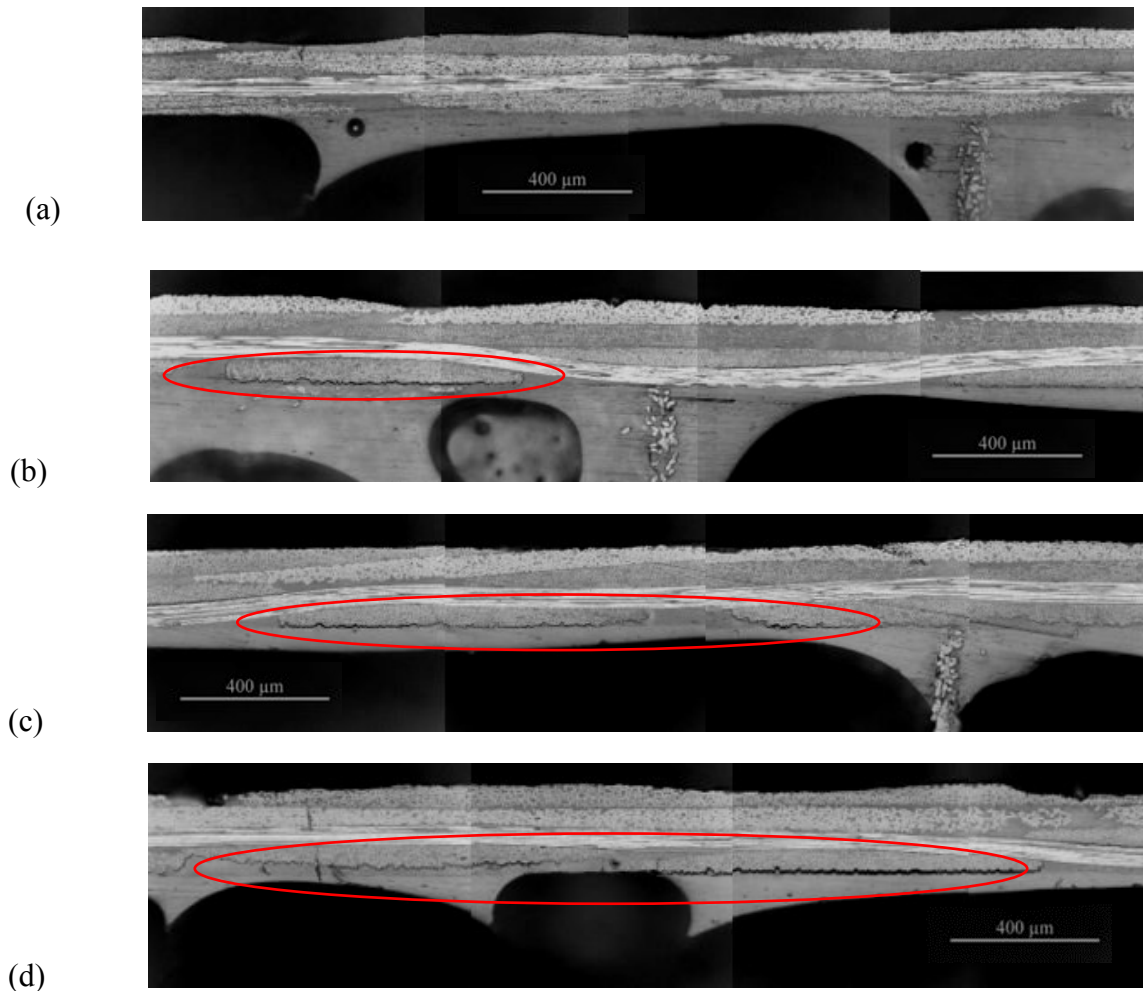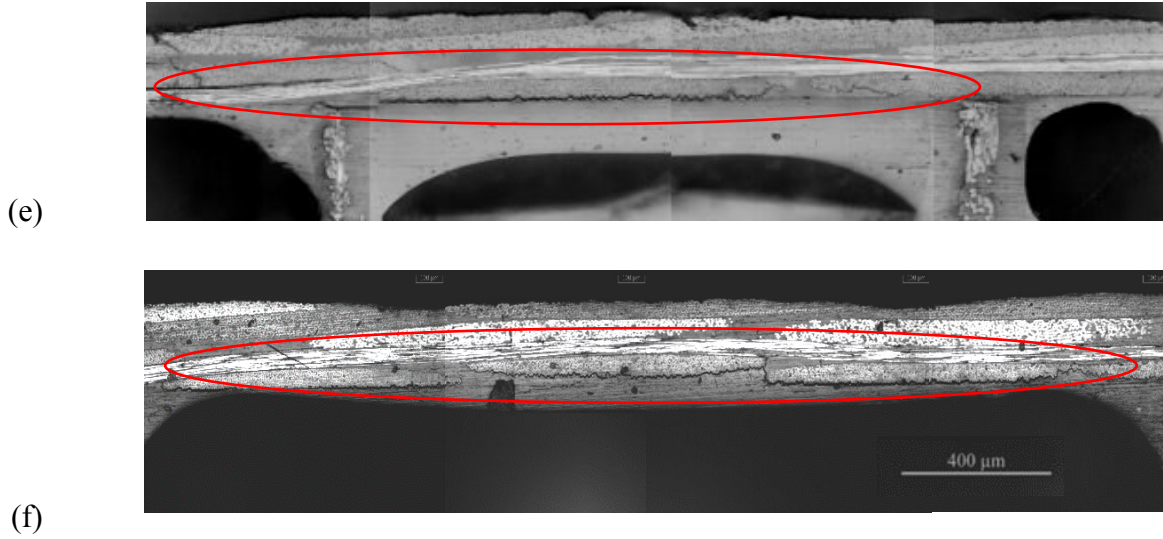
*Figure 3.5: Microscopic image taken after sample preparation, a) No thermal cycle, b) after 10 thermal cycles, c) after 20 thermal cycles, d) after 30 thermal cycles, e) After 40 cycles, f) After 60 cycles.*

### 3.6.2 Mechanics of microcrack formation

Formation of new microcracks was observed in the cold conditioning part of the cycle as the thermal strain due to the difference in the coefficient of thermal expansion (CTE) is greater in the cold cycle. Stress-free temperature is the cure temperature which was 120 °C (to bond the facesheet and core using adhesive film). The relation between thermal strain $\varepsilon_i$ and difference between process temperature and conditioning temperature is shown in equation 3.1. Hot conditioning influenced the growth of microcracks.

$$\alpha_i = ( A_{jj} N_i - A_{ij} N_j ) / ( A_{ii} A_{jj} - A_{ij}^2 ) = \varepsilon_i / \Delta T \tag{3.1}$$

Equation 3.1 is the linear in-plane hygrothermal expansion coefficient for layered structures [32], where i,j=x,y are the principal directions of laminate. $A_{ij}$ are the in-plane stiffness components, $N_i$ are the hygrothermally induced loads, $\alpha_i$ are the CTE and $\varepsilon i$ are the in-plane strains. Matrix and adhesive have positive and higher CTE compared to the carbon fiber tows which has low CTE. Due to this difference, stress is induced resulting in microcracks. Initially, microcracks appeared more on the ribbon direction side compared to the transverse ribbon direction side. This is mainly due to the more positive CTE in the ribbon direction of the core, compared to the transverse ribbon direction.

40

### 3.7    Cracks Observation at the mid-section

Composite sandwich structures are prone to microcracking on the edges (free surfaces), as the fibers are not constrained. Knowledge of whether microcracks form at the mid-section is still a void. In order to find out the presence of cracks at the mid-section, 40 thermal cycles were conducted on the sample, and a cut was made at the mid-section, as shown in Figure 3.6. The cut section was polished by following the procedure as mentioned in the previous section of the article.
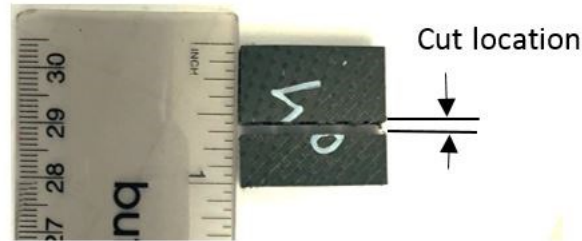


*Figure 3.6: Midsection cut for microscopic observation.*

It was observed that the microcracks were formed at the mid-section because of thermal cycling. The nature of microcracks was like the ones that were found in the previous section. The cracks were longitudinal as shown in Figure 3.7. However, no transverse microcracks were found, and the crack density was comparatively less than the ones found on the free edges.
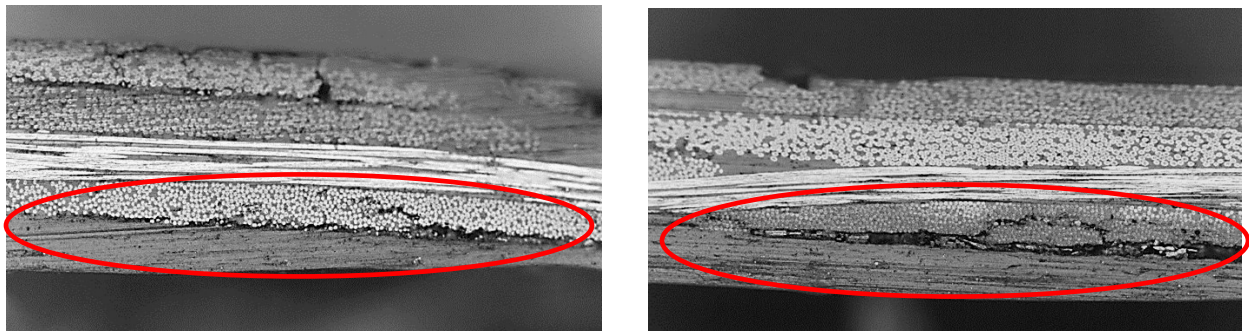


*Figure 3.7: Microcracks observed at the midsection.*

### 3.8    Quantification of Microcracks

After qualitative observation of microcracks, parameters such as crack density and crack length were used to quantify the cracks formation. Crack density is the measure of the number of microcracks per unit area as shown in equation 2.1.
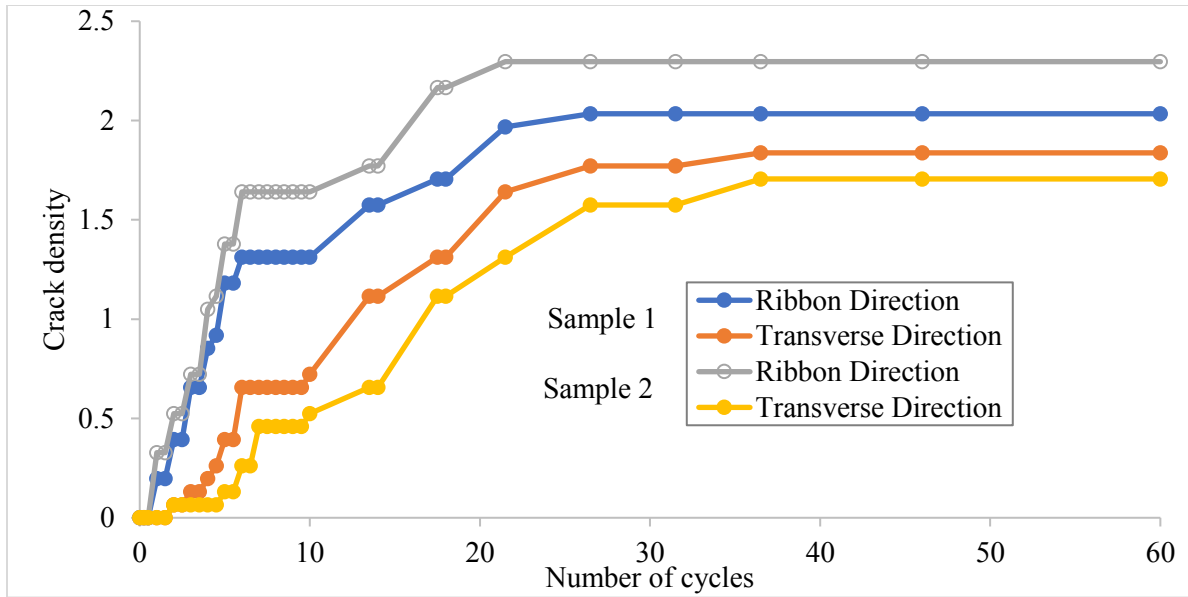
*Figure 3.8: Crack density data of two samples.*

The area under observation corresponds to the area of the facesheet cross-section multiplied by a factor of two as each side comprises of two facesheets (top and bottom). Crack length is the summation of all the cracks in ribbon and transverse ribbon direction side of the respective sample.
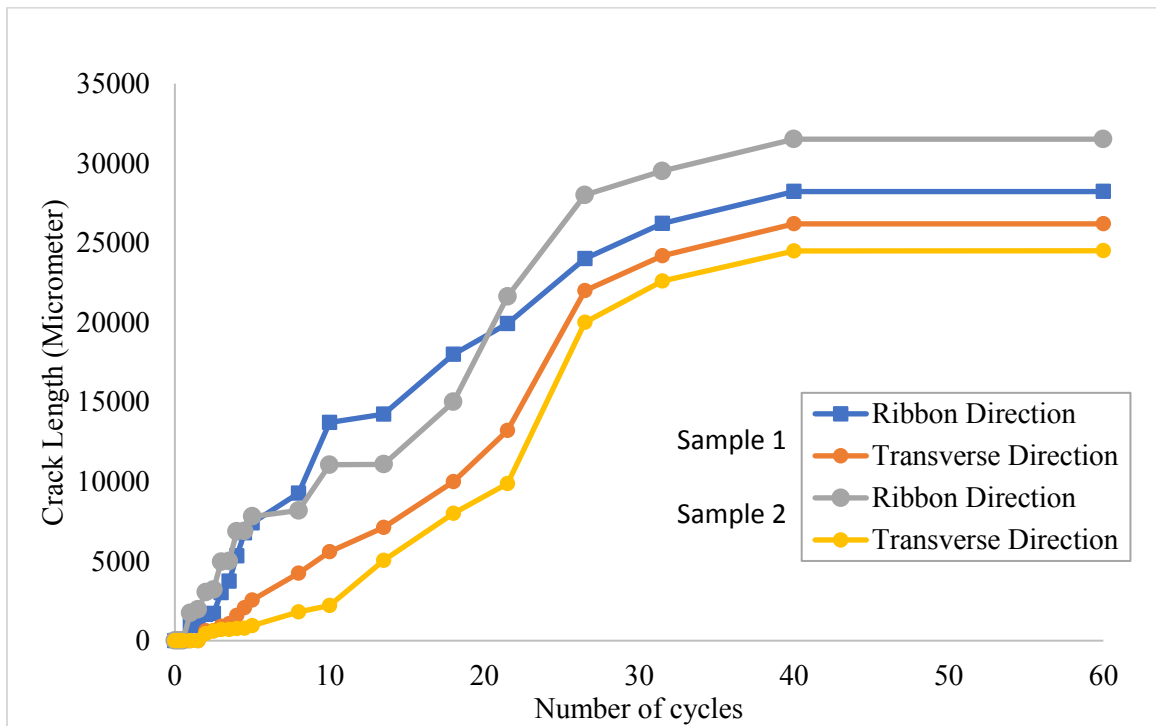


*Figure 3.9: Crack length data of two samples.*

Figure 3.8 shows the crack density in both ribbon and transverse directions for two different samples. Crack length is shown in Figure 3.9.

## 3.9 Observations from the quantification parameters

It can be noticed from crack density plot that the crack numbers steadily increase until the sixth cycle then saturates followed by increase again, between $14^{th}$ cycle to $21^{st}$ cycle. The second round of increase is mainly due to new cracks formed between the tows. The crack density on the ribbon direction side is more compared to the transverse ribbon direction initially. However, at the end of the $30^{th}$ cycle, both values merge, indicating the equal number of cracks on both sides. This is mainly is due to two geometric anisotropy of core that influences higher CTE and contraction in the ribbon direction.

Individual crack lengths were measured and added for each side of the sample, crack length shows similar behavior as crack density. However, increase in length has an upward trend until the $40^{th}$ cycle followed by saturation. It is interesting to note that although the crack density remains constant between the sixth and $14^{th}$ cycle, the crack length increases during that period. In this period of cycling, no new crack is formed, but the existing ones grow. When the system gets to a new stress condition, the new cracks start to form.

### 3.9.1 Normal distribution of crack length

Length of each microcrack was measured using image processing software named ImageJ. The crack lengths were measured initially after 10 cycles followed by second round of measurement after 50 thermal cycles, respectively. A normal distribution of crack lengths was plotted as shown in Figure 3.10. It is interesting to notice that, most cracks were ranging from 250-500 micrometer at the end of 10 thermal cycles.
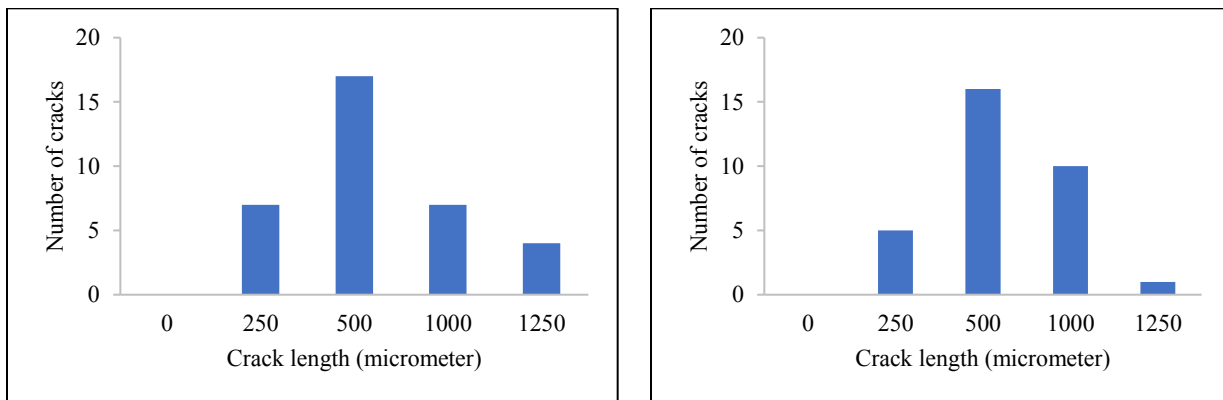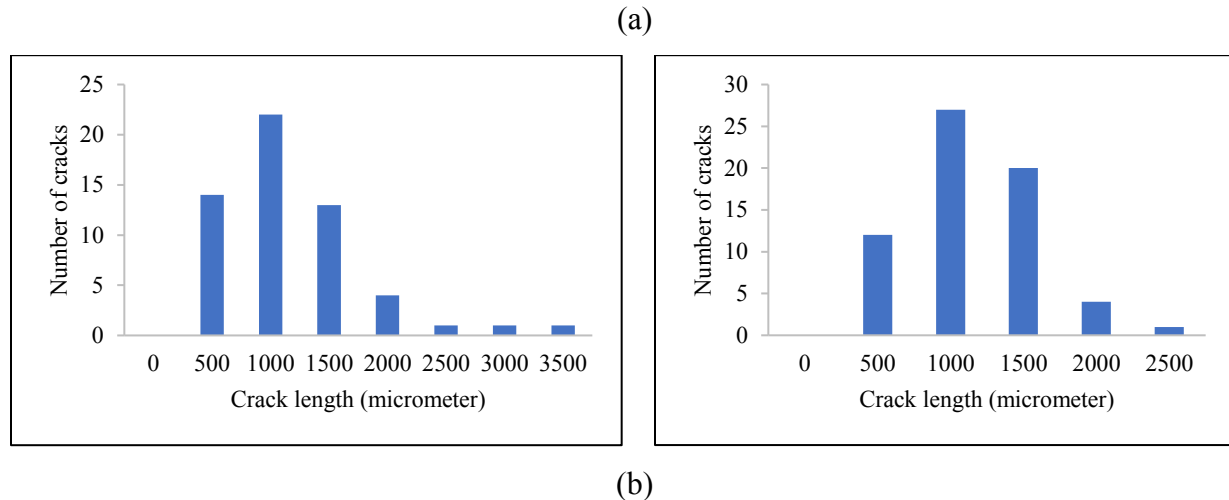
*Figure 3.10: Normal distribution of crack lengths after (a)10 and (b) 50 thermal cycles.*

The measurement of crack length was again repeated after 50 thermal cycles and it was observed that the old cracks had grown in length and new cracks had formed, which resulted in crack length ranging between 500-1000 micrometers.

Since most microcracks were present between the interface of facesheet and core, flatwise tensile test was conducted on the samples. It is the most suited test technique to measure facesheet-core debonding strength. ASTM C297 [48] was followed for sample preparation and sizing guidelines. Surface preparation of sample and loading block is very critical as it effects the bond quality between sample and loading block. Hysol 9392 Qt Aero adhesive was used to bond the sample to fixture. It was a two-part adhesive which required thorough mixing before applying on the fixture.

### 3.9.2   Sample Sizing

The core cell size of the sample size was 3mm. For 3mm cell size the required coupon size was 25.4mm by 25.4mm as mentioned in ASTM C297 standard. Care was taken while preparing the sample to make sure the edges were straight. The adhesive was cured in the oven with the attached alignment jig, as per the manufacturer's recommended curing cycle. After complete curing is achieved the sample along with the loading fixture are then clamped to the tensile machine to conduct flatwise tensile test.

## 3.10 Mechanical test



*Figure 3.11: Sample subjected to flatwise tensile loading.*

### 3.10.1 Test result

The tests were performed on displacement control mode with the rate of 0.5 mm/min and the force values are recorded at a sampling rate of 3 readings per second. The results are reported in Table 3.1.

*Table 3.1: Bond strength and failure modes of the samples after testing.*

| Sample No | Cycles | Ultimate failure load (N) | Ultimate flatwise tensile strength (MPa) | Failure Mode |
|---|---|---|---|---|
| 1 | 0 | 3130 | 5.00 | Adhesive failure of core-facing adhesive |
| 2 | 10 | 3502 | 5.42 | Adhesive failure of core-facing adhesive |
| 3 | 20 | 2932 | 4.54 | Adhesive failure of core-facing adhesive |
| 4 | 30 | 2850 | 4.41 | Adhesive failure of core-facing adhesive |
| 5 | 40 | 2662 | 4.12 | Adhesive failure of core-facing adhesive |
| 6 | 60 | 2682 | 4.15 | Adhesive failure of core-facing adhesive |

Six sets of flatwise test were conducted. For each cycle, four samples were tested to obtain statistically significant data. Samples were tested after subsequent cycles as shown in table 3.1. The bonding strength decreases with an increase in the number of cycle up to 40 thermal cycles. This result correlates with the observation from microscopy which also indicated saturation of microcrack growth/propagation around 30 to 40 thermal cycles. It can be noticed from the table 3.1 that the bonding strength reduced by 17 percent after 30 thermal cycles when compared with the strength measured of the samples without any thermal cycling.



(a)  (b)  (c)

(d)  (e)  (f)
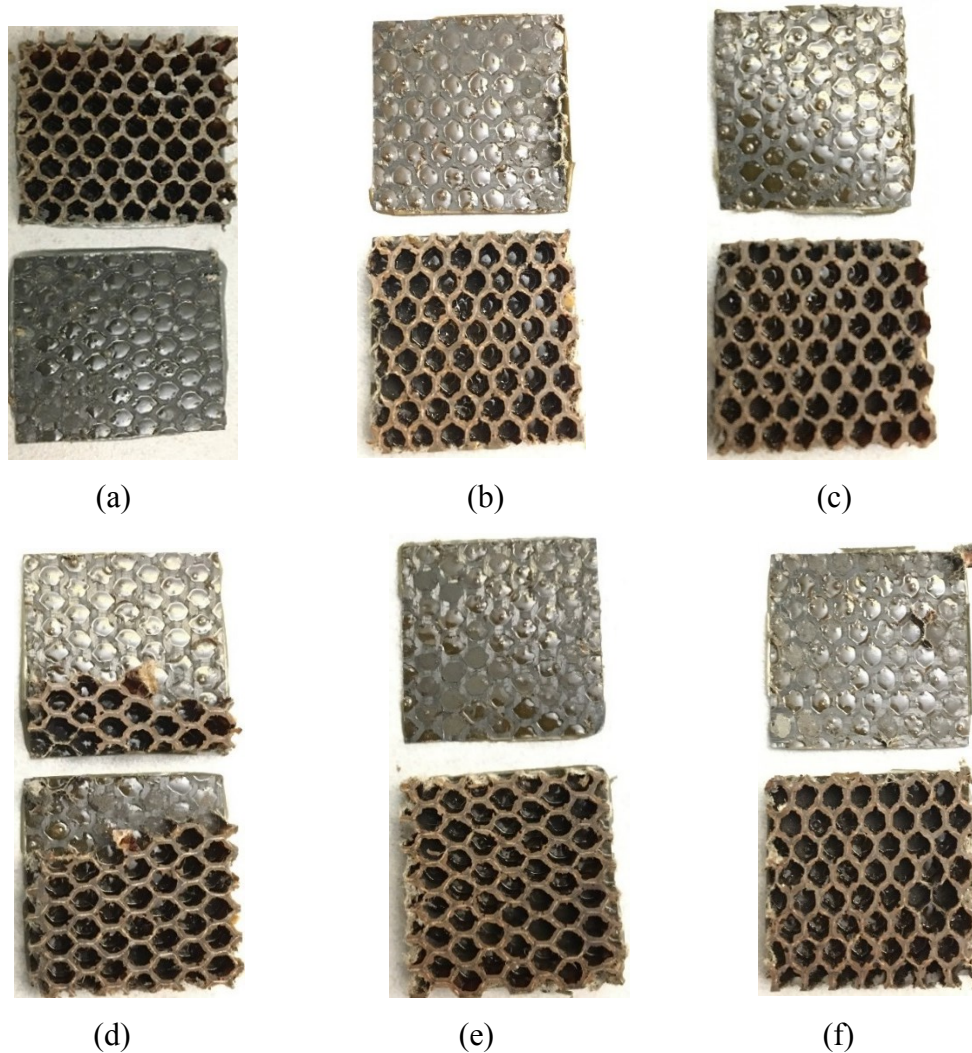
*Figure 3.12: Images indicating residue of adhesive on the core side of the sample, a) no thermal cycle, b) after 10 thermal cycle, c) after 20 thermal cycles, d) after 30 thermal cycles, e) after 40 thermal cycles, f) after 60 thermal cycles.*

The failure mode observed is the adhesive failure of core facing adhesive. The presence of microcrack between the facesheet and adhesive as shown in figure 3.5 (b) to 5 (f) effects the

bonding strength of adhesive and facesheet. Post-failure investigation of the samples indicates retention of hexagonal shaped adhesive on the facesheet and adhesive fillets on the core side.

## 3.11    Correlation between crack area and mechanical strength

The crack area was defined and calculated by multiplying the total crack length on two perpendicular edges of the adhesive-facesheet interphase on one side of the core. The cracks between the adhesive-facesheet were considered and the cracks within the facesheet were omitted, as the failure mainly occurred in that region.

Figure 3.13 shows the variation of the crack area and flatwise strength for different samples thermally cycled from zero to 60. The figure includes data points from both contact cooling and non-contact cooling conditions. It seems there is a linear relationship between the crack area and strength with the number of thermal cycles up to saturation point. The similar method to study the effect of microcrack on a mechanical property was conducted by subjecting the sample to an accelerated cooling condition. The condition is experienced by materials used for cryogenic fuel tank application where the materials come in direct contact with the cryogenic fuel. It is interesting to note from the plot that the crack area and strength reach to constant values after 40 cycles.
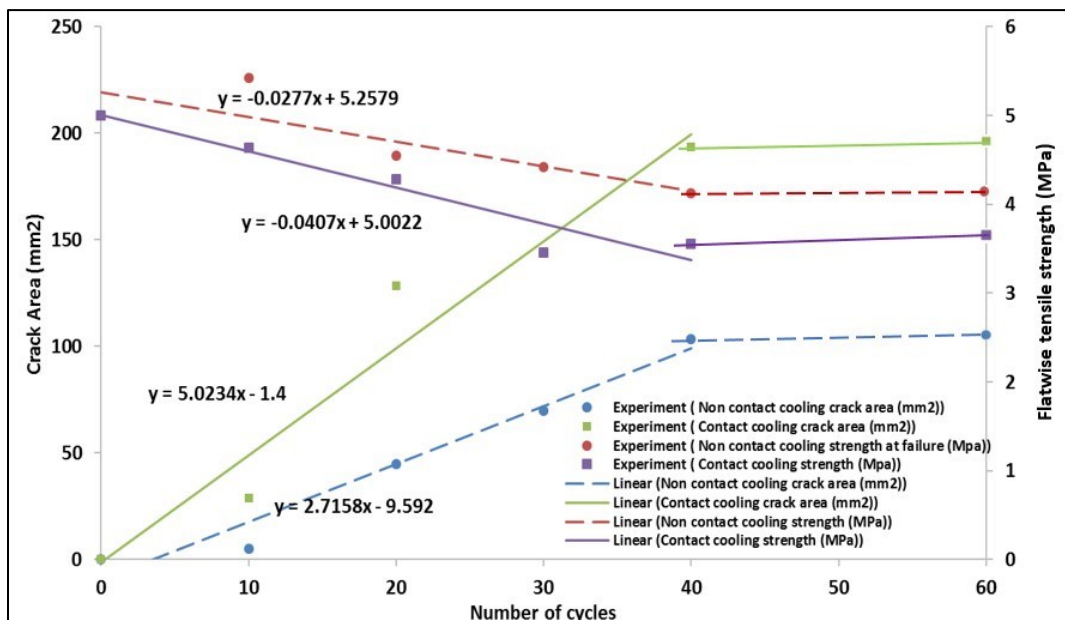


*Figure 3.13: Change in crack area and strength at failure for contact and non-contact cooling.*

It can be noticed from the plot that samples subjected to contact cooling condition exhibit lower interfacial bonding strength as compared to non-contact thermal cycled samples. This is in good

agreement with the crack area for contact cooled samples which has two times the crack area for non-contact cooled samples after 40 cycles. The relatively high degradation of bond strength for contact cooling could be primarily due to two reasons. Firstly, contact cooling involves submerging of test samples inside liquid nitrogen. During the process of cooling, the samples experience thermal shock as liquid nitrogen enters the insides of the sample due to the presence of perforations on the walls of the honeycomb core. Secondly, the samples experience the thermal environment as low as -194 ºC as compared to -170 ºC for non-contact cooling. Thermal strain increases with the decrease in conditioning temperature as given in equation 3.1.



(a)                                                     (b)
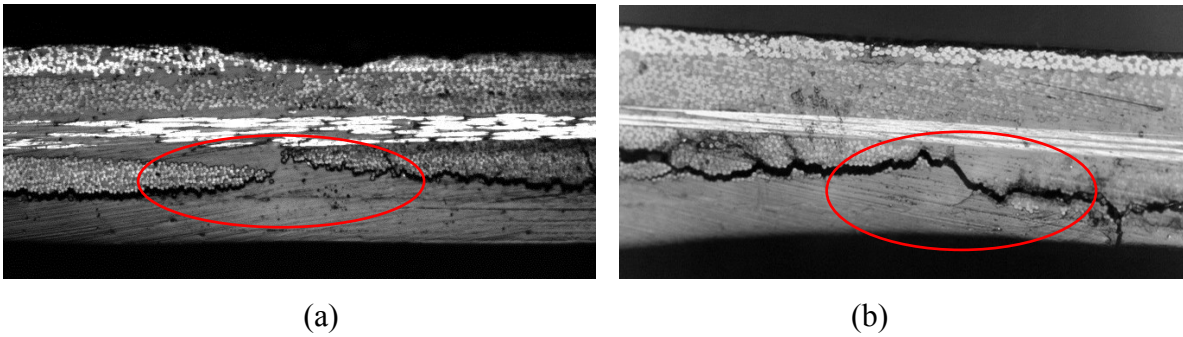
*Figure 3.14: (a) Non contact cooled sample, (b)contact cooled sample.*

Microscopic observation indicates the difference in the level of severity of microcracks for contact and non-contact cooling. Figure 3.14b indicates crack connecting each other between two adjacent 90º tows. However, for non-contact cooling cracks jump the resin region and grows in the next 90º tow as shown in figure 3.14a.



(a)                                                     (b)
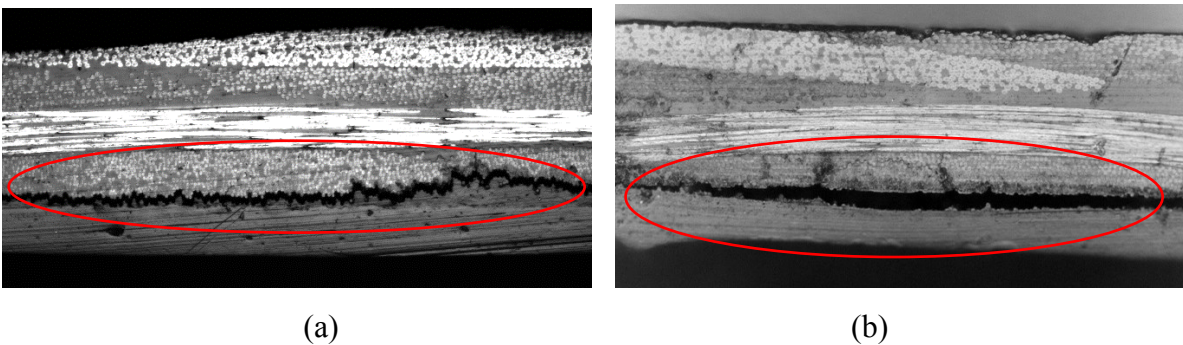
*Figure 3.15: (a) Non contact cooled sample, (b) contact cooled sample.*

It is also interesting to note the difference in the thickness of the crack. For non-contact cooled samples, the thickness of the crack is relatively small when compared with contact cooled samples as indicated in figure 3.15a and 3.15b.

## 3.12    Finite Element Analysis

After qualitative and quantitative observation of microcrack growth, finite element analysis was conducted to see if regions with high thermal strain can be predicted [51]. 3D-finite element analysis was performed on ANSYS$^{TM}$ workbench module.

### 3.12.1  Geometrical Model

A model that represents the cross-section of one of the samples tested was designed in CATIA V5$^{TM}$ software. The image was imported into the CAD software and each constituent of the sandwich was sketched as shown in Figure 3.16 (b). From the sketch, a very thin surface was extracted as shown in Figure 16 (c).
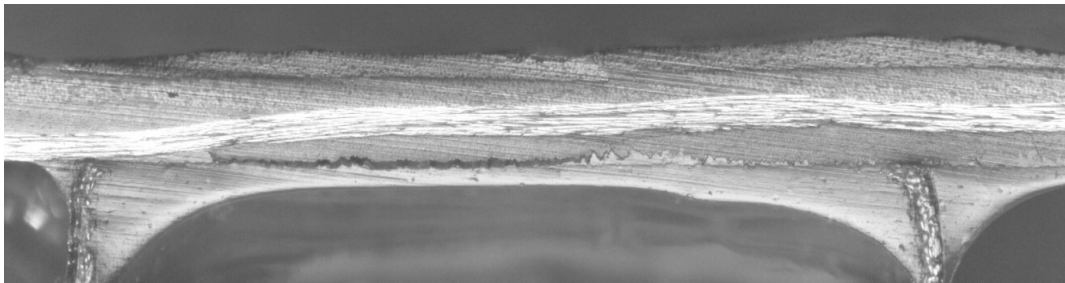


(a)
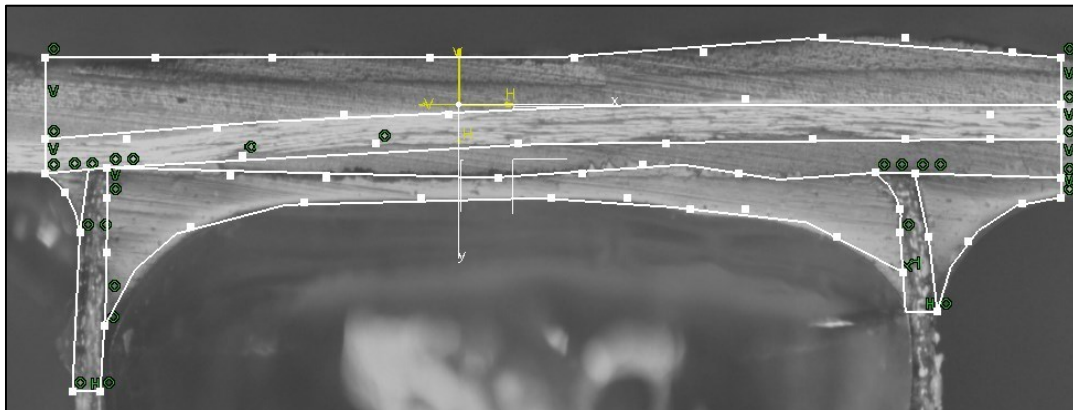


(b)
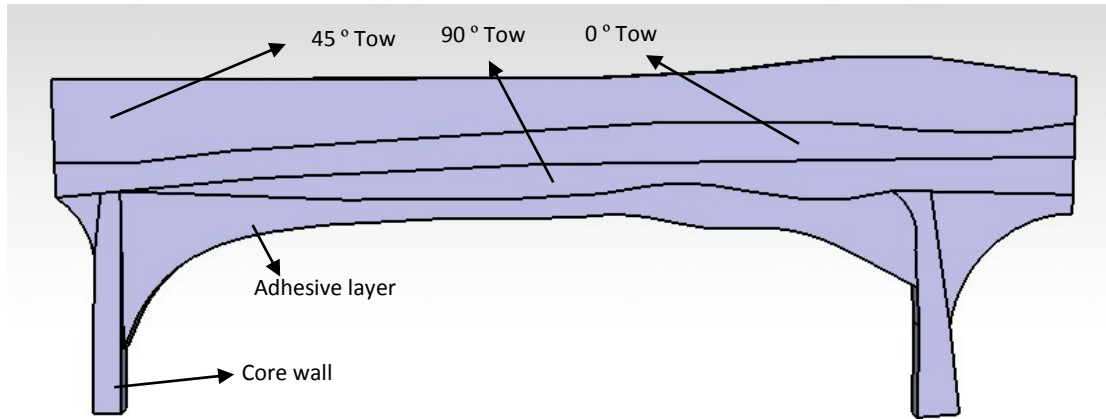
(c)

*Figure 3.16: (a) Microscopic image, (b) Sketch extracted from the microscopic image, (c) CAD model.*

### 3.12.2 Mechanical properties of elements

The properties of different sandwich constituents are summarized in table 2.

*Table 3.2: Material properties of the respective constituents used in a sandwich structure.*

| Sl. No | Material name | Density (g/cm³) | Coefficient of Thermal Expansion (C⁻¹) | Elastic Modulus (GPa) | Poisson's Ratio | Specific Heat (Cal g⁻¹ K⁻¹) | Tg °C | Tensile strength (MPa) |
|---|---|---|---|---|---|---|---|---|
| 1. | Resin | 1.19 | $43*10^{-6}$ | 3 | 0.3 | 1.2 | 254 | 80 |
| 2. | Carbon tow impregnated with resin | 2.1 | $\alpha_x = -1.8*10^{-8}$ $\alpha_y = 2.4*10^{-5}$ $\alpha_z = 2.4*10^{-5}$ | $E_x=155$ $E_y= 12$ $E_z= 12$ | 0.248 0.0193 0.0193 | 0.9 | - | 3830 |
| 3. | Kevlar paper | 1.4 | $-2*10^{-6}$ | 3.1 | 0.36 | 1.4 | - | - |
| 4. | Adhesive film | 1.2 | $75*10^{-6}$ | 5 | 0.2 | 0.2 | 148 | 7.1 |

### 3.12.3 Boundary conditions, Meshing and FEA Result

The CAD model was imported into ANSYS workbench. The size is in 1:1 ratio of the actual sample. The model was meshed using auto mesh command. The FEA model comprised of around 9,506 nodes. The mesh element chosen was 3D Solid-187 tetrahedron. Initially, the mesh size was set to 0.3 mm. To achieve convergence, mesh size was reduced by 0.05 mm in every mesh iteration.

The mesh size was finalized to 0.1 mm as the stress results tend to converge. As shown in figure 3.17 (a), the mesh elements of matrix and tows show good connectivity which is necessary to achieve the stable transfer of thermal loads. Material properties were assigned to the respective constituents as mentioned in table 3.2. The material property of the resin impregnated tow is transversely isotropic. Since the model comprised of fiber tows oriented at 45, zero and 90 degrees, the local coordinate system was changed for the respective fiber orientations to incorporate suitable directional properties.
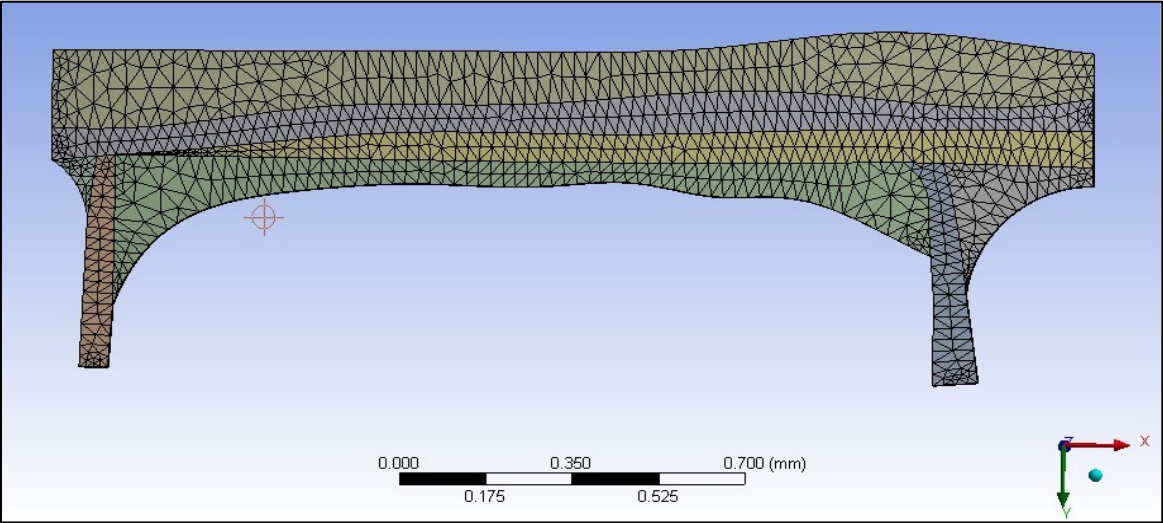


(a)
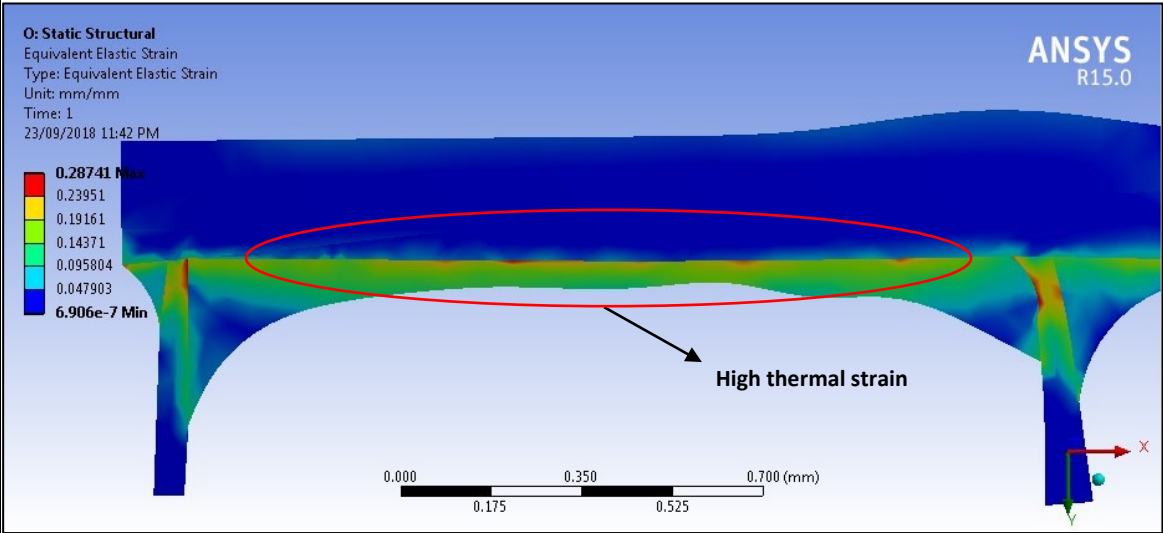


(b)

*Figure 3.17: (a) Meshed model, (b) Model indicating higher stress concentration areas.*

It is interesting to see higher strain concentration region at the boundary of adhesive and 90 degree tow. The accumulation of strain is the result of the higher difference of CTE of adhesive and resin. The results show excellent agreement between the location of crack as shown in Figure 16a to the region of higher thermal strain in Figure 3.17 (b). Therefore, FEM analysis can be used to identify the possible location of microcrack formation.

## 3.13    Conclusions

An in-house developed experimental setup is used to induce non-contact cooling (slower rate of cooling) for thermal cycling of sandwich samples. A methodology to observe crack growth/propagation and correlating them with the mechanical test was performed. It was observed that microcracks were formed at the free edges as well as at the mid-section. The nature of microcracks was the same but no transverse microcracks were found in the middle. The crack density at the middle was comparatively less than the ones found on the free edges. The experimental observation of microcracks proves that the thermal cycle of about 40 to 60 cycles is sufficient for a majority of crack formation, avoiding the need to conduct more thermal cycles. A significant difference in results for contact and non-contact cooled samples were observed by microscopic inspection and flatwise test. Crack area for contact cooled samples was two times more than non-contact cooled samples. Flatwise tensile strength for non contact cooled samples reduces by 15 percent, compared to the contact cooled samples which recorded a 30 percent reduction in bond strength. Finite element analysis was used to identify the possible location of microcrack formation. Results show good agreement between FEM analysis and experiment.

# Chapter 4: Effect of Core and Facesheet Thickness on the Mechanical property of Composite Sandwich Structures Subjected to Thermal Fatigue

## Abstract

Composite materials made of fiber reinforced polymers (FRP) are sensitive to micro-cracking. When FRP based composite materials are used in hostile thermal fatigue environments, the materials are prone to microcracking due to internal stresses. This article is focused on comparing the effect of thermal fatigue on composite honeycomb sandwich structure with different facesheet and core thicknesses. Sandwich structure under study comprises of CFRP skin bonded to the honeycomb Kevlar core. Samples were observed at the cross-section for microcrack growth and formation after subsequent thermal cycles ranging from -194 ºC to +150 ºC. Microcracks were quantified by crack length. Microcracks in the form of delaminations were observed at the facesheet and core interface. To study the effect of microcracks on mechanical property, flatwise tensile test was performed at room temperature. The results of the mechanical test were in good agreement with the microscopic inspection results. Results from microscopic inspection and flatwise test suggest that the sandwich structure made of the same material but with higher core to facesheet thickness ratio was more sensitive to microcracking.

## 4.1    Introduction

Composite materials such as Carbon Fiber Reinforced Polymer (CFRP) solid laminates or sandwich structures are most sought-after materials for complex aeronautical and space applications. To cater the rising trend in aerospace industry to accommodate higher payload mass, FRP based composite materials are judiciously used. Composite materials offer excellent mechanical and chemical properties. The ability to form into complex shapes with minimum wastage of material makes it an ideal choice for complex engineering problems. However, its heterogeneous composition makes it susceptible to defects at a micro level leading to catastrophic failure, when subjected to thermal cycling.

---

Many investigators studied various metallic and composite material based cryogenic fuel tanks [62-64]. The advantages and disadvantages were documented. Gates et al. [65] studied the correlation between the residual mechanical properties of a carbon fiber polymeric composite with the effect of temperature. Tensile modulus and strength were measured at room and cryogenic temperature. Tests were conducted on five different specimen layups to study the effect of layup on the composite performance subjected to the thermal cycling. Mechanical test and microscopic inspection at the surface show significant impact on the performance. Pannkoke and Wagner [66] conducted mechanical tests on different combination of fiber and matrix after thermal cycling at cryogenic temperature. Since microcracking occurs in the matrix, the authors used different grade of matrix such as epoxy, polycarbonate and PEEK, to observe if using matrix that have superior matrix-fiber bonding capabilities, would result in better performance. However, they did not get the expected result. They concluded that the poor matrix-fiber bonding is not the only reason for the deterioration of composite performance after thermal fatigue.

Jean-st-Laurant et al [25] studied the effect of thermal cycles ranging from -170 ºC to 145 ºC on three cyanate ester laminates reinforced with carbon fiber and a sandwich panel. Samples were subjected up to 360 thermal cycles. Microscopic observation showed three types of damages, transverse microcracks, debonding between fiber and matrix and minor delaminations. Cracks were quantified by means of crack density at the edges and at the mid-section of the samples. Mechanical test indicated effect of damage due to microcracking. Thermal cycling of composite honeycomb sandwich structure is described more in detail in [60]. Longitudinal microcracks in the form of delaminations were observed between the facesheet and the core. Cracks surfaced right from the first thermal cycle. Crack growth plateaued after 30 to 40 thermal cycles. Flatwise tensile test of the samples subjected to subsequent thermal cycles showed degradation in bond line strength. The results of mechanical test were in good agreement with microscopic inspection results. FEA (finite element analysis) of the representative sandwich model predicted the experimental observation concerning the location of microcracks. Timmerman [31] et al. studied the effect of cryogenic thermal cycling effects on symmetric carbon fiber/epoxy laminates. Laminates made out of different combinations of fiber modulus and matrix composition were studied. It was observed that laminates with higher glass transition temperature and inclusion of toughening agents in the resin showed resistance to microcracking.

Islam et al. [67] explored options such as the hybrid textile composites for composite cryogenic tank application. They manufactured composites made from carbon fiber, kevlar and hybrid composites with both carbon fiber and kevlar. Short beam shear test was conducted for both non-cycled and thermal cycled samples and results were compared. Transient thermal analysis was conducted in-order to study interfacial stresses. Mechanical test of hybrid composites indicated few combinations that performed better than the rest, after thermal cycling. Garnich et al. [68] studied the effect of moisture absorption on microcrack formation after thermal cycling. Balanced cross-ply laminates were used for the experiment. The samples were made of IM7 fibers and CYCOM 5250-4 bismaleimide matrix. Microscopic observation and crack density plot of the samples at the edges and mid-section showed that microcracking was significant on the edges of the sample in comparison to the mid-section of the sample. They also compared the microcrack density results of samples with and without moisture conditioning. Surprisingly, they found samples with 1.2 % moisture had a microcrack suppressing behavior.

During the literature study phase, it was found that most of the work dealt with thermal cycling of solid laminates. The authors believe that knowledge of the thermal cycling effects and its consequence on the mechanical property is still a void. The present study aims at determining the effects of the thermal cycling on the performance of sandwich structure, made of same facesheet and core material, but different facesheet and core thickness configuration. The work described in this article is divided into two phases. The initial phase is focused on the qualitative observation of the samples after thermal cycling. This phase involves observation of the cross-sections of the samples for microcracks, with the increase in the thermal cycles. The second phase involves quantification of microcracks followed by correlation with the flatwise tensile mechanical property.

## 4.2    Materials and Manufacturing

Sandwich samples with different core and facesheet thickness were chosen for this study. Table 4.1 gives details of the different sample configuration under investigation. The facesheet were made of 5 harness satin carbon fiber woven fabric with cyanate ester resin. The facesheets were cured separately at the laminate level and then bonded to the core using modified epoxy film adhesive. The core chosen was a Kevlar honeycomb core coated with phenolic resin. The cell size of the core was 3 mm with core wall thickness 46 micrometer and density 48 kg/m$^3$. The volume

fraction of (±45) and (0/90) fabric plies within samples was kept the same (%50) for all configuration to have almost the same in-plane stiffness properties and thermal expansion coefficients. The samples were cut to the size of 25.4 mm by 25.4 mm as shown in Figure 4.1.

*Table 4.1 Sample configuration*

| Sample ID | Configuration |
|---|---|
| Sample A | [( ±45),(0/90),core]$_S$ with 6.25 mm thick core |
| Sample B | [(0/90),( ±45)$_2$,(0/90)$_2$,( ±45)$_2$,(0/90),core]$_S$ with 6.25 mm thick core |
| Sample C | [(0/90),( ±45)$_2$,(0/90),core]$_S$ with 12.5 mm thick core |
| Sample D | [(0/90),( ±45)$_2$,(0/90),core]$_S$ with 19 mm thick core |



(a)                                          (b)



(b)                                          (d)
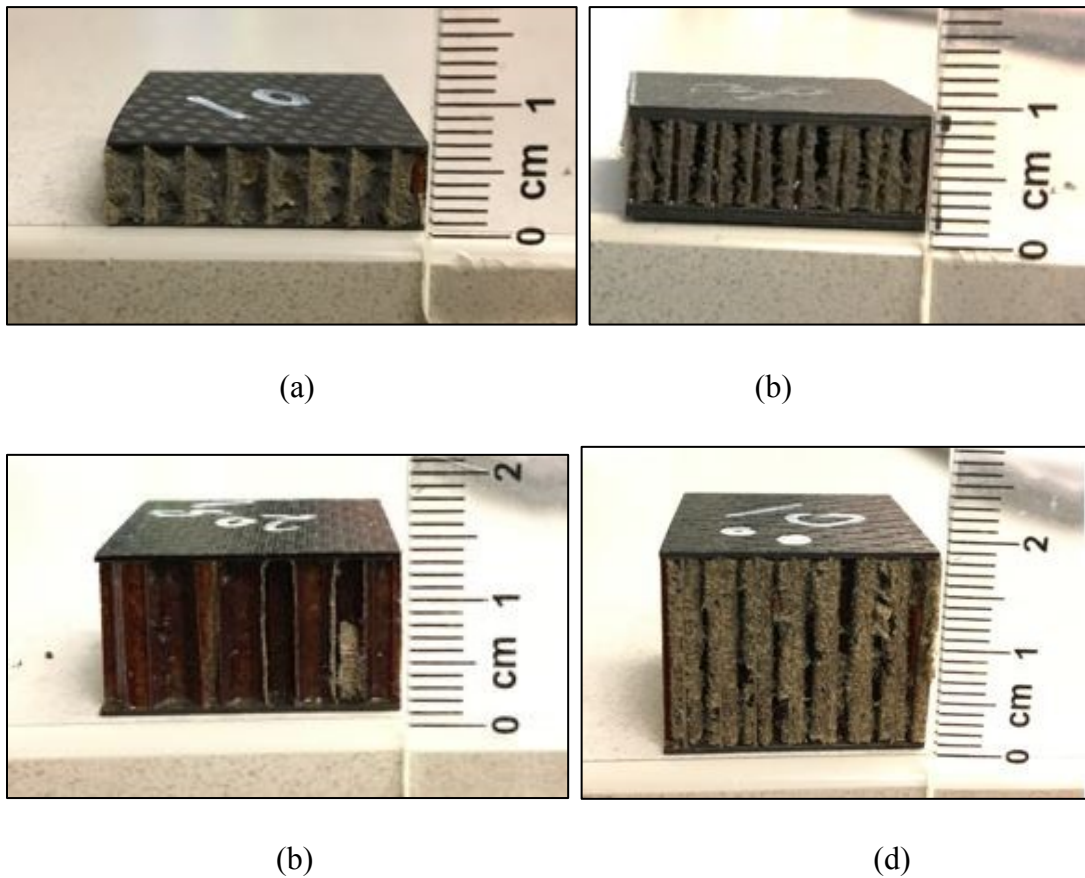
*Figure 4.1: Sample subjected to thermal cycling (a) Sample A (b) Sample B (c) Sample C (d) Sample D.*

## 4.3  Sample preparation and test plan

Samples were cut to the size of 25.4mm by 25.4mm for thermal cycling. The cutting process was performed using a diamond saw cutting tool. The tolerance of +/- 0.5 mm was achieved between the samples. Two perpendicular edges of the samples were polished for microscopic inspection. The polishing was done using a finer grit sized sand paper. Using a courser grit sized sandpaper resulted in excessive material loss during polishing, with the help of a polishing machine.

Test plan involves thermal cycling of samples as shown in Figure 4.2.  To expose the samples to cryogenic temperature, samples were placed in a metallic meshed container and then submerged into $LN_2$ as shown in Figure 2a. After cold conditioning, the samples were brought back to room temperature (RT) and then placed in a convection oven to take the samples to the elevated temperature as shown in Figure 4.2 (c).



| (a) | (b) | (c) |

*Figure 4.2: (a) Samples dipped in LN2, (b) Samples at room temperature, (c) Samples placed in convection oven*

A T-type thermocouple was inserted through a hole of 0.5 mm diameter in one of the samples to measure the change in temperature with respect to time during thermal cycling and to make sure that the center of the sample attained the conditioning temperature. The temperature history for sample A is shown in Figure 4.3. This sample is comprised of a quarter inch thick core and 2 ply's of fabric on either side of the core. It took close to 20 seconds to reach cryogenic temperature from RT and close to 15 minutes to reach +150 °C as presented in Figure 4.3. The other configuration of sample used for study had either relatively thicker core or facesheet. The similar temperature history was recorded for them. As a result, they reached the required temperature relatively slower.

However, in all the cases, cryogenic temperature was reached within 1 minute and higher temperature (150 °C) was reached in 15 minutes. To maintain consistency in the experiment, all the configuration of samples was cycled for 1 minute in $LN_2$ and 15 minutes in the oven.
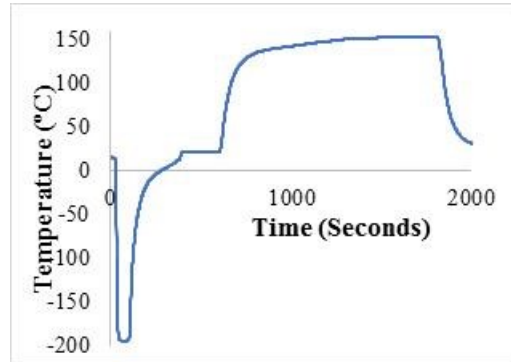


*Figure 4.3: Change in temperature with respect to time for one thermal cycle.*

## 4.4    Microscopic observation

Microscopic observation was conducted using an optical microscope. The magnification was set to clearly distinguish various constituents of sandwich material and detection of microcracks. The sample cross-sections were observed for microcrack formation and propagation. Samples were cut along ribbon and transverse ribbon direction sides. As the honeycomb core is made of combining aramid paper ribbons leading to the formation of hexagonal cells, the core has orthotropic mechanical properties in ribbon and transverse ribbon directions (Figure 4.4). This directional mechanical property also influences the thermal expansion and contraction behavior. Therefore, it was decided to conduct the microscopic observation on the above-mentioned sides. The observation was conducted for every half a cycle until 10 thermal cycles and then the observation interval was increased to 10 cycles.
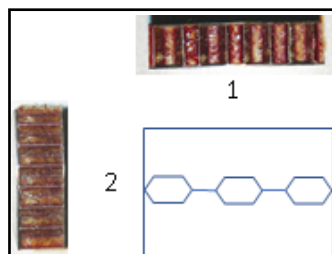


*Figure 4.4: Sandwich ribbon and transverse ribbon directions.*

## 4.5 Microcrack inspection results and quantification

As discussed in the test plan, four configurations of samples were subjected to the thermal cycling. The results from the microscopic inspection are discussed in details below.

**Sample A: [( ±45),(0/90),core]s with 6.25 mm thick core.** Sample A comprises of two fabric plies on the either side of the core with a 6.25 mm thick core. The facesheet thickness is about 0.25 mm. Figure 4.5 (a) to 4.5 (f) shows the various stages of microcrack propagation. Figure 4.5 (a) presents details of various constituents of composite sandwich. Since the facesheet was thin, no voids were observed inside the laminates. However, some voids were visible in the adhesive fillet region, as shown in Figure 4.5 (b). Microcracks started to appear right from the first cycle. Most commonly longitudinal cracks formed around the facesheet and core interface, between the 90° tow and the adhesive. With subsequent thermal cycling, existing longitudinal cracks started to grow and new microcracks formed. Cracks grow along the 90° tow until it touches the 0° tow and then jump to the adjacent 90° tow [60]. Transverse microcracks on the ply adjacent to the core started to appear after 25 thermal cycles. Longitudinal microcracks between the plies started to form after 30 cycles as shown in Figure 4 (d). Longitudinal microcracks growth saturates after 30 thermal cycle.

**Sample B: [(0/90),( ±45)$_2$,(0/90)$_2$,( ±45)$_2$,(0/90),core]s with 6.25 mm thick core.** This sample consists of eight fabric plies on either side of a 6.5 mm core. The facesheet thickness is about 1.0 mm. Voids were found in small fractions on the outermost ply and on the adhesive fillet. Figure 4.6 (a) to 4.6 (f) shows the evolution of cracks from 0 to 60 thermal cycles. Cracks did not surface after first cycle as observed in sample A. It started to appear after three thermal cycles. The microcrack growth was significant until 40 thermal cycles and then gets saturated. Microcracks did not form around the void or on the outermost ply of the sample. The crack length by the end of 60 cycle was less compared to sample A.
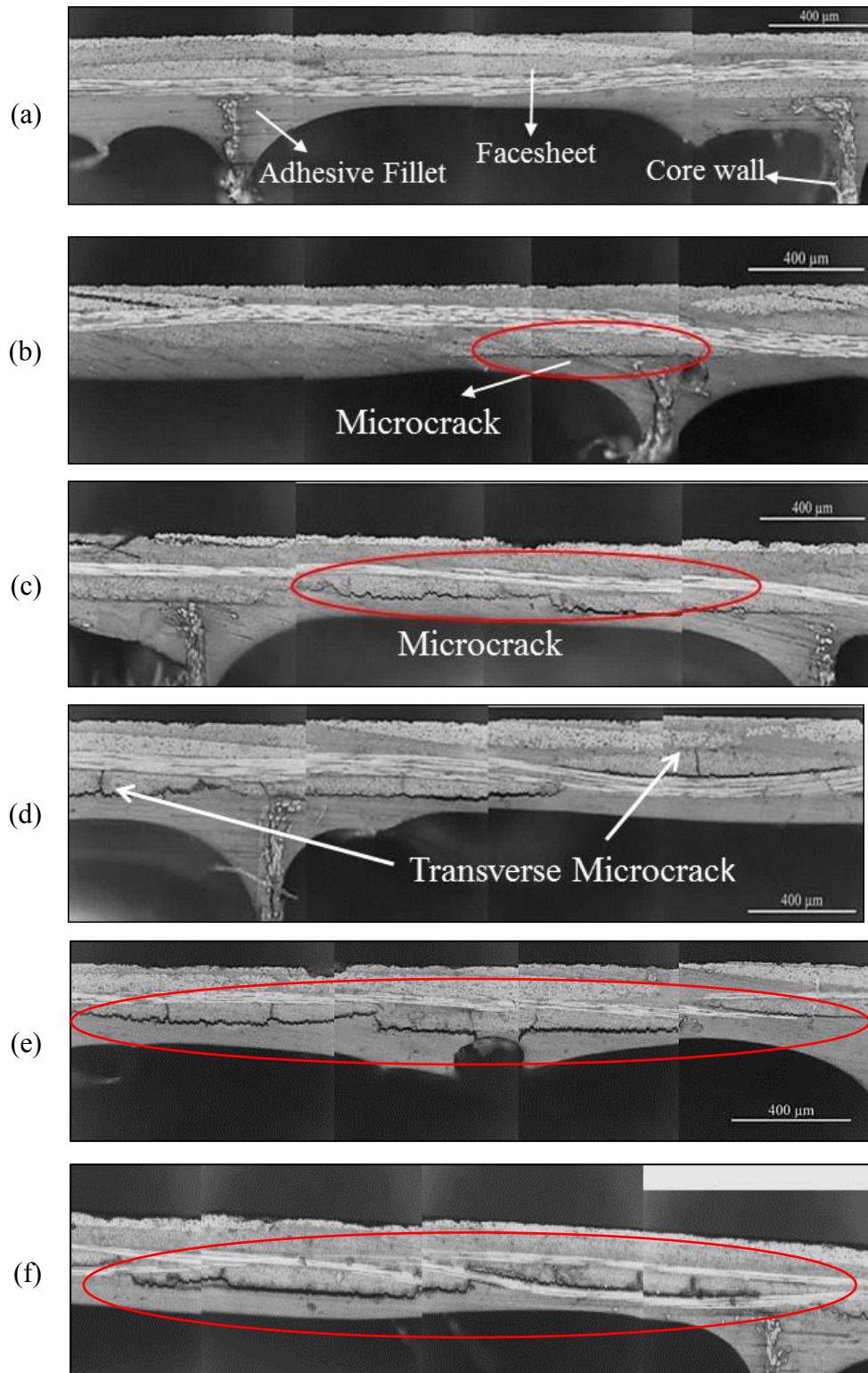
*Figure 4.5: Microscopic image taken after thermal cycling of sample A, a) No thermal cycle, b) after 10 thermal cycles, c) after 20 thermal cycles, d) after 30 thermal cycle, e) After 40 cycles, f) After 60 cycles.*
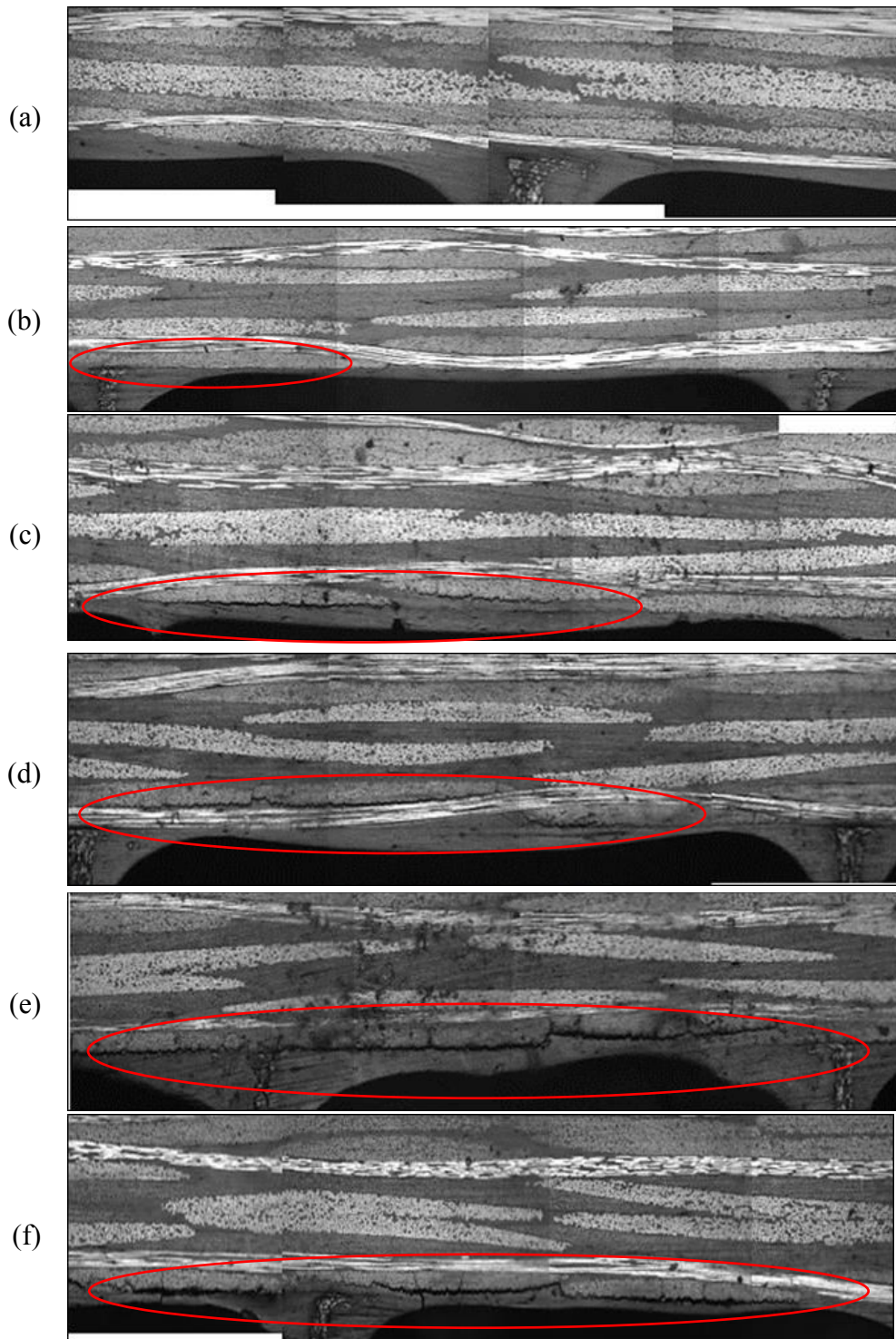
*Figure 4.6: Microscopic image taken after thermal cycling of sample B, a) No thermal cycle, b) after 10 thermal cycles, c) after 20 thermal cycles, d) after 30 thermal cycle, e) After 40 cycles, f) After 60 cycles*

**Sample C: [(0/90),( ±45)₂,(0/90),core]ₛ with 12.5 mm thick core.** Sample C comprised of four plies on the either side of the 12.5 mm thick core. The facesheet thickness is about 0.5 mm. No voids were found on the facesheet. Figure 4.7 (a) to 4.7 (f) shows the evolution of microcrack growth from 0 to 60 cycles. Cracks started to appear after third thermal cycle. Microcracks grow steadily until 40 cycles and then saturate. Longitudinal microcracks between 90° tow and core facing interface was observed similar to the cracks in sample A and B. However, cracks at the end of 60 thermal cycles were not as thick as the ones observed in Sample A.

**Sample D: [(0/90),( ±45)₂,(0/90),core]ₛ with 19 mm thick core.** This sample is comprised of four plies on the either side of a 19 mm thick core and 0.5 mm thick facesheets on either side of the core. Figure 4.8 (a) to 4.8(f) shows various stages of crack growth. Sample D had the thickest core compared to A, B and C. Longitudinal microcracks similar to sample A, B and C were observed after thermal cycling. Microcrack growth was significant in the initial set of cycles. The cracks grew thicker right after 10 thermal cycles. Crack length saturated after 20 thermal cycles which was faster compared to the previous configuration of samples.
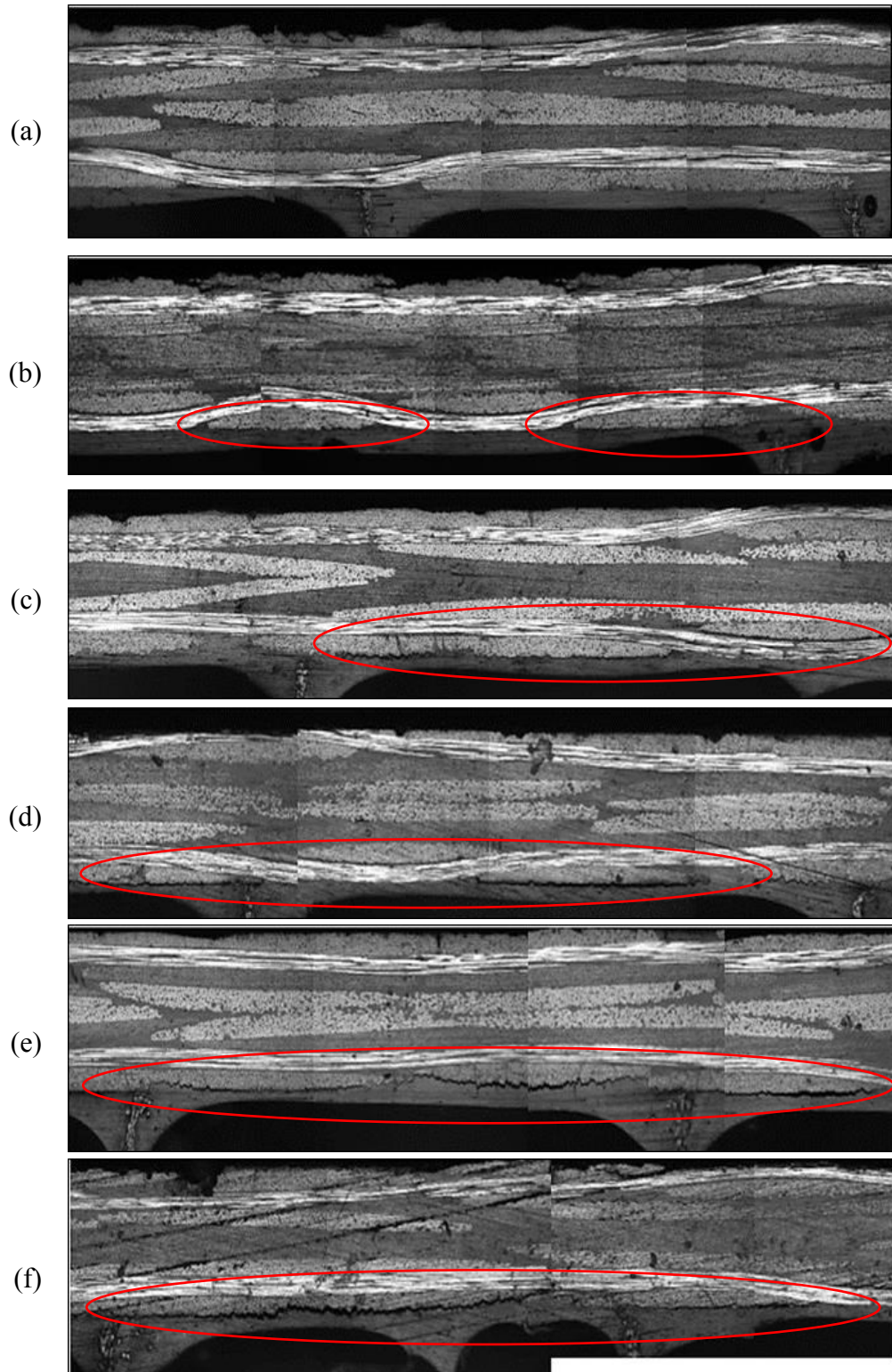
*Figure 4.7: Microscopic image taken after thermal cycling of sample C, a) No thermal cycle, b) after 10 thermal cycles, c) after 20 thermal cycles, d) after 30 thermal cycle, e) After 40 cycles, f) After 60 cycles.*
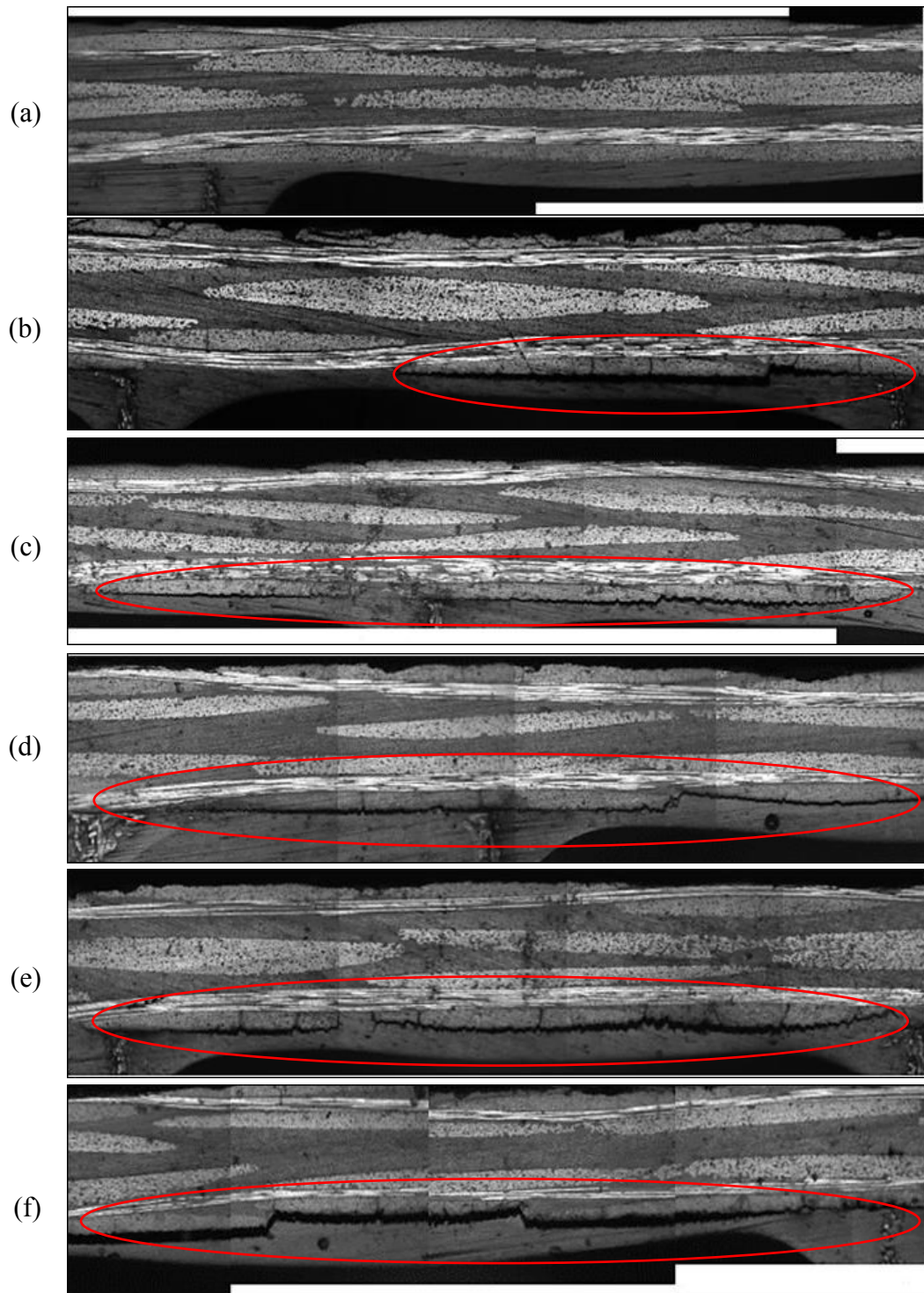
*Figure 4.8: Microscopic image taken after thermal cycling of sample C, a) No thermal cycle, b) after 10 thermal cycles, c) after 20 thermal cycles, d) after 30 thermal cycle, e) After 40 cycles, f) After 60 cycles.*

Cracks were quantified by crack lengths. Length of individual crack was measured using image processing software. After every 10 cycles the longitudinal microcracks were added. Sum of microcracks on ribbon and transverse ribbon direction were calculated separately. Figure 4.9 shows change in crack length with the increase in thermal cycles for different configurations of samples tested. Results of two samples for each configuration are presented in this figure.



(a)

(b)

(c)

(d)
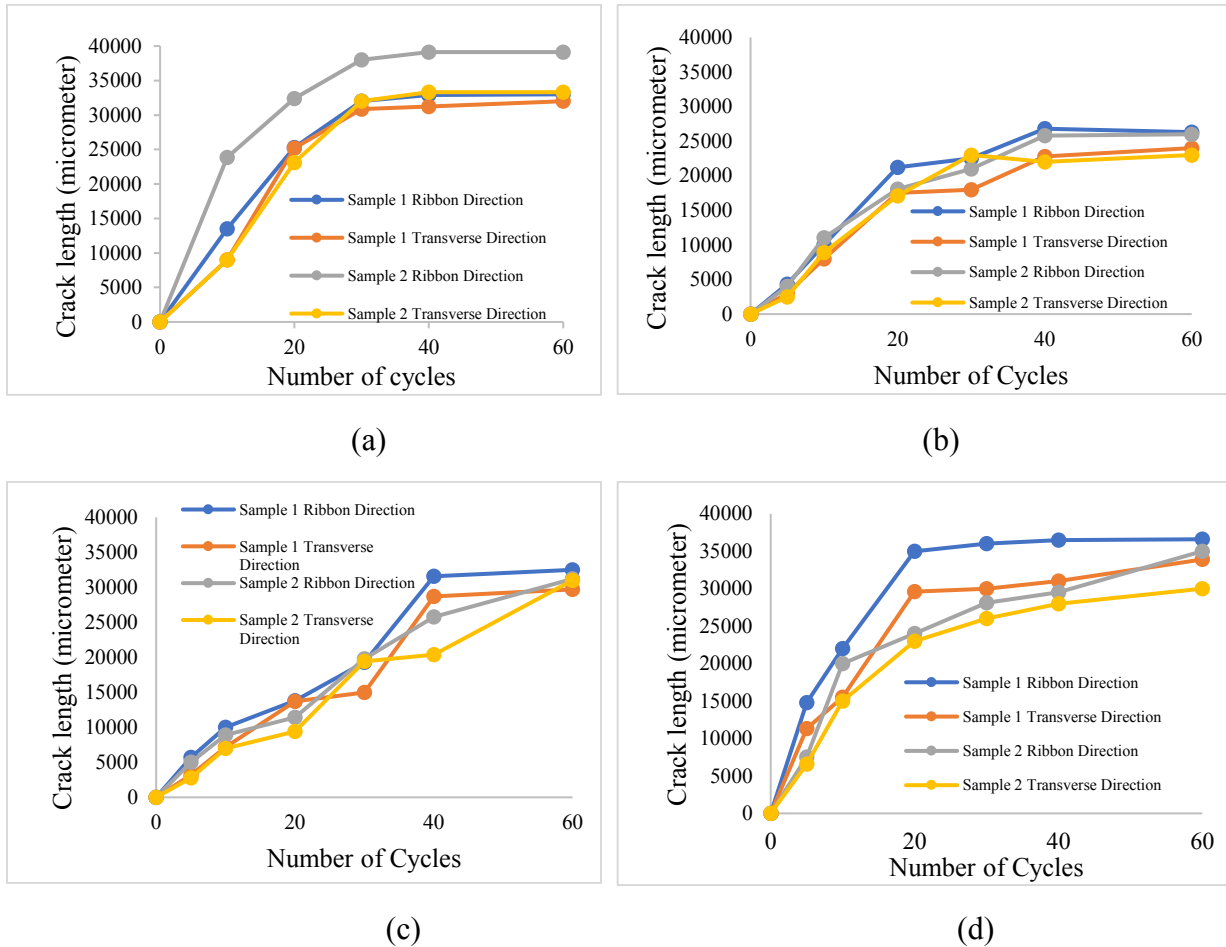
*Figure 4.9: Microcrack length with increase in thermal cycle for (a) Sample A, (b) Sample B, (c) Sample C and (d) Sample D.*

## 4.6   Discussion

The interface region between the 90° tow and adhesive was more prone to microcracking in comparison to other part of sandwich material. This is mainly due to the difference in coefficient of thermal expansion (CTE) of fiber tow and adhesive. Microcracking is more dominant in sandwich structures due to its heterogeneous composition that comprises of resin, carbon tow,

adhesive and core. In case of solid laminates microcracking is due to difference in axial and transverse CTE between each ply. The sandwich material under study is made of cyanate ester resin reinforced with carbon fiber woven fabric. Microcracks were not observed within the laminate away from the core side, as cyanate ester is less prone to microcracking. It can be inferred from all the plots that the crack length in ribbon direction is higher compared to transverse ribbon direction up to 10 thermal cycles. The anisotropy of the core due to the ribbon and transverse ribbon direction is the primary reason for this observation. The core CTE is higher in ribbon direction side.

The rationale behind observing the cross section after every half thermal cycle, for the first 10 thermal cycle was to observe the evolution of microcracks on hot and cold conditioning environment. The thermal strain is proportional to the difference in stress free temperature (temperature at cure) and process temperature (conditioning temperature). The stress component between facesheet and adhesive is higher at -194 °C as the thermal strain is higher. Therefore, cryogenic cycle had higher influence on crack formation

Sample A and Sample B have the same core thickness with different facesheet thickness. Sample C and Sample D have same facesheet thickness but with different core thickness. A comparison of the thermal cycling effect was made between samples with different core thickness and facesheet thickness. The microscopic observation and crack length corroborate the fact that Sample A with core to facesheet thickness ratio of 12.5 has higher microcrack lengths than Sample B which has a core to facesheet thickness ratio of 3.125. Sample D with core to facesheet thickness ratio of 19 has higher microcrack lengths than Sample C which has a core to facesheet thickness ratio of 12.5. It can be interpreted from the crack length and thermal cycle plot that the samples with higher core to facesheet thickness are more sensitive to microcracking.

## 4.7 Mechanical testing

To study the impact of thermally induced microcracks on the mechanical strength, flatwise tensile test was performed on the samples (Figure 4.10). Among the different types of microcracks observed, longitudinal microcracks between facesheet and core were dominant. Therefore, flatwise tensile test was chosen as it is ideal to determine the interfacial debonding strength. Other test for sandwich structure such as three-point bending, four-point bending and flatwise compression test are ideal for measuring mechanical properties of core.
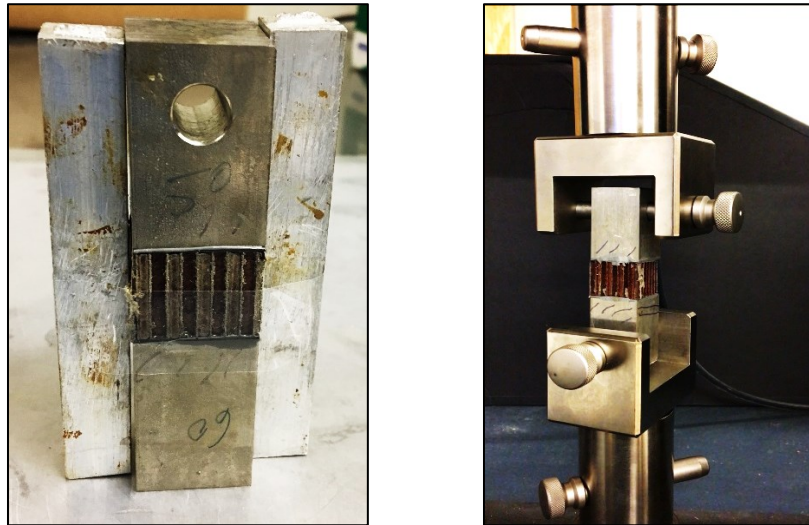


*Figure 4.10: a) sample alignment jig, b) sample under flatwise tensile loading.*

The test was conducted as per ASTM C297. Samples were cut to size of 25.4 mm by 25.4 mm. Care was taken to make sure the variation in size between the samples is less. Flatwise test was performed after 0, 10, 20, 30, 40 and 60 thermal cycles. For statistical significance three samples were tested. Test was performed using Wyoming flatwise tensile test fixture as shown in Figure 4.10b. The samples were lightly sanded on the facesheet for better adhesion with the loading blocks. The samples were bonded to the loading blocks using a two-component, high-performance aerospace grade adhesive from LOCTITE, named Hysol 9392 Qt aero. Figure 4.10a shows the sample alignment jig held together using gum tape. The samples attached to jig were placed in oven for curing at 82 °C for 1 hour. After performing flatwise test by following test parameters as mentioned in the standard, the samples were retrieved from the blocks for analysis of failure mode. The traditional method followed, is to machine the side of the block with sample attached using suitable machining process. However, this method would result in loss of sample and each time block would lose material. To retrieve the samples from blocks without damage, the blocks with

samples attached were heated in oven to 185 °C. As soon as the blocks reached the set temperature, the samples could be easily removed by gently scraping the sample using a brass scraper. This is possible as stainless-steel blocks have higher CTE, as the result, the sample would easily de-bond with help of small external force.

## 4.8 Analysis of failure mode

Figure 4.11 presents the images of different configuration of zero thermal cycled samples post flatwise tensile test. Figure 4.12 presents the images of post flatwise tensile test results of the samples subjected to 60 thermal cycles. As presented in Figure 4.11 (c), Sample C had 10 percent core failure and 90 percent adhesive failure of core facing adhesive. Figure 4.11 (d) presents sample D without any thermal cycle. The samples underwent 100 percent core failure. There is core retention on either side of the facesheet. The failure mode of 60 thermal cycled samples of sample D, as shown in Figure 4.12 (d) clearly indicates the effect of microcrack. Table 4.2 presents failure modes of four configurations of samples chosen for study. Adhesive failure of core facing adhesive was the most dominant failure mode, leaving adhesive fillet on the core side of the sample and hexagonal adhesive patches on the other facesheet.

*Table 4.2: Failure mode.*

| Number of cycles | Sample A | Sample B | Sample C | Sample D |
|---|---|---|---|---|
| 0 | AFCFA | AFCFA | 10% CF, 90 % AFCFA | 100% CF |
| 10 | AFCFA | AFCFA | AFCFA | AFCFA |
| 20 | AFCFA | AFCFA | AFCFA | AFCFA |
| 30 | 3 % FTF, 97% AFCFA | AFCFA | AFCFA | AFCFA |
| 40 | AFCFA | AFCFA | AFCFA | AFCFA |
| 60 | AFCFA | AFCFA | AFCFA | AFCFA |

AFCFA- Adhesive failure of core-facing adhesive, CF- Core failure, FTF- facing tensile failure.
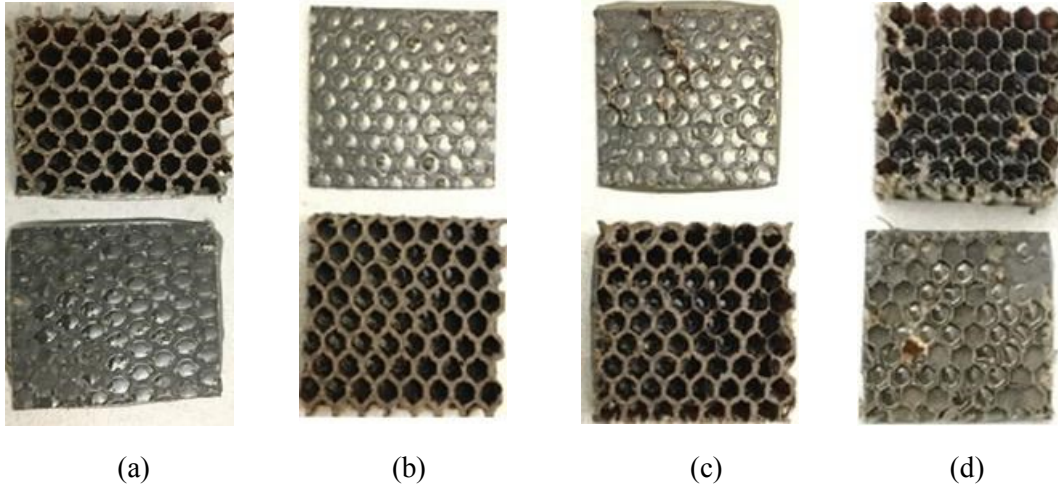
*Figure 4.11: Images of samples after flatwise test without any thermal cycle for, (a) Sample A, (b) Sample B, (c) Sample C and (d) Sample D.*
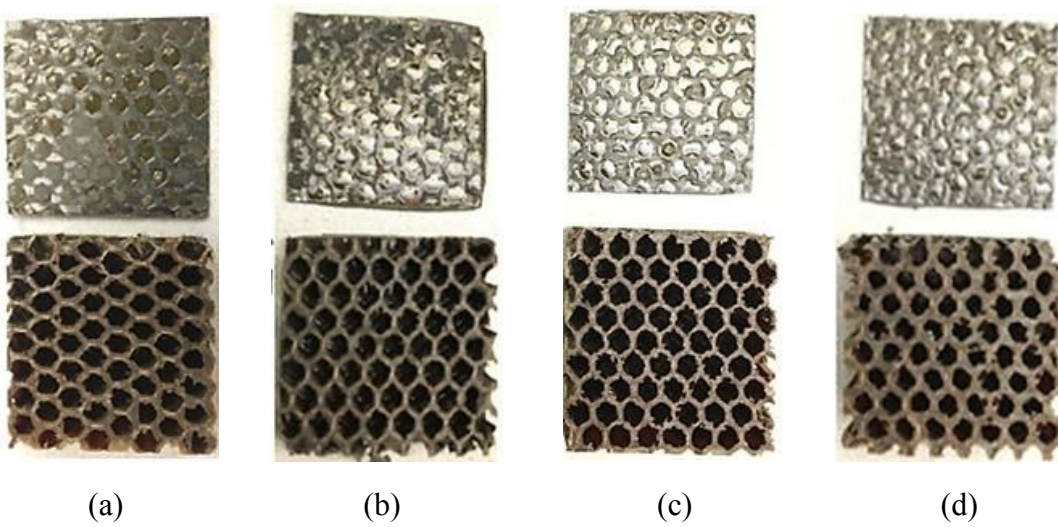


*Figure 4.12: Images of samples after 60 thermal cycles followed by flatwise test for, (a) Sample A, (b) Sample B, (c) Sample C and (d) Sample D*

It is interesting to notice higher retention of adhesive on the core side (around the core cell), for the samples that were subjected to 60 thermal cycles (Figure 4.12), in comparison to the samples that were not cycled, as shown in Figure 11. The observed retention is due to the presence of thermally induced microcracks between the facesheet and core. It is interesting to see the retention of adhesive is not just on the edges, but also at the center of the sample. One such microscopic

study of microcracks was done by Jean-st-Laurant et al [25]. The author quantified microcracks at the mid-section of the sample in terms of crack density. However, it was also reported that crack density at the mid-section is relatively lower compared to the edges of the sample. Furthermore, microcracking at the midsection can be higher for sandwich structure with honeycomb core in comparison to solid laminates as there are gaps between the adjacent cells which gives enough space for thermal strain, leading to microcracks.

## 4.9    Correlation of crack area and mechanical strength

The results from the flatwise tensile test indicated reduction in strength with increase in the number of thermal cycles. An effort was made to establish the relationship between growth of crack with decrease on the mechanical strength of the samples. Therefore, a correlation was made between crack area and strength at failure as shown in Figure 4.13.

Crack area is the product of crack length on the two perpendicular edges of the sample, on one side of the facesheet. It was decided to go for one side of the facesheet, as the failure occurred only on one side of the two facesheets. Good correlation is seen in all the configuration of samples as shown in Figure 4.13. The sample A and sample D which were most sensitive to microcracking as quantified during microscopic observation, had close to 30 percent reduction in strength; after 40 thermal cycles.  Sample B and sample C with less microcracks had recorded reduction of 11 to 14 percent in strength. It is also interesting to see saturation of both crack area and failure strength after 40 thermal cycles for all the cases.
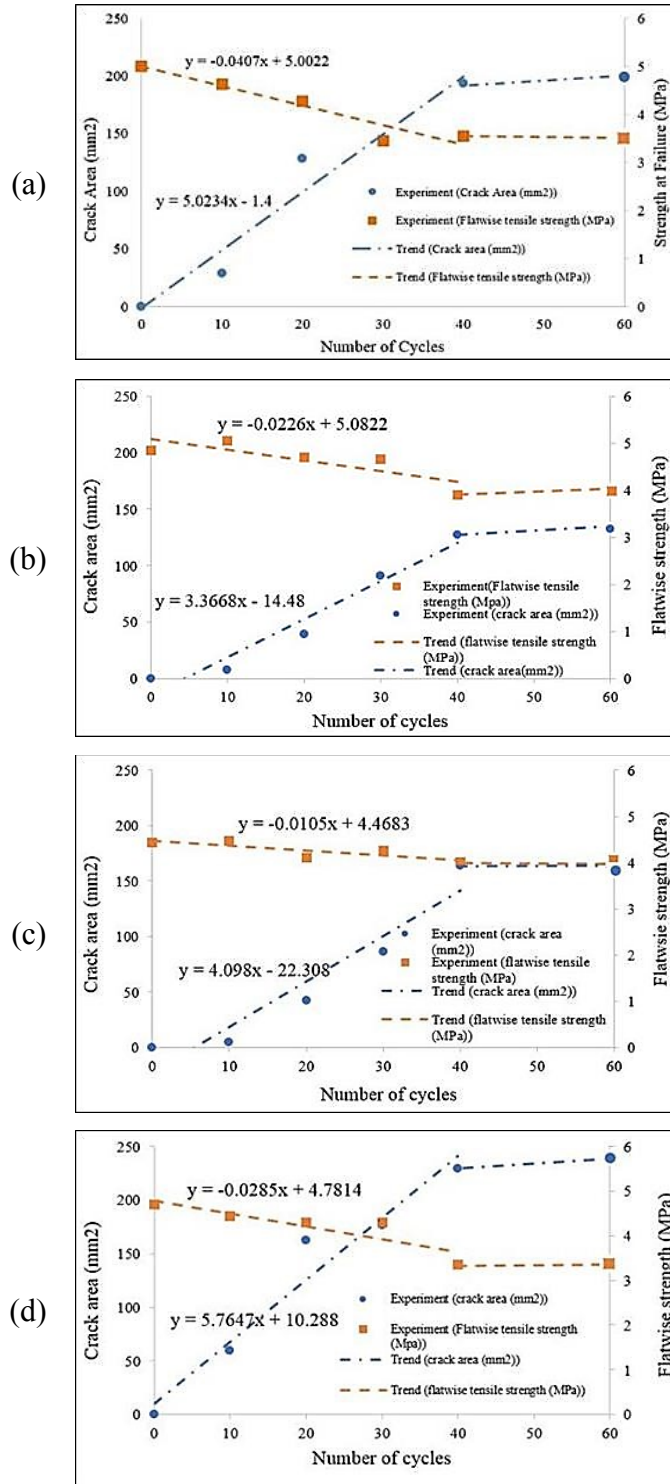
*Figure 4.13: Change in crack area and mechanical strength at failure with increase on thermal cycle for (a) Sample A, (b) Sample B, (c) Sample C and (d) Sample D.*

## 4.10 Conclusion

Performance of composite sandwich material subjected to thermal cycling was studied. Four different core and facesheet thickness configurations were chosen for study. Longitudinal microcracks in the form of delamination were observed between facesheet and core interface in all the configurations. Crack growth was monitored with increase in thermal cycles by periodic microscopic observation. Difference in CTE of the constituents was found to be responsible for the formation of microcracks. Microcracks were quantified using crack length. It was noticed that sample A and sample D were more sensitive to microcracking. Upon further investigation, it was found that between two samples studied for comparison, the one with higher core to facesheet thickness ratio was more sensitive to microcracking. The flatwise tensile test results proved that microcracks had significant effect on the debonding strength of the samples. Comparison of flatwise test results of all the configuration of samples, also suggests significant degradation of mechanical strength of samples, with higher core to facesheet thickness ratio. However, to concretely justify this trend, we need to conduct more tests with different configurations.

# Chapter 5: Conclusions, Contributions and Recommendations

## 5.1    Conclusions

In this thesis report, effect of thermal cycling on the mechanical properties of composite honeycomb sandwich structure was examined. Honeycomb sandwich structure made of cyanate ester resin reinforced with 5 harness satin fabric facesheet and Kevlar core was chosen for study. Samples were subjected to thermal cycling between the temperature ranges of -195 °C to +150 °C. For cryogenic conditioning, two different test setups were used to achieve slow and fast rate of cooling. Microscopic observation was made at the polished free edges and midsection. Microcracks were quantified and correlated with mechanical strength with increase in thermal cycles. Results of four different facesheet and core thickness configurations of samples subjected to thermal cycling were compared. 3D finite element analysis was conducted on the sandwich material geometry to predict experimental observations.

Conclusions derived from the research work presented in the preceding chapters are summarized below:

- Based on the microscopic observations made, the interface region between the adhesive fillet of the core and facesheet was sensitive to microcracking. The longitudinal microcracks observed between the facesheet and core were the result of CTE mismatch between the 90° tow and the adhesive.

- The free edges are not the only regions of the sample that are prone to microcracking. Microscopic observation at the midsection also shows presence of the microcracks. However, crack density was relatively less in the midsection and only longitudinal microcracks were observed.

- Cold conditioning had higher influence on crack formation as thermal strain is higher when samples are exposed to -194 °C. The sandwich structure was manufactured by secondary curing method. The stress-free temperature is generally the process temperature, which is 120 °C.

- Both microscopic observations and flatwise tensile mechanical test results indicate that contact cooling results in higher degradation of materials when compared to the non-contact cooling.

- The experimental results show that de-bonding strength saturates after 40 to 60 thermal cycles. This correlates well with microcrack growth, which also saturates exactly around 40 cycles or in some of the cases around 30 thermal cycles. This provides enough confidence to not go for hundreds of cycles, as the damage is already made within 40 thermal cycles.

- 3D finite element analysis in ANSYS successfully predicts the high stress and strain regions which were between the adhesive fillet and facesheet. The FEA results are in good agreement with the microscopic observation results.

- Samples made of the same facesheet and core material, but with different core and facesheet thickness were investigated. The samples with higher core to facesheet thickness ratio is more sensitive to microcracking. This conclusion is made based on the microscopic observation and mechanical test results. However, to conclusively say this, more test needs to be conducted.

## 5.2 Contributions

Some of the major contributions presented in this thesis are summarized below:

- A test plan to determine the effect of thermal cycling on the mechanical property of composite honeycomb sandwich structure was developed.

- For the first time detailed micro level images showing evolution of microcrack growth with the increase in thermal cycles was made.

- Development of a test set up to achieve lower rate of cooling. The test setup was designed to study how lower rate of cooling influences microcrack formation. The results showed significant difference in comparison to contact cooling (faster rate of cooling).

- Efficient technique of retrieving samples from flatwise test loading block for failure mode analysis. The technique also helps to increase the frequency at which tests are conducted and absolutely no loss of material from loading blocks.

- Tangible proof in the form of microscopic observation and flatwise test results explaining the factors effecting saturation of de-bonding strength for sandwich materials after limited thermal cycles.

- For the first time a 3D computer aided geometry of a representative volume element of sandwich structure was developed. The design incorporated intricate details such as

adhesive fillet, core, carbon tow and resin envelop. The finite element analysis on the geometry was able to capture experimental findings.

In addition to the above reported contributions, the following publications have been accomplished during the study:

**Journals:**

1. **Sandesh Rathnavarma Hegde**, Mehdi Hojjati," Thermally Induced Microcracks and Mechanical Property of Composite Honeycomb Sandwich Structure: Experiment and Finite Element Analysis" to appear, *Journal of Sandwich Structures and Materials*, 2018, DOI: 10.1177/1099636218802432.

2. **Sandesh Rathnavarma Hegde**, Mehdi Hojjati," Performance of Composite Sandwich Structures under Thermal Cycling" submitted to the *Journal of Composite Materials*.

3. **Sandesh Rathnavarma Hegde**, Mehdi Hojjati," Effect of Core and Facesheet Thickness on the Mechanical property of Composite Sandwich Structures Subjected to Thermal Fatigue" submitted to the *International Journal of Fatigue*.

**Conferences:**

1. **Sandesh Rathnavarma Hegde** and Mehdi Hojjati," Effect of Thermal Cycling on Composite Honeycomb Sandwich Structures" 12th International Conference on Sandwich Structures (ICSS-12), Lausanne , Switzerland, 19–22 August (2018).

2. **Sandesh Rathnavarma Hedge** and Mehdi Hojjati," Effect of Microcracks on Mechanical Property of Composite Honeycomb Sandwich Structure Subjected to Thermal Cycling" SAMPE, Long beach, California, USA, May 21-24 (2018).

3. **Sandesh Rathnavarma Hedge** and Mehdi Hojjati," Effect of Thermal Cycling on Composite Honeycomb Sandwich Structures for Space Applications" CASI-ASTRO 18, Quebec city, Quebec, Canada May 15-17 (2018).

## 5.3 Recommendations for future work

Some of the recommendations for the future work are summarized below.

- Microscopic observation at the midsection was conducted only for one of the samples after 40 thermal cycles in the presented research. However, similar inspection needs to be made for all the configurations after subsequent thermal cycles.

- Effect of fiber orientation and stacking sequence on the formation of microcracks needs to be investigated. The samples tested in this study had woven fabric oriented in 0/90 direction adjacent to the core. It would be interesting to see the effect of fiber angle.

- Carbon fiber reinforced cyanate-ester based laminates were chosen for this study. It would be interesting to conduct experiments on other most frequently used material types, for example carbon fiber with epoxy resin.

- The samples used for the study were manufactured by secondary bonding and curing process. Effect of other techniques to process may be explored to see if there is an influence of processing method.

- Other techniques of detecting microcracks could be explored, the present method involves physically cutting and polishing the samples. Other novel non-destructive methods could be explored.

- Finite element analysis to capture the effect of thermal cycling taking into consideration different core, facesheet thickness and fiber angle could prove advantageous. If the FEA model can predict the magnitude of stress and strain accurately, the need to perform the time consuming and tedious thermal cycling experiment could be avoided.

# References

1. Christos Kassapoglou, "Design and Analysis of Composite Structures: with applications to aerospace structures", Wiley, 2010.

2. Alan Baker and Murray Scott, "Composite Materials for Aircraft Structures", 3rd edition, AIAA educational series, 2016.

3. Ever J. Barbero, "Introduction to Composite Materials design", 2nd edition, CRC press, 2011.

4. S. V. Hoa, "Principles of the Manufacturing of Composites Materials", DEStech Publications, 2009.

5. R. Lukez, "The Use of Graphite/Epoxy Composite Structures in Space Applications," Morton Thiokol, Inc, Aerospace Group Brigham City Utah, USA, 1987.

6. T. C. Thompson et al., "Development of an All-Composite Spacecraft Bus for small satellite programs", Los Alamos National Laboratory, Los Alamos, New Mexico.

7. Available: https://www.ruag.com/sites/default/files/2016-12/Structures-Brochure.pdf

8. MDA Corporation brochure.

9. Available:https://spacenews.com/musk-offers-more-details-about-mars-mission-architecture/.

10. Available:http://seismocare.blogspot.com/2010/10/this-thesis-is-concerned-with-combined.html.

11. Available: http://www.admatis.com/eng/competencies_material_science_sandwich.html.

12. Kevlar Aramid Fibers, "DuPont Kevlar Technical Guide," Du Pont. pg. 1–31, 2016.

13. Hexcel Composites, "Honeycomb Attributes and Properties, A comprehensive guide to standard Hexcel honeycomb materials, configurations, and mechanical properties," Honeycomb Data Sheets, pg. 1–40, 1999.

14. The Space Environment. Available: https://www.faa.gov/other_visit/aviation_industry/designees_delegations/designee_types/ame/media/Section%20III.4.1.2%20The%20Space%20Environment.pdf.

15. J. Han and C. Kim, "Low earth orbit space environment simulation and its effects on graphite/epoxy composites," Composite Structures, vol. 72, pg. 218-226, 2006.

16. C. Soares et al., "Protection from induced space environments effects on the International Space Station," Eur. Sp. Agency, Special Publ. ESA SP, vol. 680, 2010.

17. Finckernor M. M., "Comparison of High-Performance Fiber Materials Properties in Simulated and Actual Space Environments," NASA Tech. Rep., July, 2017.

18. S. Mahdavi, "Thermal Cycling of Out‑Of‑Autoclave Thermosetting Composite Materials," Master's Thesis, Concordia University. March, 2017.

19. V. T. Bechel, J. D. Camping, and R. Y. Kim, "Cryogenic/elevated temperature cycling induced leakage paths in PMCs," Compos. Part B Eng., vol. 36, Issue no. 2, pg. 171–182, 2005.

20. Y. X. He et al., "Micro-crack behavior of carbon fiber reinforced thermoplastic modified epoxy composites for cryogenic applications," Compos. Part B Eng., vol. 44, no. 1, pp. 533–539, 2013.

21. B. R. Murray, A. Doyle, P. J. Feerick, C. O. A. Semprimoschnig, S. B. Leen, and C. M. Ó Brádaigh, "Rotational moulding of peek polymer liners with carbon fibre/peek over tape-placement for space cryogenic fuel tanks," Journal of Materials and Design., vol. 132, pg. 567–581, 2017.

22. Y. He et al., "Micro-crack behavior of carbon fiber reinforced Fe3O4/graphene oxide modified epoxy composites for cryogenic application," Compos. Part A Appl. Sci. Manuf., vol. 108, February, pg. 12–22, 2018.

23. M. Flanagan et al., "Permeability of carbon fibre PEEK composites for cryogenic storage tanks of future space launchers," Compos. Part A Appl. Sci. Manuf., vol. 101, pg. 173–184, 2017.

24. D. M. Grogan, C. M. Ó Brádaigh, J. P. McGarry, and S. B. Leen, "Damage and permeability in tape-laid thermoplastic composite cryogenic tanks," Compos. Part A Appl. Sci. Manuf., vol. 78, pg. 390–402, 2015.

25. M. Jean-St-Laurent, M. L. Dano, and M. J. Potvin, "Study of damage induced by extreme thermal cycling in cyanate ester laminates and sandwich panels," J. Compos. Mater., vol. 51, Issue no. 14, pp. 2023–2034, 2017.

26. Niu MCY. Composite airframe structures. Hong Kong: Conmilit Press Ltd.

27. Stephen W. Tsai, introduction to composite materials. Lancaster, PA, USA: Technomic Publishing Co.Inc.

28. Petras A, et al. Failure mode maps for honeycomb sandwich structures. Compos Struct 1999; 44: 237–252.

29. Kirch MT. Composite crew model: primary structure. NASA Technical Report Server, 1 November 2011, NASA Langley Research Center, Hampton, VA, https://ntrs.nasa.gov/search.jsp?R=20110020665

30. Gates TS, Su X, Abdi F, et al. Facesheet delamination of composite sandwich materials at cryogenic temperature. Compos Sci Technol 2006; 66: 2423–2435.

31. Timmerman JF, Tillman MS, Hayes BS, et al. Matrix and fiber influences on the cryogenic microcracking of carbon fiber/epoxy composites. Compos Part A: 2002; 33: 323–329.

32. Chen H, et al. Thermal expansion of honeycomb sandwich panels. Reprinted from Thermal Conductivity and Thermal Expansion, ICCM, Paris, France, 13–16 June 1999.

33. Grimsley BW, Cano RJ, Johnston NJ, et al. Hybrid composites for LH2 fluid tank structure. NASA Technical Report Server, 1 January 2001, USA, www.ntrs.nasa.gov

34. Lee HS, Hong SH, Lee JR, et al. Mechanical behavior and failure process during compressive and shear deformation of honeycomb composite at elevated temperature. J Mater Sci 2002; 37: 1265–1272.

35. Tompkins SS. Effect of thermal cycling of composite material on space structure. NASA Technical Report Server, 1 May 1989, 447-470, USA, www.ntrs.nasa.gov

36. Wienhold PD, et al. The development of high-temperature composite solar array sub- strate panels for the messenger spacecraft. In: SAMPE technical conference, Salt Lake City, UT, 11–14 October 2010.

37. Gupta S K, et al. Micro-crack detection technique in polymeric composites during thermal cycling. In: 21st International conference on composite materials, Xi'an, China, 20–25 August 2017.

38. Yu Q, et al. Effects of vacuum thermal cycling on mechanical and physical properties of high performance carbon/bismaleimide composite. Mater Chem Phys 2011; 130: 1046–1053.

39. Tsukrov I, Drach B and Gross T. Effective stiffness and thermal expansion coefficients of unidirectional composites with fibers surrounded by cylindrically orthotropic matrix layers. Int J Eng Sci 2012; 58: 129–143.

40. Sanborn J and Morel D. Effects of thermal cycling on the mechanical and physical properties of a space qualified epoxy adhesive. J Reinf Plast Compos 1998; 7: 155–164.

41. Henaff-Gardin C and Lafarie-Frenot M. Specificity of matrix cracking development in CFRP laminates under mechanical or thermal loadings. Int J Fatigue 2002; 24: 171–177.

42. Shimokawa T, et al. Effect of thermal cycling on microcracking and strength degrada- tion of high-temperature polymer composite materials for use in next generation SST structures. J Compos Mater 2002; 36: 885–895.

43. Gupta SK and Hojjati M. Thermal cycle effects on laminated composite plates contain- ing voids. J Compos Mater 2018. DOI: 10.1177/0021998318786785.

44. Polishing Machine, Mecatech 234, https://www.presi.com/en/polishing-machines/252-mecatech-234.html

45. ProgRes® Speed XT core microscope camera, http://www.rsepl.com/Progres- speedxt.php

46. Shefizadeh J. E, et al. Evaluation of the in-service performance behaviour of honeycomb composite sandwich structures. J Mater Eng Performance 1999; 8: 661–668.

47. Mahdavi S, Kumar Gupta S and Hojjati M. Thermal cycling of out-of-autoclave thermosetting composite materials. In: Canadian international conference on composite materials, Ottawa, Canada, 14–17 July 2017.

48. ASTM Standard C297-04. Standard test method for flatwise tensile strength of sandwich constructions. West Conshohocken, PA: ASTM International, 2010, pp.19428-2959, www.astm.org

49. Hysol®, EA 9392, Epoxy Paste Adhesive, Technical Data Sheet, https://northerncomposites.com/docs/default-source/data-sheets/hysol_ea_9392-en.pdf?sfvrsn=2

50. ANSYS Workbench Users Guide, Release 12.1. PA, USA: ANSYS Inc., 2009. 27.

51. Carraro PA, et al. Influence of manufacturing induced defects on damage initiation and propagation in carbon/epoxy NCF laminates. Advanced Manufacturing: Polymer and Composite Science, 8 December 2014; 1: 44–53.

52. Liu L, et al. The flatwise compressive properties of Nomex honeycomb core with debonding imperfections in the double cell wall. Compos Part B 2015; 76: 122–132.

53. S. R. Hegde, M. Hojjati. Effect of Microcracks on the Mechanical property of Composite Honeycomb Sandwich Panel Subjected to Thermal Cycling. SAMPE Conference, May 2018, Long Beach, USA.

54. A. J. Hodge. Evaluation of Microcracking Composite in Two Carbon-Fiber/Epoxy-Matrix Cryogenic Tank. NASA Technical Memorandum, Marshal Space Flight Centre, Alabama, 2001. Online: https://ntrs.nasa.gov/search.jsp?R=20010080458 2017-09-03T03.

55. T.L. Brown. Microcracking of Materials for Space. Technical report, NASA Langley Research Centre, 1998. Online: https://ntrs.nasa.gov/search.jsp?R=19990009608 2018-02-21T03.

56. Richard F. Vyhnal. The Effects of Long-Duration Space Exposure on the Mechanical Properties of Some Carbon-Reinforced Resin Matrix Composites. Rockwell International-North American Aircraft Tulsa, Oklahoma 74115, https://ntrs.nasa.gov/search.jsp?R=19930019077.

57. W. K. Stuckey. Lessons learnt from long duration Exposure Facility. Technical report, Mechanics and Materials Technology Center Technology Operations, 15 February 1993.

58. David. E. Glass. Bonding and Sealing Evaluations for Cryogenic Tanks. Technical report, Analytical Services & Materials, Inc., Hampton, https://ntrs.nasa.gov/search.jsp?R=19970029012 2018-02-26T18:25:51+00:00Z.

59. I. Tsukrov, B. Drach and T. Gross. Effective stiffness and thermal expansion coefficients of unidirectional composites with fibers surrounded by cylindrically orthotropic matrix layers. *Int. J. Eng. Sci* ;58:, pp. 129-143, 2012.

60. S. R. Hegde, M. Hojjati. Thermally Induced Microcracks and Mechanical Property of Composite Honeycomb Sandwich Structure: Experiment and Finite Element Analysis. *Journal of Sandwich Structures and Materials*, 2018, DOI: 10.1177/1099636218802432.

61. S. R. Hegde, M. Hojjati. Effect of Thermal Cycling on Composite Honeycomb Sandwich Structures. 12th International conference on Sandwich Structures (ICSS-12), 19-22 August 2018, Lausanne, Switzerland.

62. S. K. Mital, J. Z. Gyekenyesi, S. M. Arnold, R. M. Sullivan, J. M. Manderscheid, and P. L. N. Murthy, "Review of Current State of the Art and Key Design Issues With Potential Solutions for Liquid Hydrogen Cryogenic Storage Tank Structures for Aircraft Applications," *NASA STI Program Document*, pg. 3–21, October 2006.

63. M. T. Callaghan, "Use of resin composites for cryogenic tankage," *Cryogenics (Guildf).*, vol. 31, pg. 282–287, May 1991.

64. D. E. Glass, "Bonding and Sealing Evaluations for Cryogenic Tanks," NASA Contractor Report, August 1997, Online: https://ntrs.nasa.gov/search.jsp?R=19970029012.

65. T. S. Gates, K. S. Whitley, R. W. Grenoble, and T. Bandorawalla, "Thermal / Mechanical Durability of Polymer-Matrix Composites in Cryogenic Environments," pg. 1–12, 2018.

66. K. Pannkoke and H. J. Wagner, "Fatigue properties of unidirectional carbon fibre composites at cryogenic temperatures," *Cryogenics (Guildf).*, vol. 31, pg. 248–251, 1991.

67. M. S. Islam, R. Avila, A. G. Castellanos, and P. Prabhakar, "Hybrid Textile Composites as Potential Cryogenic Tank Materials," *57th AIAA/ASCE/AHS/ASC Struct. Struct. Dyn. Mater. Conf.*, January, 2016.

68. M. R. Garnich, R. W. Dalgarno, and D. J. Kenik, "Effects of moisture on matrix cracking in a cryo-cycled cross-ply laminate," *J. Compos. Mater.*, vol. 45, Issue no. 26, pg. 2783–2795, 2011.